공학박사학위논문

스트로크-보어 비에 따른 직분사 가솔린 엔진의 열효율 및 연소 현상에 대한 연구

Investigation on the Thermal Efficiency and Combustion Phenomena of a Direct-Injected, Spark-Ignited Engine with Various Conditions of Stroke-to-Bore Ratio

2019 년 8 월

서울대학교 대학원

기계항공공학부

오 세 철

스트로크-보어 비에 따른 직분사 가솔린 엔진의 열효율 및 연소 현상에 대한 연구

Investigation on the Thermal Efficiency and Combustion Phenomena of a Direct-Injected, Spark-Ignited Engine with Various Conditions of Stroke-to-Bore Ratio

지도교수 송 한 호

이 논문을 공학박사 학위논문으로 제출함

2019 년 4 월

서울대학교 대학원

기계항공공학부

오 세 철

오세철의 공학박사 학위논문을 인준함

2019 년 6 월

위 원 장 : 민 경 덕

부위원장 : 송 한 호

위 원 : 도 형 록

위 원 : 황 원 태

위 원 : 이 선 영

Abstract

Investigation on the Thermal Efficiency and Combustion Phenomena of a Direct-Injected, Spark-Ignited Engine with Various Conditions of Stroke-to-Bore Ratio

Sechul Oh
Department of Mechanical and Aerospace Engineering
The Graduate School
Seoul National University

In accordance with the strong regulation on fuel economy, gasoline-fueled spark-ignition engine for automotive application still has been researched rigorously by many researchers. However, the most investigations have been focused on the operating strategies, not on the engine design which is a key factor that determines the performance and fuel economy of engine operation. Out of the parameters related to engine design, from many studies, stroke-to-bore ratio (SB ratio) is known to significantly influence engine efficiency of SI engine operation.

With a long stroke operation (i.e. higher SB ratio), two important issues were mainly postulated in the previous literatures – cooling loss and flame propagation. First, with enlarging stroke-to-bore ratio, surface-to-volume ratio (SV ratio) at TDC timing is reduced, causing decrement in cooling loss during combustion and simultaneously increment in engine efficiency. Second, with enhanced flow dynamics by faster piston movement attributed by long stroke operation, turbulent flame propagation was enhanced, resulting in faster combustion which is

corresponding to ideal cycle (i.e. Otto cycle) for SI engine operation with improved engine efficiency. However, these works with several experiments were conducted by fixed bore condition so that the sole effect of SB ratio cannot be split from the results.

In this study, stroke-to-bore ratio with constant compression ratio and displacement volume was mainly investigated with single cylinder direct-injected spark ignition engine setup equipped with various valve timing module. With these basic investigation, two additional setups were also used – different displacement volume with similar SB ratio and enhanced tumble ratio with same SB ratio – to verify the sole effect of SB ratio and the potential of increment in burning rate on engine efficiency for various SB ratio conditions. With these approaches, firstly, valve timing variations were conducted to find the best efficiency of several operating conditions such as load, rotational speed, and SB ratio. As a result, it was concluded that the valve timing positions for the best efficiency were not significantly differed by various SB ratios – load and rotational speed were mainly influencing the positions of valve timing attributed by pumping loss and residual mass fraction for low load operation, and knock mitigation for high load operation.

By using the determined valve timing positions, several investigations related to cooling loss and knock phenomena, which was previously found to result in unexpected behaviors from preliminary tests of valve timing variation, were conducted, with low load operation for cooling loss and high load operation for knock phenomena. First of all, detailed combustion analysis based on the IVC state and in-cylinder pressure profile was used to evaluate the heat transfer and internal energy difference inside the cylinder during closed duration (from IVC to EVO timing). From these, it was shown that the amount of heat transfer around TDC or peak pressure timing was higher for long stroke operation (i.e. SB 1.47),

resulting in unexpected higher cooling loss and lower amount of the difference of internal energy between IVC to EVO timing which is related to higher exhaust heat loss evaluated by exhaust temperature. Second, knock phenomena were investigated by additional experiments with relatively strong knock occurrence. From the analysis of individual cycles, it was found that faster flame propagation caused strong knock intensity compared to non-knock cycle which had slower flame propagation. With new definition of knock-robust operation, the simulation showed that the fast burn operation still can show more knock-robust operation with enhanced engine efficiency and advanced combustion phasing. However, in the experimental data, it was shown that reduced efficiency and retarded combustion phasing were detected from longer stroke operation (i.e. SB 1.47 and tumble variation) even shorter burn duration was achieved by enhanced tumble ratio. By adopting new index representing knock intensity, it was found that the unexpected knock behavior in long stroke operation was attributed by the characteristics of geometry, especially by more compact size of cylinder around TDC timing. Therefore, in order to adopt several strategies, related to increase burning rate, to enhance engine efficiency, moderate SB ratio is recommended because of cooling loss, and knock phenomena issues as mentioned above.

Keywords: Spark-Ignited Engine, Stroke-to-Bore Ratio, 0D-Based Combustion Analysis, Knock, Cooling Loss, Exhaust Heat Loss

Student Number: 2013-23076

Contents

Abstract ii

Contents v

List of Tables ix

List of Figures x

Nomenclature xxii

Chapter 1. Introductions 1

1.1 Backgrounds 1

1.2 Literature Review 11

1.2.1 Fundamentals of SI engine operation - review 11

1.2.2 Valve timing variation in SI engine 14

1.2.3 Engine knock in SI engine 15

1.2.4 Flame speed in SI engine 22

1.2.5 Stroke-to-bore ratio 26

1.3 Motivation and Objectives 28

1.4 Organization of the Dissertation 30

Chapter 2. Combustion Analysis and Simulation Modeling 32

2.1 Thermodynamic-based analysis 32
2.1.1 Estimation of residual mass fraction and IVC condition 32
2.1.2 Heat release and combustion phasing 40
2.1.3 LHV breakdown 44
2.1.4 Energy balance in closed system 49

2.2 Knock measurement 52
2.2.1 Determination of knock-limited operation and its characteristics 56
2.2.2 Limitation of knock analysis – averaging process 66

2.3 0D simulation of SI engine operation 70
2.3.1 Basic information 70
2.3.2 Autoignition determination – Livengood-Wu integration model 78
2.3.3 Determination of knock-limited condition 80

Chapter 3. Experimental Apparatus 81

3.1 Experimental configuration 81
3.1.1 Single cylinder engine 81
3.1.2 Measurement and test facility 85
3.1.3 Experimental conditions – stroke-to-bore ratio, displacement volume, and tumble ratio 90

3.2 Approach on the reliability of data acquisition and analysis 97

Chapter 4. Preliminary Experiment – Variable Valve Timing and the Best Efficiency Point 103

4.1 Scheme for valve timing variation 104
4.1.1 Univariate search process 104

4.1.2 Design of experiment (DoE) process 106
4.1.3 Full factorial (complete enumeration) process 112

4.2 Experimental results of preliminary valve timing sweep operation 120
4.2.1 Low load operation 120
4.2.2 Middle load (WOT with N/A operation) 131
4.2.3 High load operation 136

4.3 Comparison with different displacement volume and tumble ratio conditions 142
4.3.1 Basic conditions vs. different displacement volume conditions 143
4.3.2 Basic conditions vs. different tumble ratio conditions 146

4.4 Interim summary 153

Chapter 5. Experiment and Simulation – Burning Rate and Thermodynamics in Cylinder 155

5.1 Introduction 155

5.2 Heat transfer timing and its effect 156

5.3 Experimental Results 169
5.3.1 Basic three conditions with different displacement volume 171
5.3.2 Basic three conditions with different tumble ratio 177

Chapter 6. Experiment and Simulation – Burning Rate and Knock Characteristics 183

6.1 Introduction – definition of robustness in knock 183

6.2 Experimental conditions and scheme 188

6.3 Experiment and simulation results 191
6.3.1 Burning rate on knock intensity 191
6.3.2 Geometry and other issue on knock intensity 201
6.3.3 Suggestions on simulated knock intensity 207

Chapter 7. Conclusions 213

References 217

Appendix A. Proof of the relation between heat transfer and pressure decrement in Otto cycle 231

국 문 초 록 235

List of Tables

Table 2.1 Theoretical frequencies of the pressure oscillation modes under three SB ratios [98] 63

Table 2.2 Detailed conditions used for 0D simulation 77

Table 3.1 Details of engine hardware and CVVT 84

Table 3.2 Control target of temperature and pressure in the experiment..... 89

Table 3.3 Information for gasoline used in the experiment..... 89

Table 3.4 Detailed information of stroke-to-bore ratio and Rt conditions 96

Table 3.5 Summary of the effect of error in TDC calibration 102

Table 4.1 Summary of input variables and efficiency for various methods (nIMEP 4.5 bar, 2000 RPM) 111

Table 4.2 Summary of input variables and efficiency for various methods (nIMEP 6.5 bar, 2000 RPM) 111

Table 4.3 Valve timing positions for each experiment related to chapter 5 and 6 119

Table 6.1 Operating parameters of knock-related experiments..... 190

List of Figures

Figure 1.1 CO_2 regulations for several countries 4

Figure 1.2 CO_2 emissions from several powertrain devices with different fuel conditions (redrawn from [5]) 5

Figure 1.3 Energy (1st law) and exergy (2nd law) analysis of general engine operation (redrawn from [16]) 10

Figure 1.4 Characterization of autoignition with ξ and ε values to characterize the knock phenomena, redrawn from [32], fueled by 50% of H_2 and 50% of CO. 20

Figure 1.5 Correlation between pressure rise rate and burn duration with knock cycles (expressed as green triangle with 'knocking cycle') and non-knock cycles (expressed as blue circle with 'normal cycle'), redrawn from [51] 25

Figure 2.1 Algorithm for the calculation of residual mass fraction and IVC temperature 38

Figure 2.2 Example of the estimation of residual mass fraction with respect to various intake valve timing 39

Figure 2.3 Example of the NOx emissions with respect to various intake valve timing 39

Figure 2.4 Algorithm for the calculation of heat release data 43

Figure 2.5 Energy balance of engine operation with respect to whole cycle 48

Figure 2.6 Example of pressure profiles for knock-related conditions (SB 1.47, 26mg of fuel rate and 2000 RPM) 54

Figure 2.7 Example of gross IMEP data corresponding to the conditions of figure 2.6 (SB 1.47, 26mg of fuel rate and 2000 RPM) 55

Figure 2.8 First six pressure oscillation modes of pressure wave (redrawn from [71]) 61

Figure 2.9 Normalized power spectral density of pressure profile with knock occurrence for three different SB ratio (redrawn from [98]) 62

Figure 2.10 Example of in-cylinder and filtered pressure data of knock cycle (SB 1.47, 26 mg of fuel rate, and 1500 RPM, #130 cycle of total 5000 cycles experiment) 64

Figure 2.11 Example of in-cylinder and filtered pressure data of non-knock cycle (SB 1.47, 26 mg of fuel rate, and 1500 RPM, # 128 cycle of total 5000 cycles experiment) 64

Figure 2.12 Comparison of MAPO knock incidence and ISPO knock intensity, redrawn from [71] 65

Figure 2.13 Example of the stochastic knock behavior (SB 1.0, 34 mg of fuel rate, 1500 RPM) 68

Figure 2.14 Example of section-divided averaging method redrawn from [76] (a): Guideline for averaging method by unburned mass fraction (b): Results of averaging method 68

Figure 2.15 Example of the result of averaging method (SB 1.0 and 1.47, 34 mg of fuel rate, 1500 RPM) x-axis: averaged unburned mass fraction at knock onset y-axis: averaged MAPO by each section of unburned mass fraction..... 69

Figure 2.16 Ignition delay map from constant-volume chamber simulation. The value at each iso-ignition delay line means ignition delay with millisecond unit. 79

Figure 3.1 Single cylinder DISI engine..... 83

Figure 3.2 Details of CVVT operations 83

Figure 3.3 Test Facilities for measurement and control processes 87

Figure 3.4 Engine parameters measured and controlled in the experiment..... 88

Figure 3.5 Total geometry conditions for the experiment 94

Figure 3.6 Details of the design related to packaging constraint..... 94

Figure 3.7 The cylinder heads (upper: A, middle: B, lower: C) 95

Figure 3.8 Camshaft and the ‘half moon’ part..... 101

Figure 3.9 CMPS signal derived from absolute position of half-moon part 101

Figure 4.1 Experimental results of maximum efficiency point using various methods (nIMEP 4.5 bar 2000 RPM, 6.5 bar 2000RPM), redrawn from [100] 110

Figure 4.2 Operating points for complete enumeration experiments 115

Figure 4.3 Net efficiency results of complete enumeration process for nIMEP 4.5 bar, 2000 RPM (a: SB 1.0, b: SB 1.2, c: SB 1.47) 116

Figure 4.4 Net efficiency results of complete enumeration process for nIMEP 8.5 bar, 2000 RPM (a: SB 1.0, b: SB 1.2, c: SB 1.47) 117

Figure 4.5 Gross efficiency results of complete enumeration process for gIMEP 10.5 bar, 2000 RPM (a: SB 1.0, b: SB 1.2, c: SB 1.47).....118

Figure 4.6 Experimental results of intake valve timing sweep for nIMEP 4.5 bar, 1500 RPM, and three SB ratios (1.0, 1.2, and 1.47) (a) Residual mass fraction (b) NOx emissions (c) CO emissions (d) UHC emissions 125

Figure 4.7 Experimental results of intake valve timing sweep for nIMEP 4.5 bar, 1500 RPM, and three SB ratios (1.0, 1.2, and 1.47) (a) Initial flame speed (ignition to CA10) (b) Main flame speed (CA10 to CA90) (c) The maximum in-cylinder pressure 126

Figure 4.8 Experimental results of intake valve timing sweep for nIMEP 4.5 bar, 1500 RPM, and three SB ratios (1.0, 1.2, and 1.47) (a) Internal energy extraction normalized by fuel LHV (in closed duration) (b) Exhaust loss normalized by fuel LHV (c) Net indicated efficiency (d) PMEP 127

Figure 4.9 Cooling loss results with intake valve timing sweep for nIMEP 4.5 bar and three SB ratios (1.0, 1.2, and 1.47) (a) 1500 RPM (b) 2000 RPM 128

Figure 4.10 Experimental results of intake valve timing sweep for nIMEP 4.5 bar, 2000 RPM, and three SB ratios (1.0, 1.2, and 1.47) (a) Exhaust loss normalized by fuel LHV (b) PMEP (c) Net indicated efficiency 129

Figure 4.11 Experimental results of exhaust valve timing sweep for nIMEP 4.5 bar, 2000 RPM, and three SB ratios (1.0, 1.2, and 1.47) (a) Residual mass fraction (b) Exhaust loss normalized by fuel LHV (c) PMEP (d) Net indicated efficiency 130

Figure 4.12 Experimental results of intake valve timing sweep for nIMEP 8.5 bar, 2000 RPM, and three SB ratios (1.0, 1.2, and 1.47) (a) NOx emissions (b) CO emissions (c) UHC emissions (d) The maximum in-cylinder pressure 133

Figure 4.13 Experimental results of intake valve timing sweep for nIMEP 8.5 bar, 2000 RPM, and three SB ratios (1.0, 1.2, and 1.47) (a) Initial flame speed (b) Main flame speed (CA10-CA70) (c) CA50..... 134

Figure 4.14 Experimental results of intake valve timing sweep for nIMEP 8.5 bar, 2000 RPM, and three SB ratios (1.0, 1.2, and 1.47) (a) Exhaust loss normalized by fuel LHV (b) Cooling loss normalized by fuel LHV (c) PMEP (d) Net indicated efficiency..... 135

Figure 4.15 Experimental results of intake valve timing sweep for gIMEP 10.5 bar, 2000 RPM, and three SB ratios (1.0, 1.2, and 1.47) (a) Volumetric efficiency (b) PMEP..... 138

Figure 4.16 Experimental results of intake valve timing sweep for gIMEP 10.5 bar, 2000 RPM, and three SB ratios (1.0, 1.2, and 1.47) (a) NOx emissions (b) CO emissions (c) UHC emissions (d) The maximum in-cylinder pressure 139

Figure 4.17 Experimental results of intake valve timing sweep for gIMEP 10.5 bar, 2000 RPM, and three SB ratios (1.0, 1.2, and 1.47) (a) Initial flame speed (b) Main flame speed (CA10-CA70) (c) CA50..... 140

Figure 4.18 Experimental results of intake valve timing sweep for gIMEP 10.5 bar, 2000 RPM, and three SB ratios (1.0, 1.2, and 1.47) (a) Cooling loss normalized by fuel LHV (b) Exhaust loss normalized by fuel LHV (c) Gross indicated efficiency 141

Figure 4.19 Pumping loss data for intake valve timing sweep with nIMEP 4.5 bar, 1500 and 2000 RPM, and five SB ratios (1.0, 1.2, 1.47, 1.19 and 1.42) (a) 1500 RPM (b) 2000 RPM 144

Figure 4.20 Cooling loss data for intake valve timing sweep with nIMEP 4.5 bar, 1500 and 2000 RPM, and five SB ratios (1.0, 1.2, 1.47, 1.19 and 1.42) (a) 1500 RPM (b) 2000 RPM 144

Figure 4.21 Exhaust loss data for intake valve timing sweep with nIMEP 4.5 bar, 1500 and 2000 RPM, and five SB ratios (1.0, 1.2, 1.47, 1.19 and 1.42) (a) 1500 RPM (b) 2000 RPM 145

Figure 4.22 Net indicated efficiency data for intake valve timing sweep with nIMEP 4.5 bar, 1500 and 2000 RPM, and five SB ratios (1.0, 1.2, 1.47, 1.19 and 1.42) (a) 1500 RPM (b) 2000 RPM..... 145

Figure 4.23 Combustion efficiency data for intake valve timing sweep with nIMEP 4.5 bar, 1500 and 2000 RPM, and five different conditions (SB 1.0, 1.2, 1.47, 1.2 high Rt, and 1.47 high Rt) (a) 1500 RPM (b) 2000 RPM 148

Figure 4.24 Flame speed data for intake valve timing sweep with nIMEP 4.5 bar, 1500 and 2000 RPM, and five different conditions (SB 1.0, 1.2, 1.47, 1.2 high Rt, and 1.47 high Rt) (a) Initial flame speed for 1500 RPM (b) Initial flame speed for 2000 RPM (c) Main flame speed for 1500 RPM (b) Main flame speed for 2000 RPM..... 149

Figure 4.25 Pumping loss data for intake valve timing sweep with nIMEP 4.5 bar, 1500 and 2000 RPM, and five different conditions (SB 1.0, 1.2, 1.47, 1.2 high Rt, and 1.47 high Rt) (a) 1500 RPM (b) 2000 RPM 150

Figure 4.26 Cooling and exhaust loss data for intake valve timing sweep with nIMEP 4.5 bar, 1500 and 2000 RPM, and five different conditions (SB 1.0, 1.2, 1.47, 1.2 high Rt, and 1.47 high Rt) (a) Cooling loss normalized by fuel LHV for 1500 RPM (b) Cooling loss normalized by fuel LHV for 2000 RPM (c) Exhaust loss normalized by fuel LHV for 1500 RPM (b) Exhaust loss normalized by fuel LHV for 2000 RPM..... 151

Figure 4.27 Net indicated efficiency data for intake valve timing sweep with nIMEP 4.5 bar, 1500 and 2000 RPM, and five different conditions (SB 1.0, 1.2, 1.47, 1.2 high Rt, and 1.47 high Rt) (a) 1500 RPM (b) 2000 RPM 152

Figure 5.1 In-cylinder pressure profile of the best efficiency condition with SB 1.0, nIMEP 4.5 bar, and 2000 RPM and its adiabatic pressure profile..... 163

Figure 5.2 The effect of heat transfer timing on the summation of adiabatic work, expressed as subtraction between total adiabatic work and pseudo adiabatic work (nIMEP 4.5 bar, 2000 RPM)..... 164

Figure 5.3 The effect of heat transfer timing on the summation of adiabatic work with real heat transfer value at the relevant crank angle timing (nIMEP 4.5 bar, 2000 RPM)..... 164

Figure 5.4 Correlation between heat transfer and work loss during closed duration for each SB ratio condition with knock-free data (< nIMEP 6.5 bar), normalized by relevant fuel LHV (a): all conditions (b): SB 1.0 with 1st order curve fitting (c): SB 1.2 with 1st order curve fitting (d): SB 1.47 with 1st order curve fitting 165

Figure 5.5 Correlation between the difference between heat transfer and work loss during closed duration and the difference of internal energy from IVC to EVO with knock-free data (< nIMEP 6.5 bar), normalized by relevant fuel LHV

(a) basic three SB ratio with tumble ratio enhanced conditions (b) same graph with (a) but conditions marked..... 166

Figure 5.6 Trends of heat transfer during main flame propagation (CA10 to CA70) with relevant burn duration for basic three SB ratio and different tumble ratio, normalized by total amount of heat transfer during closed duration..... 167

Figure 5.7 Correlation between the remainder of internal energy at EVO timing and exhaust loss for all operating conditions under knock-free operation (including basic three SB ratio, different displacement volume and tumble ratio conditions)..... 168

Figure 5.8 Instantaneous are at each crank angle for basic three SB ratio and different displacement volume conditions. (a): whole crank angle (compression + expansion stroke) (b): same with (a) but magnified, targeted to firing TDC timing (c): same with (b) but normalized by the volume of firing TDC timing for SB 1.47 condition..... 170

Figure 5.9 Experimental data for basic three SB ratio with different displacement volume (nIMEP 4.5 bar, 1500 RPM with the best efficiency operation) (a): estimated heat transfer during closed duration (b): estimated convective heat transfer coefficient (from single zone approach) (c): mass-averaged single zone temperature..... 173

Figure 5.10 Experimental data for basic three SB ratio with different displacement volume (nIMEP 4.5 bar, 1500 RPM with the best efficiency operation) (a): burn duration from CA10 to CA90 (b): estimated heat transfer and work extraction during closed duration, normalized by relevant fuel LHV (c): fuel LHV breakdown 174

Figure 5.11 Experimental data for basic three SB ratio with different displacement volume (nIMEP 4.5 bar, 2000 RPM with the best efficiency operation) (a): estimated heat transfer during closed duration (b): estimated convective heat transfer coefficient (from single zone approach) (c): mass-averaged single zone temperature 175

Figure 5.12 Experimental data for basic three SB ratio with different displacement volume (nIMEP 4.5 bar, 2000 RPM with the best efficiency operation) (a): burn duration from CA10 to CA90 (b): estimated heat transfer and work extraction during closed duration, normalized by relevant fuel LHV (c): fuel LHV breakdown 176

Figure 5.13 Experimental data for basic three SB ratio with different tumble ratio (fuel rate 14mg per cycle, 1500 RPM with the best efficiency operation) (a): estimated heat transfer during closed duration (b): estimated convective heat transfer coefficient (from single zone approach) (c): mass-averaged single zone temperature..... 179

Figure 5.14 Experimental data for basic three SB ratio with different tumble ratio (fuel rate 14 mg per cycle, 1500 RPM with the best efficiency operation) (a): initial flame speed from spark timing to CA10 (b): burn duration from CA10 to CA90 (c): estimated heat transfer and work extraction during closed duration (d): fuel LHV breakdown 180

Figure 5.15 Experimental data for basic three SB ratio with different tumble ratio (fuel rate 14mg per cycle, 2000 RPM with the best efficiency operation) (a): estimated heat transfer during closed duration (b): estimated convective heat transfer coefficient (from single zone approach) (c): mass-averaged single zone temperature..... 181

Figure 5.16 Experimental data for basic three SB ratio with different tumble ratio (fuel rate 14 mg per cycle, 2000 RPM with the best efficiency operation) (a): initial flame speed from spark timing to CA10 (b): burn duration from CA10 to CA90 (c): estimated heat transfer and work extraction during closed duration (d): fuel LHV breakdown 182

Figure 6.1 In-cylinder pressure data of four different SB ratio conditions (1500 RPM, 1 bar and 380 K with stoichiometric condition at IVC timing) – Simulation data..... 186

Figure 6.2 MFB and knock onset results of four different SB ratio conditions (1500 RPM, 1 bar and 380 K with stoichiometric condition at IVC timing) – Simulation data..... 186

Figure 6.3 Results of Livengood-Wu integration of four different SB ratio conditions (1500 RPM, 1 bar and 380 K with stoichiometric condition at IVC timing) – Simulation data 187

Figure 6.4 Burned mass fraction of 10000 individual cycles with fixed-operating condition with marked MAPO value, redrawn from [72] 195

Figure 6.5 Correlation between burn duration and in-cylinder pressure at knock onset timing of 10000 individual cycles, redrawn from [72] 195

Figure 6.6 Burned mass fraction of 5000 individual cycles with fixed-operating condition with marked MAPO value (a): SB 1.0, 1500 RPM with 34 mg of fuel rate per cycle (b): SB 1.0, 1500 RPM with 30 mg of fuel rate per cycle (c): SB 1.47, 1500 RPM with 34 mg of fuel rate per cycle (d): SB 1.0, 2000 RPM with 34 mg of fuel rate per cycle..... 196

Figure 6.7 Correlation between burn duration (from spark timing to CA70) and duration from spark timing to knock onset timing 197

Figure 6.8 Simulation data with different combustion phasing with knock onset mark (SB 1.0, 1500 RPM)..... 197

Figure 6.9 Simulation data from adiabatic process under the same knock criterion (SB 1.0, 1500RPM) 198

Figure 6.10 Experimental data for basic three SB ratio with different tumble ratio (fuel rate 26 mg per cycle, 2000 RPM with the best efficiency operation) (a): burn duration from CA10 to CA70 (b): CA50 combustion phasing (c): net indicated efficiency 199

Figure 6.11 Experimental data for basic three SB ratio with different tumble ratio (fuel rate 30 mg per cycle, 1500 RPM with the best efficiency operation) (a): burn duration from CA10 to CA70 (b): CA50 combustion phasing (c): gross indicated efficiency 200

Figure 6.12 Correlation between burn duration (from spark timing to CA70) and MAPO with averaging process for SB 1.0 and 1.47 conditions. (1500 RPM, fuel rate 26 mg per cycle, and ~35% of knock incidence) 204

Figure 6.13 Correlation between instantaneous volume at knock onset timing and MAPO with averaging process for SB 1.0 and 1.47 conditions (same as figure 6.13)..... 204

Figure 6.14 Correlation between unburned mass fraction and MAPO with averaging process for 1500 and 2000 RPM of SB 1.0 conditions with fuel rate 26 mg per cycle 205

Figure 6.15 Correlation between burn duration and MAPO with averaging process for SB 1.2 and 1.47 with 2000 RPM, fuel rate 34 mg per cycle 205

Figure 6.16 Configuration of flame propagation for SI engine operation with flame radius (R) and L value for the newly defined 'shape factor' 206

Figure 6.17 Correlation between 'shape factor' and unburned mass fraction with raw data of each individual cycle for SB 1.0, 1.2, and 1.47 conditions. 206

Figure 6.18 Incidence of moderate intensity of MAPO values for each MFB value for SB 1.0, 1.2, and 1.47 with 2000 RPM, fuel rate 34 mg per cycle, normalized by total number of knock cycle for each operating condition 210

Figure 6.19 Correlation between unburned mass fraction or fuel LHV remainder in unburned mass at knock onset timing and MAPO with averaging process for all knock experiments (a) unburned mass fraction and MAPO (b) fuel LHV remainder at knock onset timing and MAPO 211

Figure 6.20 Correlation between newly suggested $KI_{simulated}$ and MAPO with averaging process with 1st order curve fitted equation shown in the box..... 212

Nomenclature

A	area [m^2]
AHRR	accumulated heat release rate [J/cycle]
aTDC	after TDC [CA]
B	bore length [m]
BDC	bottom dead center
BMEP	brake mean effective pressure [bar]
bTDC	before TDC [CA]
CA	crank angle [deg]
CA10	crank angle at 10% of mass burned [CA aTDC]
CA50	crank angle at 50% of mass burned [CA aTDC]
CA70	crank angle at 70% of mass burned [CA aTDC]
CA90	crank angle at 90% of mass burned [CA aTDC]
CMPS	camshaft position sensor
c_p	specific heat with isobaric process (constant pressure) [J/kgK]
CR	compression ratio
c_v	specific heat with isochoric process (constant volume) [J/kgK]
CVVT	continuous various valve timing
DBL	detonation border line
DISI	direct-injected spark ignition
EGR	exhaust gas recirculation
EIVC	early intake valve closing
EV	electric vehicle
EVC	exhaust valve closing timing [CA]
EVO	exhaust valve opening timing [CA]
ExCAM	exhaust camshaft timing [CA]

f	frequency [Hz]
GIE	gross indicated efficiency
gIMEP	gross indicated mean effective pressure
H	convective heat transfer coefficient [W/m^2K]
h	intensive enthalpy [J/kg]
H/C	the ratio of hydrogen atom to carbon atom in specific fuel
HEV	hybrid electric vehicle
HRR	net heat release rate [J/deg]
ICE	internal combustion engine
ICEV	internal combustion engine vehicle
IMEP	indicated mean effective pressure [bar]
InCAM	intake camshaft timing [CA]
IVC	intake valve closing timing [CA]
IVO	intake valve opening timing [CA]
KL-CA50	CA50 timing at knock-limited operation [CA aTDC]
KLSA	knock limited spark advance [CA aTDC]
LCA	life cycle analysis
LHV	lower heating value [J/kg]
LIVC	late intake valve closing
m	mass [kg/cycle]
MAPO	maximum amplitude of pressure oscillation
MFB	mass fraction of burned mixture
MW	mean molecular weight [kg/kmol]
N	cycle number
NIE	net indicated efficiency
nIMEP	net indicated mean effective pressure [bar]
NOx	nitrogen oxides emissions

OF	overlap factor
P	pressure [pa], unless noted
PFI	intake port fuel injection type
PHEV	plug-in hybrid electric vehicle
PMEP	pumping mean effective pressure [bar]
PRF	primary reference fuel
PRF 91.5	Fuel with 91.5 % of iso-ocatne and 8.5 % of n-heptane, volume
Q	heat [J/cycle]
R	gas constant [J/kgK]
RCM	rapid compression machine
RMF	residual mass fraction [%]
RMSE	root mean square error
RPM	revolution (rotation) per minute
S	stroke [m]
SB ratio	stroke-to-bore ratio
SI	spark ignition
SOI	start of injection [CA aTDC]
SV ratio	surface-to-volume ratio
T	temperature [K]
t	time [sec]
TDC	top dead center
THC	unburned hydrocarbon emissions
U	extensive internal energy [J]
u	intensive internal energy [J/kg]
UHC	unburned hydrocarbon emissions
V	volume [m^3]
x	Mole fraction

y	Mass fraction

Subscript

B	burned
cycle	per cycle
cool	cooling loss
e	exhaust
filt	filtered signal
gross	gross indicated parameters
i	intake
incomplete	incomplete combustion loss
pump	pumping loss
ref	reference state
sens	sensible term
u	unburned

Greek Letters

γ	specific heat ratio [-]
η	efficiency [-]
θ	crank angle [deg]
τ	ignition delay [ms]
ϕ	equivalence ratio [-]

Chapter 1. Introductions

1.1 Backgrounds

After the Industrial Revolution from 18th century, it has been necessarily required to satisfy enormous amount of energy demand corresponding to the development of technology for mankind. The chemical energy inside petroleum, in the form of complicate chemical bonds, has been a major source of the demand up to now, while several approaches called 'renewable energy' (e.g. solar energy) have been not only investigated but also conducted to overcome the deficit from petroleum-based power generation such as emission issues. According to the demand, transportation has considerable portion, up to 29% at 2017 [1], which implies that the deficit related to petroleum-based energy conversion will be significantly generated by transportation portion. Thus, it is not surprising to apply a strict regulation on both fuel economy and emissions from transportation market, especially for internal combustion engine, in order to reduce the CO_2 emissions, related to from fuel economy (microscopic viewpoint) to global warming issues (macroscopic viewpoint), and other emissions such as PM, NOx. Therefore, two things should be briefly reviewed – fundamentals of internal combustion engine and the up-to-date regulations applied to transportation market – to understand the up-to-date situation related to the development of internal combustion engine and the motivation of this work for the purpose of overcoming those issues suggested in this chapter.

For the regulation issues, the strong regulations on both fuel economy and emissions have been proposed to internal combustion engine, both gasoline SI and diesel CI engine, which are typical types of internal combustion engine for transportation market. Since an internal combustion engine is mainly operated by

usage of petroleum-based hydrocarbon such as gasoline and diesel, CO_2 emissions are inevitably emitted no matter how state-of-the-art combustion strategies are applied. As related to this issue, many of countries made several regulations to restrict fuel economy of ICEV as shown in figure 1.1 – for USA, Corporate Average Fuel Economy (CAFE) was suggested, which contains the target of fuel economy as 54.5 mpg (mile per gallon) at 2025, compared to 40 mpg for the average value at 2017, as directly related to the improvement of CO_2 emissions [2] . In the case of Europe, ultimately 59 g/km of CO2 emission is set as a target for 2030, which is less than half of the current (2015) averaged-value – 130 g/km [3]. For China, which has the largest population in the world, graduated plan with CAFC (Corporate Actual Annual Fuel Consumption) value was proposed where the phase 3 and 4 included target CAFC value from 7.5 L per 100 km to 5.0 L per 100 km, corresponding to 2012 and 2020 target values [4]. Considering these details of regulations for each country, it is certain that ICEV now meets severe challenges to satisfy those strong regulations and it is why several substitutes, such as electric vehicle (EV) and fuel cell electric vehicle (FCEV), have been proposed, since they do not emit such emissions directly from their tailpipe (FCEV) or even have no tailpipe (EV). Here, it should be noted that all the processes of power generation for transportation devices, which are operated by hydrocarbon fuel directly (e.g. internal combustion engine) and indirectly (e.g. fuel cell, electric vehicle), inevitably produce CO_2 emissions so that they cannot be free from the argument related to CO_2 emissions – the only difference in CO_2 emissions is whether it comes directly or not. For example, in the case of an internal combustion engine, CO_2 emissions from power generation process (i.e. combustion inside cylinder) are emitted from tailpipe[1]. Instead, in the case of battery or fuel cell electric vehicle, most of CO_2 emissions are produced from the generation process of electricity at power plant or secondary fuel (e.g. hydrogen)

[1] In fact, CO_2 is also produced from the life cycle of fuel from its well-to-wheel process, based on the concept of life cycle analysis (LCA).

from reforming process, respectively. Therefore, it should be discussed from the viewpoint of the whole process including not only power generation itself but also the source of the power generation, also known as well-to-wheel emissions based on the life cycle analysis [5-9]. Based on the result from the reference [5], several issues should be noted – depending on which fuel is used for electric power generation, electric vehicles can even show more Greenhouse gas emissions (GHG), i.e. CO_2, than conventional internal combustion engine vehicles; for the detail, shown in figure 1.2 which was redrawn from [5], about 200 g-CO_2-eq/km of GHG emissions was produced from EV with only coal power generation case, while 216 g-CO_2-eq/km for pure gasoline-based ICEV, 160 g-CO_2-eq/km for gasoline HEV, and 142 g-CO_2-eq/km for gasoline PHEV. These were attributed by comparable amount of GHG emissions of power generation process for EV operation with that of vehicle operation for typical ICEV operation. Although another choice of fuel as a source of electricity for EV can change this trend, one thing can be clearly concluded that GHG emissions are not so different for each operating scheme in the viewpoint of whole process.

Another thing which should be noted is that due to the characteristics of fast reaction from combustion process which is hardly controlled, critical emissions such as NOx, UHC, and PM are also emitted, which is possibly able to be reduced for other power generation process such as fuel cell operation fueled by hydrocarbon-reformed hydrogen. For instance, related to Europe, about 68% reduction of NOx emissions is required to meet the latest EURO 6 regulation compared to EURO 4 regulation, where the target values are 80 mg/km and 250 mg/km for each regulation, respectively. In the case of PM, about 82% reduction is required, where the target values are 4.5 mg/km and 25 mg/km, respectively. For USA case, As mentioned, since these regulations were particularly set to ICEV, several developments related to reduction in emissions should be conducted to meet the latest regulations successfully.

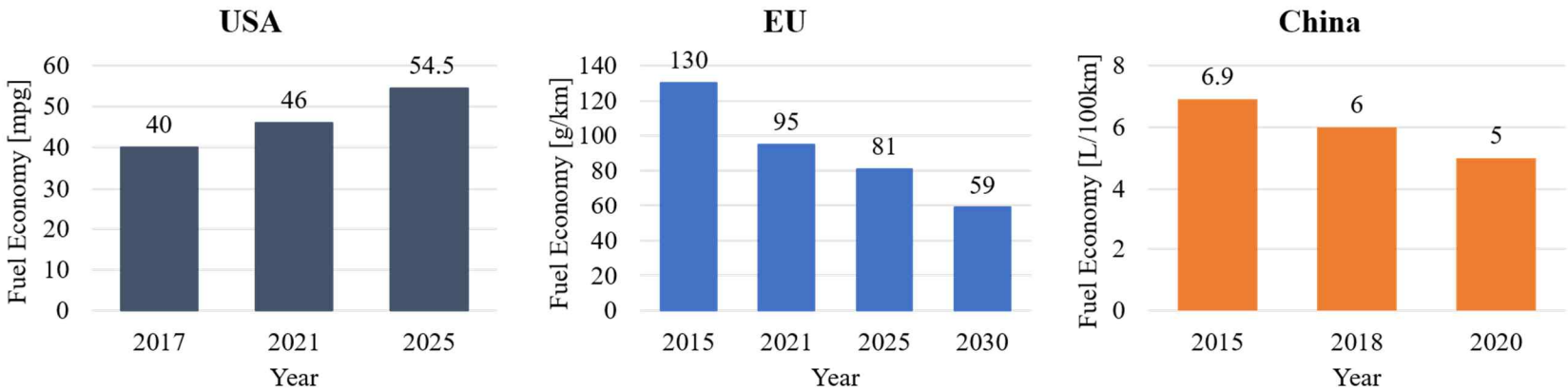

Figure 1.1 CO_2 regulations for several countries

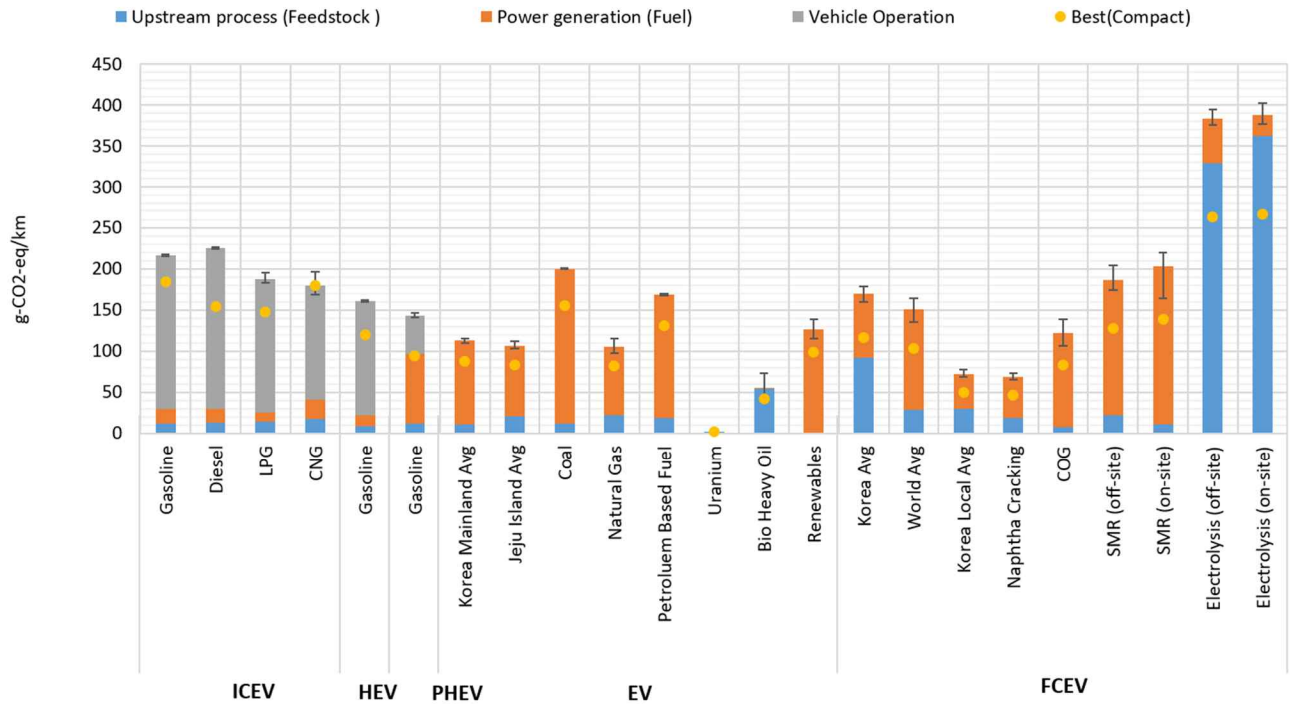

Figure 1.2 CO_2 emissions from several powertrain devices with different fuel conditions (redrawn from [5])

An internal combustion engine is a typical medium- or small-size heat engine that converts the chemical energy of fuel into mechanical energy through a combustion reaction in a closed system (i.e., a cylinder). In the case of the commonly used spark ignition (SI) engine, fuel and air are mixed in a stoichiometric composition. At the end of the compression, a spark plug mounted in the combustion chamber starts combustion by spark ignition. The combustion in the engine proceeds while spreading for a certain period. Effective combustion can be conducted by minimizing the heat rejection, mechanical friction, and exhaust gas loss, where the relevant equation was listed below.

enthalpy of the inlet mixture formation (mainly fuel lower heating value (LHV)) + sensible enthalpy of the inlet mixture =
pumping work + gross work + sensible enthalpy in exhaust gas + enthalpy of formation in exhaust gas + cooling loss + engine blow-by[2]

To maximize the conversion from energy input factors on the left side to mechanical work, the remaining terms of the right side should be reduced. Therefore, further discussion related to these terms is required. (It is assumed that the quantity of engine blow-by is too low to be ignored within the range currently discussed.)

In the case of a work term, pumping work and gross work separately exist. In general, combustion of the fuel in one cycle creates work by expanding the piston during an expansion stroke. Therefore, it contributes to the gross work term. The pumping work is required to bring air and fuel into the combustion chamber at the gas exchange period (i.e., from EVO to IVC). The sum of these two terms is the net indicated work. Therefore, even if the same amount of fuel is injected and the same gross work is produced by proper combustion, the net indicated

[2] Corresponding contents were also mentioned in chapter 2.1.3, except for engine blow-by which was assumed to be too small to affect the experimental results in this study.

efficiency could be different when there is a difference in the pumping work. This difference is due to external factors, such as the engine geometry (e.g., valve diameter, manifold design, piston motion). In the case of the SI engine, the amount of air is controlled by a throttling process in the naturally aspirated, part-load region. In this process, the pumping loss is dominant compared with other combustion regimes because the intake air pressure is lower than the exhaust pressure.

In the case of sensible enthalpy in exhaust gas, also known as "exhaust loss," the main factors are the peak temperature determined by the combustion duration and mixture composition, combustion phasing, engine expansion ratio, and exhaust valve timing. As some of the chemical energy of fuel is destined to be converted into heat (as in the definition of "heat engine"), exhaust loss is similar to cooling loss. However, since the amount of heat inside the cooling loss is completely dissipated from the mixture to the outside, it is almost impossible to produce work using a general concept of the heat engine. On the other hand, in the case of exhaust loss, the heat is inside the exhaust mixture in the form of sensible enthalpy with a relatively high temperature. Therefore, heat recovery can be conducted to obtain more work from the exhaust loss. In fact, many studies to date have examined these issues [10-13], which were related to using organic Rankine cycle to recover certain amount of wasted heat included in engine exhaust gas.

In the case of enthalpy of formation in the exhaust gas, also known as "incomplete combustion loss," many factors—such as the thermal boundary thickness, operation load, and crevice volume—can affect this term. However, its absolute value is relatively small (approximately 5%) compared to other terms. In the case of a normal SI engine, the stoichiometric composition needed to achieve

proper flame propagation in the SI engine makes it easy to drive the remainder of the reaction through the three-way catalyst.

Meanwhile, the primary means of cooling loss (heat rejection), which mainly occurs after the ignition timing, is the convective heat transfer between the mixture and the combustion chamber components: the cylinder head, intake and exhaust valve, piston top surface, and cylinder liner. It should be noted that the radiation heat transfer mode also occurs. However, since the ranges of temperature and injection pressure of a direct injection spark ignition (DISI) engine used in this study are not adequately high to generate soot emission—the main source of radiation heat transfer—it is ignored. As mentioned above, it is pure loss; to achieve efficient operation, it should be firstly reduced. Accordingly, many topics, such as low heat rejection by actual combustion chamber coating [14] and improved combustion strategies [15], have been actively researched.

The summary of aforementioned issues with additional approach based on 2nd law of thermodynamics was shown in figure 1.3, redrawn from the reference [16]. According to this, several parameters related to real vehicle driving were also included in this figure such as friction and accessory work. In this article, important issue was highlighted, mentioned as "IC engines are not Carnot heat engines and therefore are not limited by Carnot efficiency" [16], because it is basically open cycle that fresh reactant gas (fuel and air mixture[3]) and product gas are exchanged during exhaust and intake stroke, which does not occur in conventional closed heat engine cycle (e.g. steam turbine). Thus, as mentioned in the reference [16], the maximum theoretical efficiency of internal combustion engine is 100%, whereas several issues related to real operation (mentioned as "practical efficiency limits" in the reference) mainly affects the total engine

[3] Allocated exhaust gas, called external exhaust gas recirculation (EGR), can be also included.

efficiency such as friction and cooling loss. The details of this issue will be reviewed in the next chapter with other reference [17].

Aforementioned contents are the fundamentals for general internal combustion engine with all the types of combustion regimes such as SI and CI engines. Instead, as focusing on an SI engine operation, which is the main issue in this study, abnormal combustion called 'knock' can be also a main issue that affects thermal efficiency. Knock is defined as a ringing sound occurring inside the cylinder induced by autoignition of hot spot in the unburned zone with severe intensity. Normally, it occurs when the flame propagation induced by spark ignition does not reach certain hot spot of which temperature and pressure are high enough to be autoignited[4] – and if the autoignition is too strong to induce certain amount of pressure wave (i.e. non-equilibrium pressure field inside the cylinder, thus pressure oscillation), the pressure wave starts to oscillate, resulting in very specific sound like 'knock' with destruction of thermal boundary layer inside a cylinder. If this continues with certain time duration (~ 10 min), several parts of engine cylinder such as piston, piston ring, and liner can be damaged, causing serious problem for SI engine operation. In general, knock is a main constraint of limiting engine efficiency for high load operation, because the thresholds of temperature and pressure to be autoignited are considerably high. Therefore, along with several parameters directly related to engine efficiency (e.g. cooling loss), knock should be also considered as a main parameter to determine SI engine efficiency.

[4] Noted that pre-ignition, which occurs before the start of turbulent based flame propagation, is also considered as knock, while it is not the scope of this work.

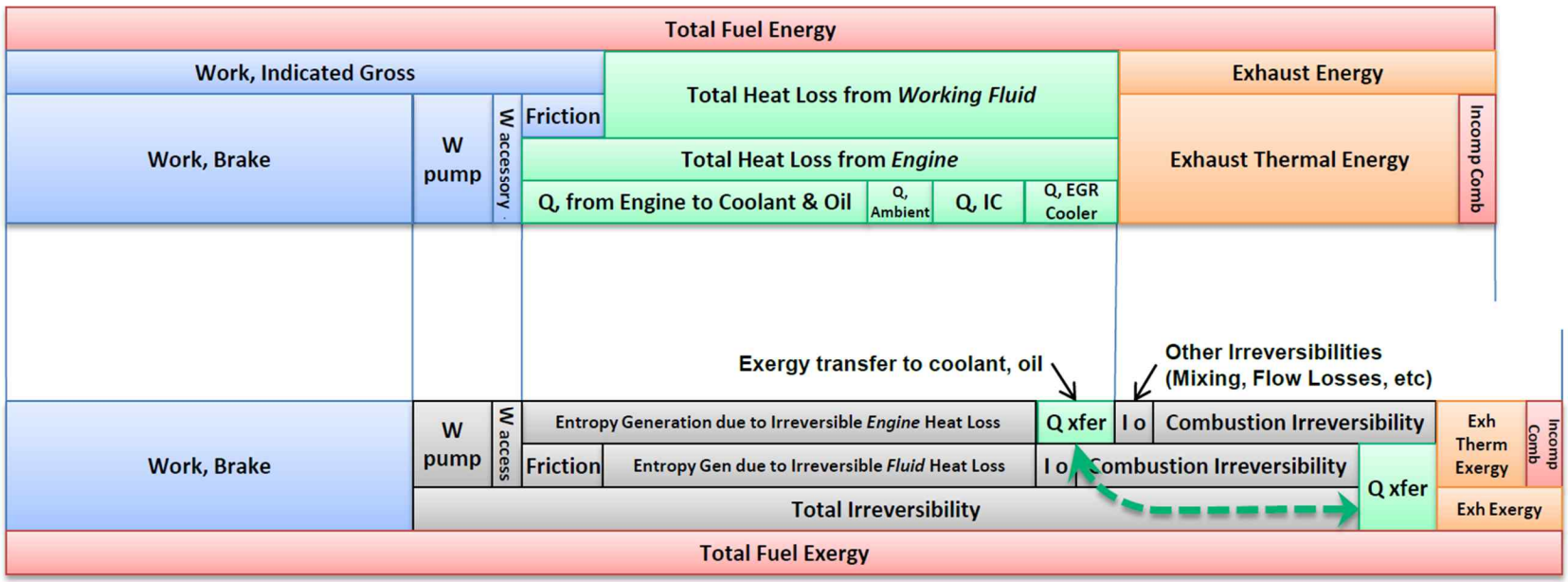

Figure 1.3 Energy (1st law) and exergy (2nd law) analysis of general engine operation (redrawn from [16])

1.2 Literature Review

Considering several issues related to engine efficiency and performance as mentioned in previous chapter, the state-of-the-art researches and developments from not only academia but also various OEM have been conducted. Here, firstly, the fundamentals of investigations of SI engine were reviewed. After that, several studies related to the motivation and main purpose of this work were reviewed.

1.2.1 Fundamentals of SI engine operation - review

According to the several studies [16, 17], several approaches related to the increment in engine efficiency were suggested. While these were mainly related to the fundamental aspects with macroscopic viewpoint, it can be postulated that the details of the future investigations for SI engine should be based on the contents mentioned in the references.

Firstly, Caton et al. suggested the way of engine operation with high efficiency by several schemes as listed below [17].

1) Increasing compression ratio of an engine

2) Lean burn operation (i.e. equivalence ratio under unity)

3) External exhaust gas recirculation

4) Faster burning rate

It should be noted that each term is related to the ideal cycle for general internal combustion engine such as Otto cycle (constant-volume cycle) [18]. The equations of total efficiency for Otto cycle were listed in eq. 5.1.

$$\eta_{Otto} = 1 - \frac{1}{CR^{\gamma-1}} \qquad \text{eq. 1.1}$$

Here, it is clearly shown that increment in both compression ratio (and also expansion ratio) and constant value of specific heat ratio can increase the total efficiency of Otto cycle, which is directly related to the first, second, and third term. In addition, since Otto cycle is assumed to be operated with instantaneous heat addition (corresponding to chemical reaction for converting chemical energy into sensible energy in real engine) at TDC timing, fast burning rate is required to make a real operation similar to ideal case, which is related to the fourth term. In the reference, the simulation process with the operating condition relevant to real engine operation (2000 RPM with 9 bar of BMEP) was conducted to quantitatively evaluate the effect of each term for increasing engine efficiency. According to this, it was figured out that increasing compression ratio is found to have the highest effect on the increment in engine efficiency, followed by lean burn operation, EGR addition, and fast burn duration. Two things related to the results should be noted; first, abnormal combustion such as knock which can occur in higher compression ratio was not considered in this approach. Second, expansion ratio was considered as same value with compression ratio, which implies that the effect of increment in compression ratio is also related to that of expansion ratio[5]. Although the approach was conducted with simulation process, the direction of engine development for better efficiency can be signposted by this work, with a macroscopic point of view.

In addition, Dean et al. suggested more practical issues related to the engine efficiency from a point of 1st and 2nd law of thermodynamics of which contents

[5] The details of this, especially for different expansion and compression ratio, was reviewed in chapter 1.2.2, in terms of valve timing variation strategies.

were briefly mentioned in the previous chapter [16]. In addition to the several terms, such as cooling loss, directly related to engine efficiency, fuel characteristics and complicate association between the efficiency-related terms were investigated in the reference. First of all, fuel should be carefully selected in order to minimize the irreversibility (exergy destruction) generated during combustion process. In general, lower irreversibility during combustion process was generated for fuels which have simple structure such as hydrogen and methane, as mentioned in the reference. However, it should be noted that such fuels are normally not directly extracted from nature, rather generated by certain reforming process such as steam reforming or partial oxidation reforming. Therefore, it should be considered that during those reforming processes, certain amount of exergy destruction was inevitably generated [19] so that the whole process needed to use simple fuel for internal combustion engine should be understood with life cycle of fuel usage. Second, complicate linkage between efficiency-related terms were reviewed in the reference, such as relation between reduction in cooling loss and exhaust heat loss. That is, specific heat ratio is decreased as increment in temperature (and pressure) by reducing cooling loss, which can cause higher remainder of sensible energy at exhaust stroke with little gain in piston work. According to this, Dean et al. mentioned that “reduction of one loss term tends to result in an increase of another”. Therefore, several strategies related to engine efficiency should be investigated carefully prior to its application.

Finally, in recent times, comprehensive investigations have been conducted to match engine characteristics with those of fuel to obtain synergy related to tailored fuel-engine operation [20, 21]. With these approaches, aimed are enhancing knock resistance and reducing emissions for contemporary SI engine of which details were reviewed in chapter 1.2.3.

1.2.2 Valve timing variation in SI engine

As mentioned before, compression and expansion ratios are very important factors for engine efficiency. However, it should be noted that the most part of 'positive' work extraction is produced during expansion stroke, where compression work has negative value. That is, the amount of compression is only needed to make the temperature and pressure of reactant mixture to be increased for suitable combustion process. Thus, it can be postulated that the actual effect of nominal compression ratio on engine efficiency is attributed by corresponding expansion ratio. As regard to this, several strategies have been conducted to differentiate compression and expansion ratio by adjusting intake and exhaust valve timing, especially for IVC and EVO timing. Since EVO timing is inevitably confined because of expansion work extraction, these studies were mainly related to late intake valve closing (LIVC) and early intake valve closing (EIVC) strategies focusing on improving the pumping loss of SI engine and the mitigation of knocking phenomena by making a difference between the compression and expansion ratio [22-25]. Li Tie et al. conducted an experimental comparison between LIVC and EIVC operation [22]. Based on the results of this study, improvements in brake specific fuel consumption of 6.8% and 7.5% for LIVC and EIVC operation, respectively, were attained, mainly owing to the reduction of pumping loss. In addition, at high load operation, LIVC (CR 12) was improved by about 4.7% compared to the conventional production engine (CR 9.3), where EIVC could not make such improvement. In addition, from the point of knock resistance, LIVC was more effective at high-load operation. Zheng Bin et al. conducted a subsequent study developed from the above study [24]. From this study, it was found that LIVC operation at high load has the effect of reducing the fuel consumption rate owing to better combustion characteristics, which were

attributed to the high turbulence intensity as compared with that of EIVC operation.

Luisi et al. investigated the effects of the knock mitigation of LIVC and EIVC operation [23]. They suggested that in the case of EIVC, any flow source that can compensate the viscosity loss was not added into the cylinder in the EIVC-BDC duration, which eventually led to a substantial amount of turbulent kinetic energy dissipation. Moreover, a certain amount of temperature decreased owing to the expansion after EIVC, which led to an adverse effect on the vaporization of the direct-injected fuel mixture. Soderberg et al. investigated the combustion stability of LIVC and EIVC operation [25]. From the experimental results, it was shown that EIVC operation makes CA00–CA10 longer than that of a throttled conventional operation, although it results in a faster burning rate. This circumstance was attributed to the low lift of the EIVC operation, as investigated. The low lift caused more shearing flow, which resulted in the fuel droplets breaking apart. Moreover, unlike in previous literature, the experimental data showed that the combustion stability of EIVC operation is higher than that of LIVC. Although improvements in pumping loss from both LIVC and EIVC operations were reported in every previous literature, from the point of combustion characteristics, there were still various results. However, it can be postulated that the split of valve timing, especially for IVC timing, to differentiate compression and expansion ratio is a proper way to increase engine efficiency by reducing pumping loss and enhancing knock behavior as mentioned above. In this work, used was LIVC operation with dual CVVT camshaft for both intake and exhaust valve of which details were introduced in chapter 3.

1.2.3 Engine knock in SI engine

As mentioned before, knock is induced by strong autoignition at the unburned gas zone of which types can be classified as three modes: deflagration, thermal explosion, or developing detonation [26]. From the numerical studies, König et al. [27] identified these modes and showed that auto-ignition of the hot-spot can lead to pressure spikes. Knock occurrence in spark-ignited engine must be avoided during operation because it can cause serious engine failure and damage [28, 29].

The fundamentals of knock phenomena were comprehensively investigated by several studies [30, 31] . In these works, criteria that defines the cause and intensity of knock from certain autoignition were investigated. First, from Yelvington et al., knock phenomena for high load operation of HCCI engine were investigated. Here, it was proposed that locally high pressure induced by fast heat release from the autoignition of hot spot can induce non-equilibrium of pressure (mentioned as "local overpressures" in the reference) between hot spot and other mixture which results in pressure oscillation if the rate of heat release by autoignition exceeds certain level, where the related equations were listed below [18, 30].

$$\frac{dP}{dt} = -\frac{\gamma P}{V}\frac{dV}{dt} + \frac{\gamma - 1}{V}\frac{dQ_{ch}}{dt} \qquad \text{eq. 1.2}$$

$$\dot{q} = \frac{1}{V}\frac{dQ_{ch}}{dt} \qquad \text{eq. 1.3}$$

$$\beta = \frac{V}{A}\frac{(\gamma - 1)}{\gamma P}\frac{\dot{q}}{a} \qquad \text{eq. 1.4}$$

Here, $\dot{q}$ is a volumetric heat release rate (heat release rate normalized by control volume), and all the parameters including V (volume) and A (area) were relevant to hot spot where an autoignition occurs. It should be noted that the value for the determination of knock phenomena (β) was obtained by dividing first term of RHS (mentioned as "rate work down by volume expansion" in the reference) by second term of RHS (mentioned as "rate of chemical heat release" in the reference), as qualitatively described before. Yelvington et al. proposed that if the β value is lower than unity, knock would not be expected. Despite the difference in operating conditions between the reference and many of SI engine-related study (e.g. air-fuel ratio), it can be postulated that the knock phenomena can be described as a competition between local heat release and volume expansion rate of hot spot which is autoignited, based on the notion from the reference.

As related to the reference, Bradley et al. classified the several modes of knock occurrence with using two parameters – ξ and ε, where the definitions for each term was listed below, respectively [32].

$$\xi = \frac{a}{u_a} \qquad \text{eq. 1.5}$$

$$\varepsilon = \left(\frac{r_0}{a}\right) / \tau_e \qquad \text{eq. 1.6}$$

Here, u_a means the rate of propagation of autoignition from hot spot, r_0 means the assumed radius of hot spot, and τ_e is the excitation time for energy release by autoignition. Based on the meaning of each term, ξ represents the competition between autoignition propagation speed and sound speed, and ε

represents the hot spot reactivity – the competition between the time for the acoustic waves to remain and the time for heat release from autoignition to maintain. For example, considering ξ value with split into numerator (sound speed) and denominator (autoignition propagation speed), qualitative explanation can be introduced as listed below.

1) Autoignition propagation speed $\ll$ sound speed ($\xi \gg 1$)
   : Pressure equilibrium can be conducted easily attributed by dominant sound speed compared to the rate of autoignition from hot spot (deflagration)

2) Autoignition propagation speed $\cong$ sound speed ($\xi \sim 1$)
   : Unique "resonance" between the propagation of autoignition and shock wave occurs. Because of this, the pressure and, resultantly, temperature of mixture near the hot spot increases, which can also enhance the shock wave and same pattern continues like 'resonance'. Therefore, it results in severe knock intensity (detonation).

3) Autoignition propagation speed $\gg$ sound speed ($\xi \ll 1$)
   : Regardless of the size of initial hot spot or sound speed, almost instantaneous autoignition occurs (thermal explosion).

Considering these, suggested was the specific region of ξ and ε, related to the severe knock intensity autoignition, which was called 'detonation peninsula' as shown in figure 1.4 redrawn from the reference [32]. Therefore, usual SI engine should be operated without encountering such region to prevent severe knock damage as mentioned later.

Furthermore, Kalghatgi et al. suggested knock index of relevant fuel and engine operating conditions [33], where the details of the index were listed below.

$$OI = (1 - K)\,(RON) + K\,(MON) \qquad \text{eq. 1.7}$$

Here, OI is octane index "which describes the anti-knock quality" of relevant fuel [33], RON and MON are research octane number and motor octane number for relevant fuel which is derived by CFR engine operation as a standard of fuel's anti-knock quality [18]. It should be noted that OI can be suggested as a replacement of RON and MON, because those octane number values were obtained by CFR engine operation which is not proper for contemporary SI engine operation. In order to determine OI value, K has to be assigned, which can be a representative of engine operating conditions such as rotational speed and compression ratio, by conducting knock-limited experiment to find KLSA [33].

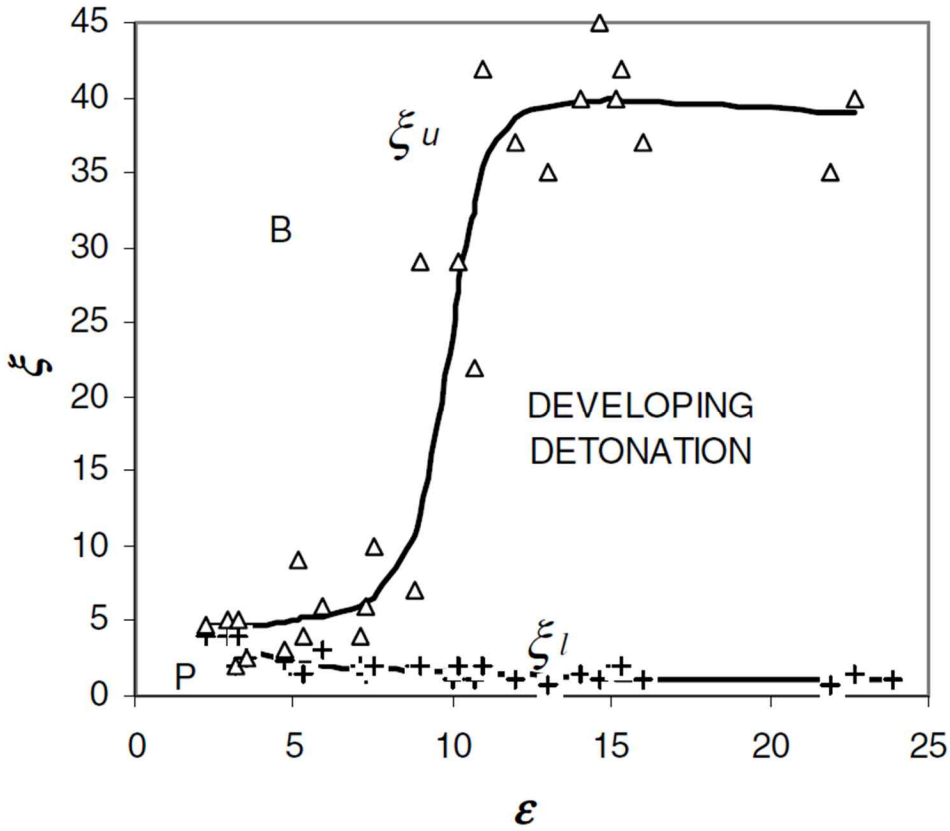

Figure 1.4 Characterization of autoignition with ξ and ε values to characterize the knock phenomena, redrawn from [32], fueled by 50% of H_2 and 50% of CO.

According to this, introduced are practical and fundamental methods to reduce knock occurrence. One is the enhancement of flame speed during the combustion process to reduce the time for hot spot in unburned gas to be autoignited. That is, under the enhanced flame speed, the air-fuel mixture in the unburned end-gas area can be consumed before the in-cylinder condition reaches the auto-ignition point. Use of advanced ignition systems not only can increase the efficiency but also has an effect of knock suppression [34-36]. Introducing a high-tumble port design is also one of the most effective ways to produce fast combustion, which can produce higher turbulent intensity to increase flame speed [37-40].

Another method of improvement uses an EGR system. EGR is a very promising method for knock mitigation that reduces the in-cylinder temperature and reactivity of unburned end-gas [41-43]. Several approaches from OEM companies were conducted to put a great deal of effort into EGR systems because of its potential. Matsuo et al. improved the manifold design to enhance the EGR distribution of each cylinder [44]. Cooled EGR [34] and improved EGR cooling units [43] have recently been adapted to mass production engines. According to this, EGR strategy, especially for knock mitigation, is comprehensively reviewed in the reference [45].

Asif et al. investigated the effect of coolant on KLSA using a multi-cylinder DISI engine with dual CVVT (continuous variable valve timing) system [46]. They showed in their recent study that the temperature between the exhaust valve bridge decreases by only 1 °C, while the coolant flow decreases by 20%. KLSA was not significantly affected by the reduction of the flow. Moreover, they observed KLSA was retarded from approximately 0.5 CA to 1 CA while the coolant temperature increased from 90 °C to 100 °C. They explained this variation

cannot be considered a significant change in the paper. An overview and the principle of knock is comprehensively reviewed in the study [47].

1.2.4 Flame speed in SI engine

As mentioned in the previous chapter, enhancement in flame propagation speed is generally required to increase anti-knock quality for SI engine operation. Recently, however, several studies proposed the opposite trend of flame speed in terms of its anti-knock quality [48-52], where the corresponding issue can be summarized as followed; "Does a faster burning rate always increase knock resistance for SI engine operation?" Related to this, many of studies were conducted to verify the effect of enhancing flame propagation speed by several ways such as additive (e.g. hydrogen) [52], and enhanced turbulent intensity [50]. First of all, Yu Chen et al. studied the influence of burning rate on knock by using both simulations and experiments [51]. By applying newly developed method called SWE (sine wave estimation) to smooth the pressure oscillation caused by knock occurrence for a pressure profile of each individual cycle, it can be concluded in the reference that the cycles with knock occurrence showed shorter burn duration (defined as the duration from spark timing to CA70) and higher pressure rise rate (defined as $\Delta P/\Delta\theta$). In order to supplement the experimental data, they conducted simulations with MACZ (multi-step adiabatic constant-volume zero-dimensional) model with Cantera software [53], which is also used in this study, showing good agreement with the experimental results, by presenting a meaningful equation quoted below [51].

$$\theta_{auto\ knock} = 1.16 \times MFB_{0-70\%} - 29 \qquad \text{eq. 1.8}$$

Here, $\theta_{auto\ knock}$ means the crank angle with the onset of autoignition (CA aTDC), and $MFB_{0-70\%}$ means the duration from spark timing to 70% of mass fraction burned timing. It should be noted that if the slope is less than unity, fast burn can diminish knock occurrence by its meaning, provided that advanced knock onset timing causes severe intensity of knock occurrence. However, as shown in eq. 1.8, the value of slope exceeds unity. Thus, it can be postulated that fast burn operation can cause more severe knock occurrence, where the data supplementing these trends indirectly were shown in figure 1.5 redrawn from the reference [51]. Here, blue circles and green triangles are non-knock and knock cycles, respectively. From this figure, in can be concluded that the individual cycles with knock occurrence showed higher pressure rise rate than non-knock cycles, with shorter burn duration.

Lin Chen et al. investigated the effect of turbulent intensity on knock intensity with using 3D CFD simulations [50]. They conducted simulations with different combustion phasing by adjusting initial swirl ratio to facilitate turbulent intensity. Here, it was found that under low degree of swirl ratio, the more turbulent intensity (by enhancing swirl ratio), the harsher knock occurrence due to the additional compression effect on unburned mixture by faster turbulent flame propagation. Instead, under high degree of swirl ratio, usual suspect happens – that is, the effect of enhanced turbulent flame speed can induce faster consumption of unburned mixture, resulting in reduction in knock intensity by lower unburned mass fraction at knock onset timing. Therefore, from the reference [50], it can be postulated that even if the same engine setup is used, different operating strategies (i.e. flow dynamics) can cause the opposite trends for knock intensity.

Hao Yu et al. suggested the relationship between knock intensity and important parameters – burning rate, unburned mass fraction, and volume at autoignition onset timing by conducting 1D flame propagation simulation with

detailed chemistry for simple and specific calculation of both laminar flame speed and autoignition of two fuels – hydrogen and iso-octane [49]. Here, important issues were mentioned that the occurrence of maximum pressure by autoignition showed opposite trends, depending on the range of burned mass fraction as classified into “regime I” and “regime II” in the reference. First, with moderately larget unburned mass fraction at autoignition onset timing, the maximum value of pressure induced by autoignition was increased as burning rate increased and/or the volume of unburned zone at autoignition onset timing decreased (called “regime I” in the reference). On the other hand, with lower unburned mass fraction at autoignition onset timing, usual suspect happened – enhanced flame speed caused lower value of the maximum pressure induced by autoignition. Thus, from the reference, it can be postulated that enhancement in flame speed should be considered as a promising strategy of knock mitigation only for the case of certain amount of unburned mass remaining in cylinder. It should be noted that this will be comprehensively reviewed with experimental data in chapter 6.

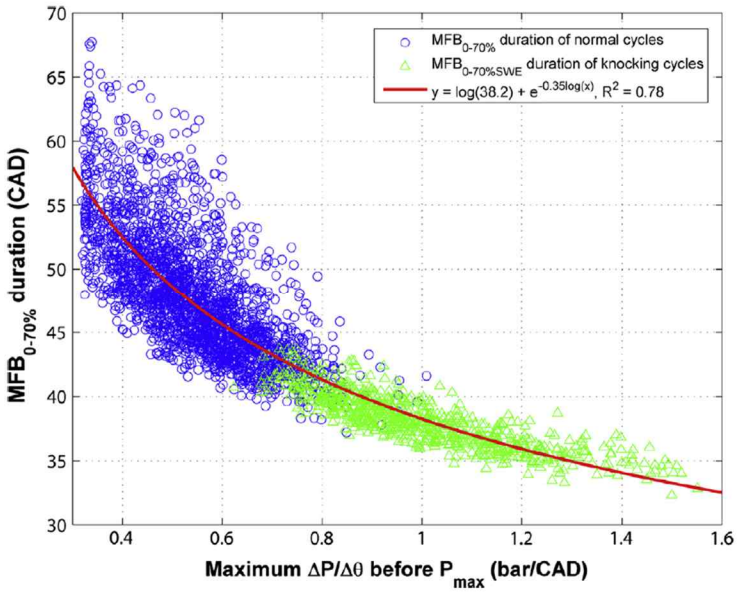

Figure 1.5 Correlation between pressure rise rate and burn duration with knock cycles (expressed as green triangle with 'knocking cycle') and non-knock cycles (expressed as blue circle with 'normal cycle'), redrawn from [51]

1.2.5 Stroke-to-bore ratio

Aforementioned issues are highly related to the strategies for engine operation to obtain higher efficiency. However, all the engines have specific design for their purposes. Valve set angle, for example, was designed to maximize the tumble motion inside a cylinder which can make higher turbulent intensity during compression and combustion process [37]. Furthermore, piston shape, for example, can be designed differently to enhance knock resistance of SI engine operation [54]. However, more important issue can arise with summarized as a following question; "in which 'geometries' should these strategies be applied?" In fact, there are many parameters that are important for engine geometries such as displacement volume, compression (and also expansion) ratio, bore and stroke length, and connecting rod length. Since the up-to-date trend of SI engine design has been set to downsizing with higher compression ratio [18], former two parameters – displacement volume and compression ratio are supposed to set in this study. In addition, connecting rod length is also usually set by relevant stroke, displacement volume, and compression ratio to adjust clearance volume, which is related to the real engine size (normally total height)[6]. While, how about stroke and bore length? With general notion, in fact, all the parameters and operation strategies mentioned earlier such as cooling loss, flame speed, knock phenomena are deeply related to the stroke-to-bore ratio (SB ratio) [18]. For example, considering general notion, increment in SB ratio results in reduced surface-to-volume ratio (SV ratio) at firing TDC timing at which the most part of heat transfer is generated. Thus, one can expect that cooling loss can be reduced by increasing SB ratio [55-58]. In addition, turbulent flame speed also should be mentioned

[6] This will be mentioned as 'packaging constraint' in the following chapters.

because it is highly related to SB ratio. That is, with longer stroke, flow dynamics inside cylinder are enhanced, attributed by fast piston movement. Therefore, one can expect that the turbulent intensity, which is directly related to turbulent flame speed [55, 59]. Therefore, the most important mention in this study can be postulated that SB ratio is directly, and importantly related to many of parameters which is favorably associated with engine efficiency as mentioned earlier.

There are a number of both experimental and computational studies on the stroke-to-bore ratio (SB ratio) of the engine. Filipi et al. analyzed the effects of three different ratios (0.7, 1.0, and 1.3) through simulations [55]. In this study, with a fixed engine displacement volume and compression ratio (400 cc, CR 9), the change in the burning rate in the SB ratio 0.7 to the SB ratio 1.0 was larger than that of the SB ratio 1.0 to the SB ratio 1.3, which is nonlinear. Moreover, comparing the effect of change in geometry and turbulence characteristics, they suggested that the change in the SB ratio is more important than that of the turbulence toward cooling loss and combustion characteristics. Ikeya et al. conducted experiments for five different SB ratio conditions (1.2, 1.35, 1.5, 1.6, and 2.0) with the same bore size [57]. From this, it was confirmed that the cooling loss decreased to the point of the SB ratio 1.5, and the change became small thereafter. Instead, PMEP and FMEP (implemented by modeling because of the characteristics of torque output from single cylinder engine) increased quite steadily. As caused by the combination of these two effects, the maximum value of the brake thermal efficiency was observed around the point of the SB ratio 1.5. Tsuchida et al. analyzed the effects of longer strokes in terms of the usage of the variable compression ratio (VCR) strategy by both experiment and CFD 3D simulation [56]. Through these approaches, it was experimentally proven that VCR operation is efficient in the long stroke of SB ratio 1.28 and CR 18. This is attributed to the reduction in cooling loss and exhaust enthalpy loss. Hoag et al. carried out experiments at three SB ratios (1.00, 1.1395, and 1.3372) under the

fixed bore condition [58]. From the experimental results of this study, it was shown that the nisfc was improved up to an SB ratio of 1.1395 (bore 86 mm, stroke 98 mm). Thereafter, the SB ratio showed no additional benefit or even increment in nisfc in part of the experimental region. The researchers suggested that these results were attributed to the reduction in cooling loss caused by a lower surface-to-volume ratio (S/V ratio) near TDC at a higher SB ratio, but also a decrement in burn duration caused by higher turbulence kinetic energy (TKE) at a higher SB ratio where the piston speed is increased owing to the relatively long stroke operation.

However, it must be noted that all the experiments in the references were conducted with fixed bore condition. Thus, one can claim that it is not clear whether the results obtained from the experiments in several references were simply the outcomes of the change in SB ratio, or inevitable change in displacement volume attributed by fixed bore condition. Unfortunately, there are no experimental studies related to the operating conditions of fixed volume with various SB ratio conditions so that only simulations have been conducted. Thus, it is desirable to investigate sole effect of SB ratio on the various parameters for SI engine operation such as cooling loss and knock phenomena, with sophisticated setup for experiments, which is the main scope of this work.

1.3 Motivation and Objectives

As mentioned in the previous chapter, the important issue dealt with this work is that SB ratio is comprehensively related to many of parameters that directly affects the efficiency of SI engine. Since there were no studies related to the investigation of sole effect of SB ratio on the mentioned parameters experimentally, the sophisticated engine setup was adopted to investigate the effect, with fixing other geometric parameters such as compression ratio and

displacement volume which will be comprehensively reviewed in chapter 3. In conclusion, the main objective of this work is to find the effect of SB ratio on the engine efficiency and performance, and finally suggest the proper value of SB ratio for the operation of contemporary SI engine with grounds of experimental data.

In order to guide this work appropriately, several questions directly related to this work can be suggested, which will be considered in the following chapters.

1) How to evaluate the sole effect of SB ratio while maintaining other important variables? (chapter 3)

2) What is the relation between valve timing and SB ratio for the best efficient operation? (chapter 4)

3) What are the key parameters to explain the different values of efficiency for various SB ratio? (chapter 4, 5, and 6)

4) In terms of the heat transfer, and work extraction from the difference of internal energy at closed duration, which SB ratio can result in the best efficiency for SI engine operation? (chapter 5)

5) In terms of the knock characteristics, dominating the efficiency of high load operation, which SB ratio can show high knock resistance? (chapter 6)

With answering these questions, eventually, final question can arise as listed below.

- Is it proper way to increase engine efficiency by enhancing burning rate through increment in SB ratio? If not, what is the adverse and unexpected effect that cause the results?

1.4 Organization of the Dissertation

The work contains seven main chapters including current chapter in which the brief explanation of SI engine efficiency and several parameters related to that was introduced with the highlight of importance of SB ratio.

In chapter 2, the method to analyze raw experimental data (especially in-cylinder pressure data) and the configuration of 0D simulation used in this study will be explained.

In chapter 3, the details of experimental setup will be explained with sophisticated design for the sole effect of SB ratio, which is eventually the main novelty of this work.

In chapter 4, the experimental data of preliminary test with various valve timing operation will be introduced to obtain the best efficiency of each condition of load, rotational speed, and SB ratio, for the main experiments used in the next two chapters. In addition, unexpected tendency, which will be mainly investigated in the next two chapters, will be briefly mentioned.

In chapter 5, the parameters directly related to engine efficiency as a part of LHV breakdown – cooling and exhaust heat loss – will be investigated for each SB ratio with usage of specific method of combustion analysis mentioned in chapter 2. Here, the effects of both SB ratio and displacement volume can be split to ensure the sole effect of SB ratio for those important, efficiency-related parameters.

In chapter 6, knock phenomena for each SB ratio will be investigated with additional knock experiments. Here, detailed 0D simulation and newly suggested parameters that can explain the behavior of each SB ratio will be considered.

In chapter 7, overall conclusion of this work will be introduced.

Chapter 2. Combustion Analysis and Simulation Modeling

Since the data from the engine experiments are normally based on the 0D bulk motion based in-cylinder pressure data for each crank angle, one cannot fully understand all the phenomena inside the cylinder. Therefore, additional two tracks exist; visualization of cylinder status using laser diagnostics and spectroscopy [60], and 3D CFD simulation [50]. Before conducting those strategies, however, it is strongly believed that comprehensive analysis by exploiting in-cylinder pressure data should be achieved preferentially, because not only it is well-known method for combustion analysis but also, we can get a lot of information from the data with few reasonable assumptions.

At the first part of this chapter, detailed combustion analysis used in this study was covered, which was mainly based on the in-cylinder pressure data. After that, covered were basic information and detailed configuration of 0D simulation, found to be a good supplement of experimental results which were limited by several issues mentioned earlier.

2.1 Thermodynamic-based analysis

2.1.1 Estimation of residual mass fraction and IVC condition

The residual mass fraction (RMF) is one of the most important parameters that change the temperature and pressure in the IVC as well as the in-cylinder thermodynamic characteristics. In general, because of larger clearance volume

corresponding to smaller compression ratio compared to CI engine, SI engine is significantly affected by residual mass fraction. Typically, although it strongly depends on load and the RPM condition, residuals occupy approximately 5–30% [18] of the mass fraction in normal part-load SI engine operation.

It is not easy to conduct an experiment while measuring the actual residual value on a cycle-by-cycle basis. Therefore, many researchers have indirectly performed residual estimation using other parameters [61-64]. Considering Fox et al., the 'overlap factor' was firstly introduced to quantify the effect of overlap period on the residual mass fraction. The definition was listed below [61],

$$OF = \frac{D_i A_i + D_e A_e}{V_d} \qquad \text{eq. 2.1}$$

$$A_i = \int_{IVO}^{Lift\ t_i = Lift\ t_e} L_i(\theta)\, d\theta \qquad \text{eq. 2.2}$$

$$A_e = \int_{Lift\ t_i = Lift\ t_e}^{EVC} L_e(\theta)\, d\theta \qquad \text{eq. 2.3}$$

where D_i and D_e are the inner seat diameters of the intake and exhaust valves, L_i and L_e are instantaneous valve lift of intake and exhaust valves, and V_d is the displacement volume of the engine. Using this concept, they suggested the estimation of residual mass fraction as listed below,

$$x_r = C_1 \left(\frac{P_e}{P_i}\right)^{\frac{\gamma_{in}+1}{2\gamma_{in}}} \left(\frac{OF}{N}\right) \sqrt{P_e - P_i} + C_2 \frac{\left(\frac{P_e}{P_i}\right)^{\frac{1}{\gamma_{in}}} \phi}{CR} \qquad \text{eq. 2.4}$$

where N is rotational speed of which unit is rev/sec, and P_i and P_e are intake and exhaust pressure of which unit is bar. Here, C_1 and C_2 are fitting constant of which values were set to be 1.266 and 0.632 by assuming constant specific heat ratio (1.35) and ambient air density. With this estimation and measured data of residual mass fraction by sampling CO_2 process, parameter sweep was conducted for OF, equivalence ratio, engine rotational speed, and inlet pressure, showing good correlation. However, it was found to be not appropriate for this study because in the model, pressure at IVC timing was not used which is a direct barometer of the total mass for the relevant individual cycle. In addition, combustion-related parameters were also not directly used, where the intake and exhaust pressure were only used. As considering these reasons, advanced models suggested from [63, 64], which were modified and improved based on the model from [61], were also not used in this study. In this study, an improved model was used by applying some of the contents of the reference [62]. Details of modification process based on the model from the reference was covered below.

Passing IVO and EVC timing, the residual remains in the cylinder and the intake mixture of the intake manifold newly enters the cylinder. In addition, back flow from cylinder to intake manifold occurs. Thus, the total mass of a single cycle is not determined until the IVC timing occurs. Based on the measured cylinder pressure, the partial pressures for each the intake mixture and the residual at IVC timing are defined in the eq. 2.5.

$$P_{IVC} = P_{IVC,intake} + P_{IVC,residual} \qquad \text{eq. 2.5}$$

In the reference, suggested were three factors which affect the intake mixture temperature at IVC timing; 1) compression of the mixture from intake manifold to cylinder 2) heat transfer to the wall and 3) a fuel charge cooling effect. Based on the reference, it was assumed that the effects of 2) and 3) are canceled, and thus the intake mixture is adiabatically compressed from the intake manifold to the cylinder IVC. Therefore, the temperature of the intake mixture at the IVC timing can be calculated by applying the adiabatic compression equation of ideal gas, as listed in eq. 5.1,

$$T_{IVC,intake} = T_{in}\left(\frac{P_{in}}{P_{IVC,intake}}\right)^{\frac{1-\gamma_{in}}{\gamma_{in}}} \qquad \text{eq. 2.6}$$

where T_{in} and P_{in} are the temperature and pressure at the intake manifold, respectively, $P_{IVC,intake}$ is the partial pressure of the intake mixture at IVC timing, and $T_{IVC,intake}$ is the estimated temperature of intake mixture at IVC timing. For residual gas, the exhaust temperature measured at the exhaust manifold was used as its temperature at the IVC timing, provided that the exhaust temperature measured at the exhaust manifold was affected by the heat transfer from exhaust valve to measured position and isentropic expansion into exhaust manifold pressure, which are similar to the case of residual gas remaining in the cylinder. The total mass of the air in the fresh mixture can be calculated from the fuel flow rate measured in the fuel flow meter, the H/C ratio of the fuel, and the lambda value measured in the exhaust manifold. Therefore, if the RMF is evaluated, the temperature at IVC can also be calculated. Figure 2.1 presents a flowchart showing the calculation process of RMF estimation. When the RMF value is given, whether by initial assumption or iteration, the average temperature at the IVC timing can be calculated by applying the energy balance using the temperature and mass values calculated by eq. 5.1.

$$T_{IVC} = \frac{(1-rmf)c_{v,intake}\,T_{IVC,intake} + rmf\,c_{v,rmf}T_{IVC,rmf}}{(1-rmf)c_{v,intake} + rmf\,c_{v,rmf}} \qquad \text{eq. 2.7}$$

Here, $c_{v,intake}$ and $c_{v,rmf}$ are the specific heat at constant volume of the intake mixture and residual at the IVC timing, respectively. With this process, thermodynamic properties at the IVC timing can be completely obtained through the calculated composition from the calculated average temperature, measured pressure, and RMF value. The product of this density and the instantaneous volume at the IVC timing was compared with the total mass value obtained from the RMF value and the intake mixture mass value. The iteration proceeded by adjusting the RMF and ended if the difference between present and previous values is smaller than the tolerance.

The examples of estimated residual mass fraction and NOx emissions data were shown in figure 2.2 and 2.3. The values of x-axis in both figures are the degree of intake cam shifting – if the values are decreased, IVC and IVO timing are advanced simultaneously. Thus, it can be expected that with fully advanced condition (i.e. -40 InCAM position), actual compression ratio defined by the volume of IVC timing is the largest of all InCAM position, which means peak temperature may be also the highest. As shown in figure 2.3, however, NOx emissions, which is highly related to peak temperature [18], were decreased as intake valve timing was advanced. Thus, it can be concluded that even if the actual amount of compression was increased, other variables such as composition-related parameters might cause NOx decrement – residual mass fraction is the proper answer. Considering the trends shown in figure 2.2 and 2.3, estimated residual mass fraction shows very related tendency with NOx emissions. For general case of SI gasoline engine operation, increased amount of hot residual gas makes specific heat ratio of the gas during compression stroke lower by thermal

effect (hot temperature) while the chemical effect has opposite effect but not dominant compared to former effect[7]. In addition, more inert gas (i.e. residual) leads to decrement of temperature rise caused by combustion process. Thus, more residual mass fraction can cause decrement in NOx emissions, which was clearly shown in figure 2.2 and 2.3. Therefore, although the quantitative validation was not conducted, this model can be proved to be used properly with various valve timing conditions.

The experimental values required when using the model were listed below.

- Pressure and temperature of the intake mixture
- Mass flow rate of fuel
- H/C ratio of fuel
- Air–fuel ratio (i.e., lambda)
- In-cylinder pressure
- Gas concentration of exhaust mixture (dry basis is adequate for the estimation)

[7] Although the number of atoms of N_2 and O_2 (the main species of fresh mixture) is higher than H_2O and CO_2 (the main species of exhaust gas), the specific heat ratio of exhaust gas is higher than that of the fresh mixture (air + fuel) if those are in the same temperature, because the large number of atoms in fuel component (gasoline) has dominant effect on the determination of specific heat ratio of fresh mixture – provided general case of gasoline SI engine operation with ambient air and stoichiometric condition.

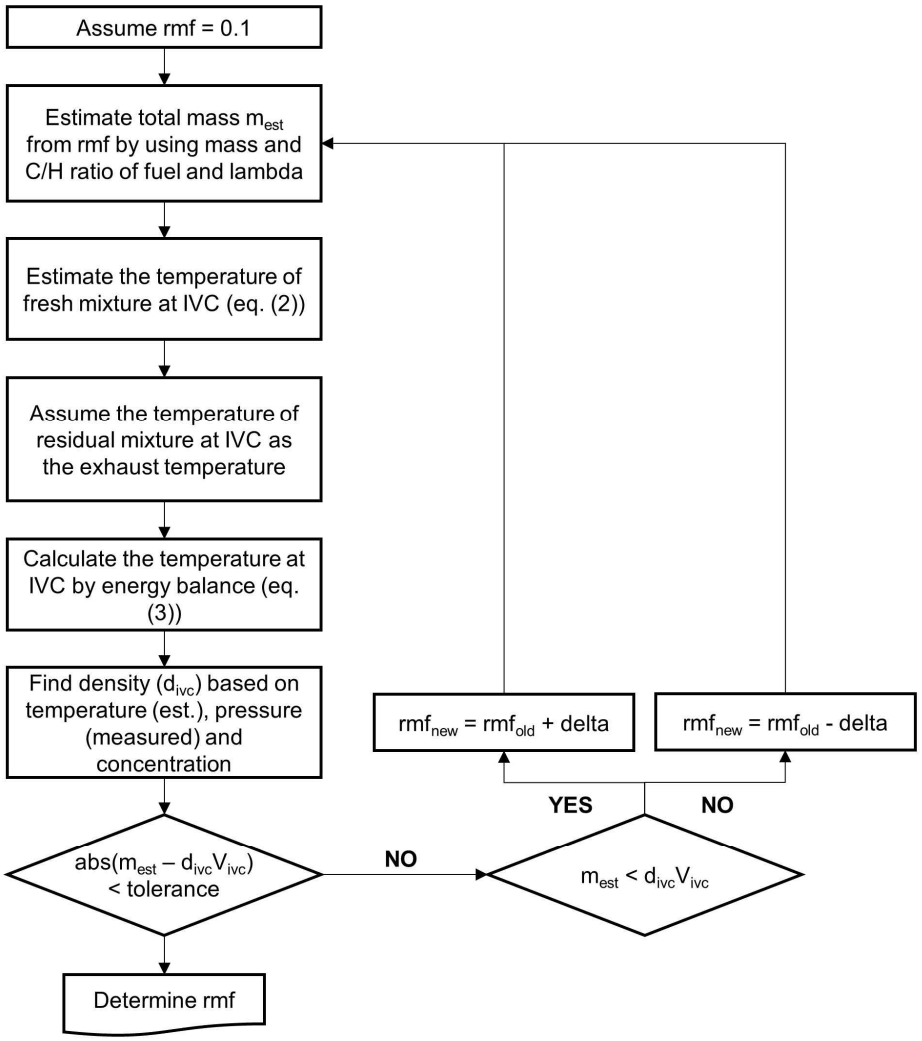

Figure 2.1 Algorithm for the calculation of residual mass fraction and IVC temperature

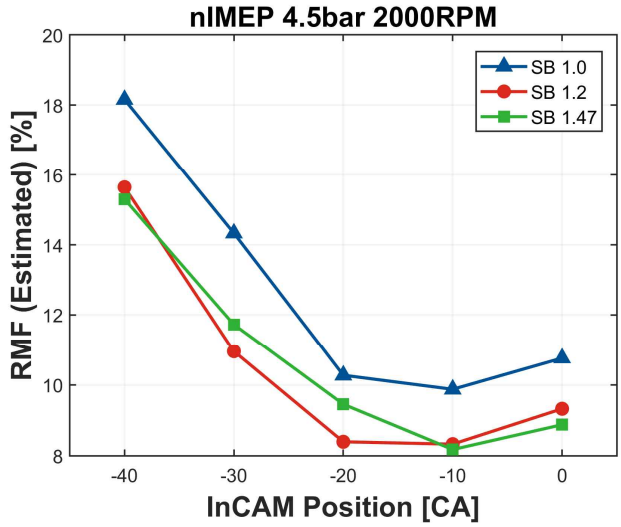

Figure 2.2 Example of the estimation of residual mass fraction with respect to various intake valve timing

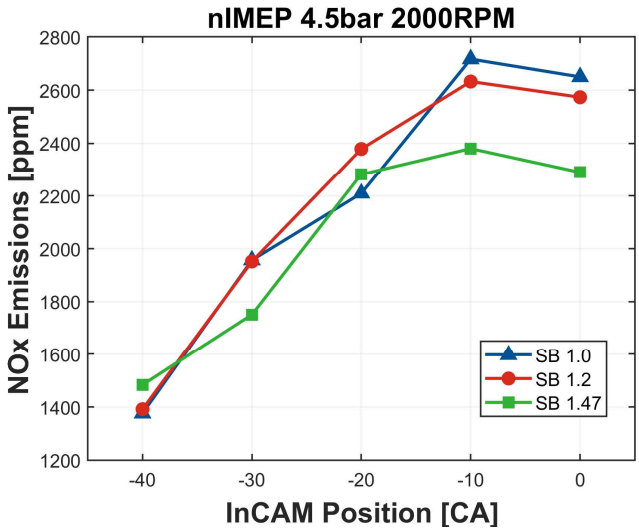

Figure 2.3 Example of the NOx emissions with respect to various intake valve timing

2.1.2 Heat release and combustion phasing

Heat release calculation has been widely used to analyze the combustion phenomena inside the engine, especially for combustion phasing, regardless of the engine type [18, 65, 66]. From a point of mass burned fraction, calculation without using heat release estimation also exists [67], which has been also widely used for engine combustion analysis. In this study, heat release calculation with using accurate properties was used to estimate combustion phasing inside the cylinder.

Estimation of accurate total mass of pertinent individual cycle and IVC temperature is the key thing to achieve proper combustion analysis. From that reason, estimation of residual mass fraction and IVC state was covered in the previous chapter. In addition, after IVC timing, it is also important to estimate the accurate specific heat ratio of the gas during the calculation of the heat release rate (from IVC to EVO timing) when the inside of the cylinder is closed [66, 68]. In this study, the specific heat ratio values at each crank angle of cylinder gas were estimated through iteration so that the heat release rate calculation result was converged with satisfying certain tolerance. The process of calculating the heat release rate was shown in figure 2.4. First, the initial value of the gas state before entering the iteration (loop statement) was set. The composition of the intake mixture can be calculated by using the measured fuel rate, H/C ratio of the fuel, the lambda value measured in the exhaust manifold, and estimated residual mass fraction. In addition, the composition of the exhaust mixture including H_2O and H_2 can be calculated by measuring the dry basis concentration of the exhaust gas with atom balance of the composition of each intake and exhaust mixture. Thus, the temperature, pressure, composition of the cylinder gas, and specific heat ratio at IVC timing were obtained. The calculated specific heat ratio value was applied as a constant value at the initial heat release rate calculation loop where the

composition of the cylinder mixture for each CA is not yet known. The equations used to calculate the heat release rate and accumulated heat release rate (AHRR) were expressed in eq. 2.8 and eq. 2.9, with an assumption of ignoring the blow-by effect to the crevice.

$$HRR(\theta) = \frac{\gamma(\theta)}{\gamma(\theta)-1} p(\theta) \frac{dV(\theta)}{d\theta} + \frac{1}{\gamma(\theta)-1} V(\theta) \frac{dp(\theta)}{d\theta} + \frac{dQ_{ht}}{d\theta} \qquad \text{eq. 2.8}$$

$$AHRR(\theta_{i+1}) = AHRR(\theta_i) + HRR(\theta_i)\, d\theta \qquad \text{eq. 2.9}$$

During the process, whole cylinder was assumed to be filled with single-zone, homogenous charge. It is noted that the heat transfer term (last term in eq. 2.8) is assumed to be zero for the first iteration. The crank angle where the AHRR has its maximum value is assumed to be the end of combustion (EOC). Henceforth, the burned mass fraction (MFB) can be calculated using the normalized AHRR values from ignition timing to EOC. Additionally, the gas composition in each CA also can be calculated using eq. 2.10.

$$y(\theta) = y_{in} \left(1 - MFB(\theta)\right) + y_{out}\, MFB(\theta) \qquad \text{eq. 2.10}$$

Here, y_{in} was assumed to be the composition calculated at IVC timing, and y_{out} was assumed to be the composition of wet basis exhaust gas composition. Since the single zone density can be estimated by using total estimated mass per cycle and volume profile, the mass-averaged temperature, satisfying the density at the pressure and composition, can be calculated for each crank angle, where the revised specific heat ratio can be also calculated simultaneously. Afterwards,

internal energy was estimated for each crank angle by using the pressure (measured), temperature (estimated as single value), and composition of each crank angle. Finally, heat transfer between θ_i and θ_{i+1} can be estimated with simple first law of thermodynamics, as expressed in eq. 2.11.[8]

$$\frac{dQ_{ht}}{d\theta}(\theta_i) = m_{cyde}\ \left(u(\theta_i) - u(\theta_{i+1})\right) - \frac{\left(P(\theta_i) + P(\theta_{i+1})\right)}{2}\left(V(\theta_{i+1}) - V(\theta_i)\right)$$

eq. 2.11

After repeating the above process using the revised specific heat ratio and heat transfer, allocated for each crank angle, the iteration was stopped, and the result was outputted if the difference between the calculated HRR and the previous one is less than the tolerance.

The experimental values required when using the model were listed below.

- Pressure and temperature of the intake mixture
- Mass flow rate of fuel
- H/C ratio of fuel
- Air-fuel ratio (i.e., lambda)
- In-cylinder pressure
- Gas concentration of exhaust mixture (dry basis is adequate for the estimation)

[8] These will be explained in chapter 2.1.4 in detail.

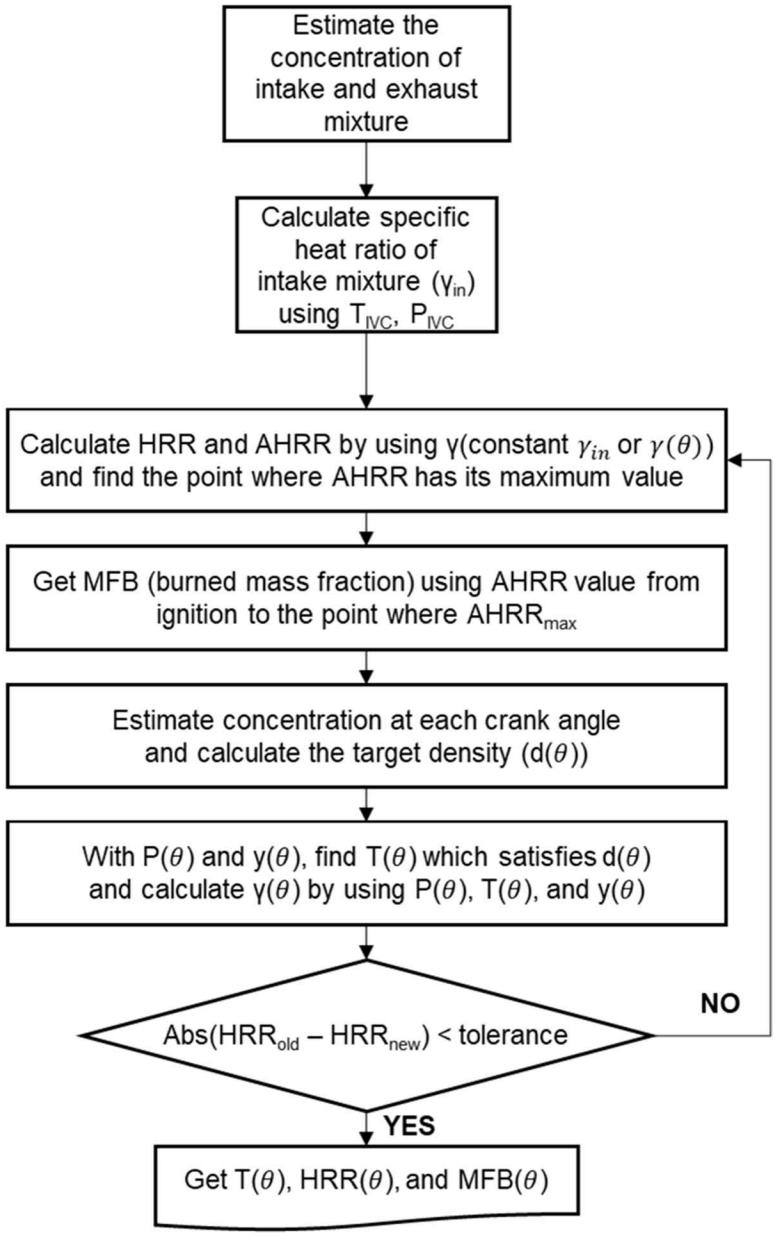

Figure 2.4 Algorithm for the calculation of heat release data

2.1.3 LHV breakdown

Since the internal combustion engine is also a type of heat engine, thermodynamic-based energy flow should be conducted to understand its performance comprehensively. Here, LHV breakdown process was covered. Figure 6 shows the mass flow, heat, and work flowing into and out of the engine combustion chamber in analyzing the operation during one cycle of the four-stroke gasoline SI engine, specifically from the gas exchange top dead center (TDC) to the next gas exchange TDC. Using 1st law of thermodynamics, the relationship is summarized in the eq. 5.1.

$$LHV_{in}\, m_{fuel} + h_{sens,in}\, m_{mix} + W_{pump} = LHV_{ex}\, m_{incomplete} + h_{sens,ex}\, m_{mix} + Q_{cool} + W_{gross} \quad \text{eq. 2.12}$$

Noted that the order of terms used in this equation is same with figure 2.5. Each term except 'Cooling loss' was described in detail;

1) 'Enthalpy of formation (i.e. fuel LHV)' is the energy term corresponding to the chemical energy that fuel contains. In order to estimate this, fuel rate and LHV of fuel are required.

2) 'Sensible enthalpy of intake mixture' is the energy term corresponding to the sensible energy that fuel and air mixture contains. It becomes non-zero value if the intake temperature is different from the temperature of reference state[9]. The calculation process is listed below.

[9] In this work, 25 Celsius and 1 atm was chosen as the reference temperature and pressure.

$$h_{sens,in}\, m_{mix}$$

$$= \left(m_{fuel} + m_{air}\right)\left(h(T_{in}, P_{in}, x_{in}) - \left(T_{ref}, P_{ref}, x_{in}\right)\right) \qquad \text{eq. 2.13}$$

3) Pumping work is calculated by in-cylinder pressure and volume profile of intake and exhaust stroke. The definition is listed below.

$$W_{pump} = \left| \int_{BDC'}^{BDC''} P(\theta) dV \right| \qquad \text{eq. 2.14}$$

Here, BDC' means the first BDC timing after the expansion stroke, and BDC'' means the first BDC timing after the intake (induction) stroke. In general, the term inside the absolute bracket has negative value, due to the higher pressure during the exhaust stroke for normal throttled SI engine operation.

4) 'Enthalpy of formation for exhaust mixture' (i.e. incomplete combustion) means the chemical energy which remains in exhaust gas, caused by incomplete combustion. The typical species related to this term are CO and UHC[10], which can be measured by the emission analyzer. It should be noted that UHC cannot be measured as a single species; its unit is ppmC, which means total number of carbons for any UHC in exhaust gas. In this study, propane (C_3H_8) was used to represent the total emissions of

[10] In fact, the species included in NOx emissions (NO or NO_2) also have a slight chemical energy which can be called heating value. However, even if the engine combustion is ideal so that the oxidation of all the fuel species is achieved, NOx cannot be completely removed because it is generally formed by after-combustion process; N_2 and O_2 oxidation in burned zone, followed by flame propagation, are the main source of NOx emissions. Thus, it is not usually considered as a 'incomplete combustion' term.

UHC since it was used as a calibration species of UHC in emission analyzer; for example, 3000 ppmC of UHC is displaced by 1000 ppm of propane. With these processes, chemical energy remaining in CO and UHC was calculated to obtain this term.

5) 'Sensible enthalpy of exhaust mixture' (i.e. exhaust loss) is directly related to the exhaust gas temperature, where the definition is similar to that of 'Sensible enthalpy of intake mixture', listed below.

$$h_{sens,ex} m_{mix} = \left(m_{fuel} + m_{air}\right)\left(h(T_{ex}, P_{ex}, x_{ex}) - h\left(T_{ref}, P_{ref}, x_{ex}\right)\right) \quad \text{eq. 2.15}$$

6) 'Gross work' is calculated by in-cylinder pressure and volume profile of compression and expansion stroke. The definition is listed below.

$$W_{gross} = \int_{BDC''}^{BDC'} P(\theta) dV \quad \text{eq. 2.16}$$

The same notion for each BDC timing was used. In general, gross work is highly related to the burning rate and heat transfer inside the cylinder during closed duration (i.e. from IVC to EVO timing).

'Cooling loss', which was not introduced above, means the total amount of heat transfer for a whole cycle. However, it cannot be measured directly from engine experiment data. Thus, 'Cooling loss' was in-directly estimated by using 1st law of thermodynamics (i.e. eq. 5.1) and the other parameters which can be directly estimated from the experimental data. Two things should be noted. First,

unintended values such as blow-by which was not included in eq. 5.1 can be contained in this term, caused by the method of calculating ‘Cooling loss’. Second, since the exhaust temperature, used to calculate ‘Sensible enthalpy of exhaust mixture’, was measured at the point of the exhaust manifold, as close as possible to exhaust valve. Therefore, ‘Cooling loss’ contains heat transfer from not only the cylinder but also the exhaust port [69]. However, since the most part of ‘Cooling loss’ is undoubtedly comprised of heat transfer inside the cylinder, it is reasonable to use this term to compare the relative heat transfer behavior between experimental conditions.

The experimental values required to calculate each term are listed below.

- Mass flow rate of fuel
- Low heating value of fuel
- H/C ratio of fuel
- Air–fuel ratio (i.e., lambda)
- Pressure and temperature of the intake mixture
- In-cylinder pressure
- Pressure and temperature of the exhaust mixture
- Gas concentration of the exhaust mixture (dry basis is adequate for the estimation)

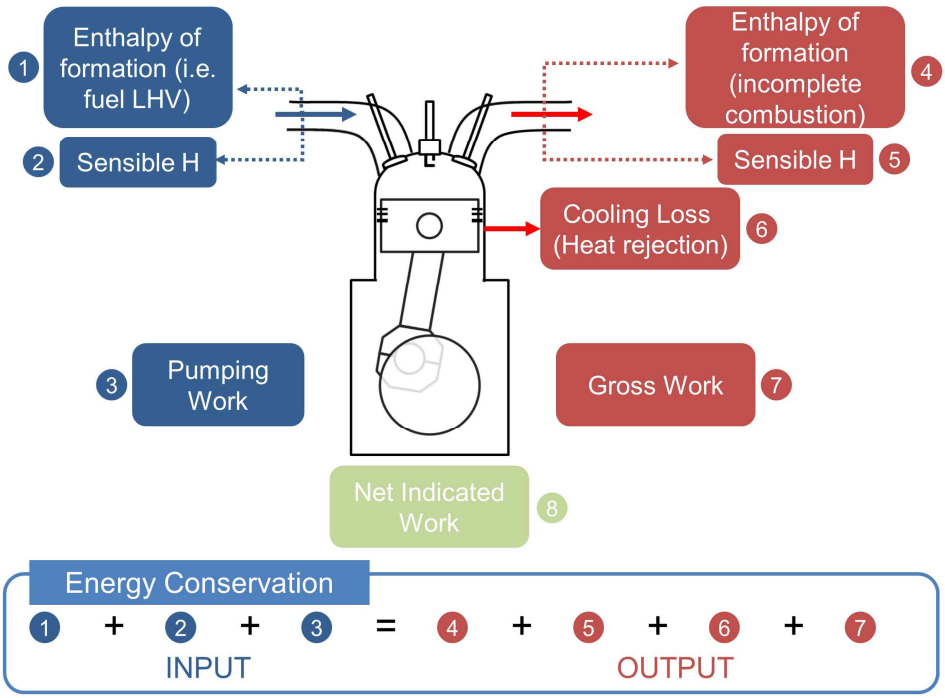

Figure 2.5 Energy balance of engine operation with respect to whole cycle

2.1.4 Energy balance in closed system

In general, most of the work from four-stroke internal combustion engine is produced by the combustion process between IVC and EVO timing (called 'closed duration' in this study). Since the volume, pressure, and resultantly temperature profiles were different for each SB ratio condition with almost same input parameters (e.g. fuel rate, rotational speed), detailed analysis which is related to the information from each crank angle was inevitably required. Thus, based on the in-cylinder pressure data measured at each crank angle, thermodynamic analysis with estimation of the balance between work and heat transfer (1st law) was conducted to comprehensively understand the phenomena inside the cylinder during closed duration. The details were listed below.

1) The in-cylinder pressure was measured and referenced with intake manifold pressure[11].

2) The properties at IVC timing (temperature and composition) was determined with the measured pressure and the method previously covered in chapter 2.1.1.

3) Mass-averaged temperature (single-zone) was estimated (during the calculation of heat release rate) with the method mentioned in chapter 2.1.2.

4) Internal energy per each crank angle was estimated based on the estimated single-zone temperature, composition, and measured in-cylinder pressure.

[11] The details were covered in chapter 3.2.

5) Using PdV work rate per each crank angle, calculated with measured in-cylinder pressure, heat transfer rate was estimated using 1st law of thermodynamics for each interval between θ_i and θ_{i+1}, as shown in eq. 2.11.

In this procedure, it was the most important process to estimate internal energy precisely. According to this, it should be noted that the actual internal energy of the mixture used in the experiment cannot be estimated because of the difference in the composition of unburned mixture. However, this process has two degree of freedom – estimation of composition and heat transfer – with one constraint – measured in-cylinder pressure. Due to this, the estimated heat transfer may have lots of sources for error range. Therefore, additional approaches such as 3D CFD will be needed to validate the estimated data, where 3D CFD analysis can reduce the degree of freedom into one because of the boundary condition between wall and mixture which can produce the results of convective heat transfer independently.

For the entire combustion analysis, PRF 91.5 (91.5 % of iso-octane and 8.5 % of n-heptane with volume fraction) was used as a substitute of gasoline used in real engine experiment. Thus, it was assumed that the tendency of internal energy and the others related to the rest of combustion analysis mentioned earlier was not significantly changed by using thermodynamic properties of PRF 91.5 instead of gasoline of which properties cannot be estimated due to the complexity of its composition. Furthermore, because of low temperature at IVC timing, the usage of ideal gas law may not be appropriate in terms of compressibility factor. However, the IVC conditions of each data to be mainly compared in this study were not so different because the experiments were conducted with same load or fuel rate. Therefore, it was assumed that the discordance of compressibility factor

(with unity corresponding to ideal gas) will be equally biased in the region of IVC temperature of the experimental data to be compared.

2.2 Knock measurement

As mentioned in chapter 1, knock phenomena significantly affects the performance of SI operation. The example of knock-related operation was plotted in figure 2.6, where the heavy knock, knock-limited and retarded operations were shown[12]. The corresponding gIMEP data were listed in figure 2.7. It was shown that with the same fuel rate and rotational speed, relatively 2% of gIMEP was increased from the most retarded spark timing to the heavy knock (beyond KLSA) condition, corresponding to around 0.7 – 0.8% absolute difference of net indicated efficiency. Therefore, above all the state-of-the-art technologies related to modern SI engine, knock mitigation is mostly required to achieve the latest regulation of emissions and fuel economy related to automotive SI engine. In addition, it should be noted that the determination of knock standard has significant effect on the best efficiency chosen for corresponding operating condition – if the spark timing of heavy knock in figure 2.7 is selected as a KLSA of corresponding condition, changed is the best efficiency of which tendency for various SB ratio cannot be predicted easily. Therefore, it should be noted that in the process of the determination of knock standard, comprehensive study related to every condition of the experiments should be covered.

In order to analyze the knock phenomena in SI engine operation, the standard for knock determination should be required. For this, two things should be clarified.

[12] The pressure oscillation corresponding to knock occurrence was diminished by ensemble averaging process (300 cycles) with zero-phase filtering process used in the reference [71].

1) What is the criterion to determine whether knock occurs or not in certain individual cycle? (related to knock onset and intensity)

2) If knock occurs in the cycle, what criterion can be used to classify the knock characteristics of the cycle? (related to knock intensity)

These were covered in the following sections. In addition, the problems related to the stochastic behavior of knock phenomena were reviewed, which led to the alternative approach on the data from individual cycles.

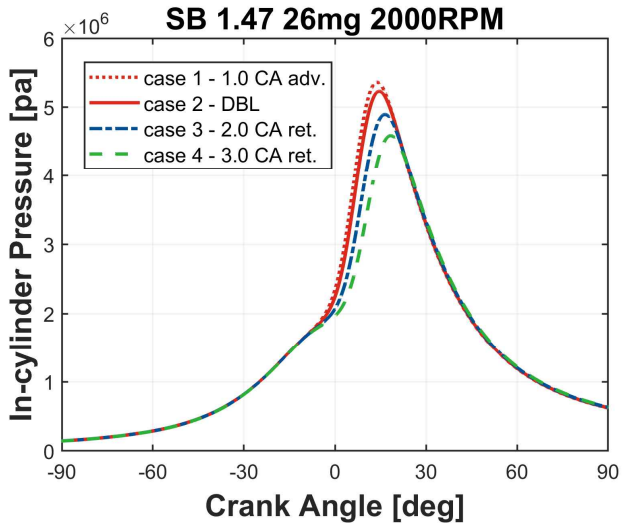

Figure 2.6 Example of pressure profiles for knock-related conditions (SB 1.47, 26mg of fuel rate and 2000 RPM)

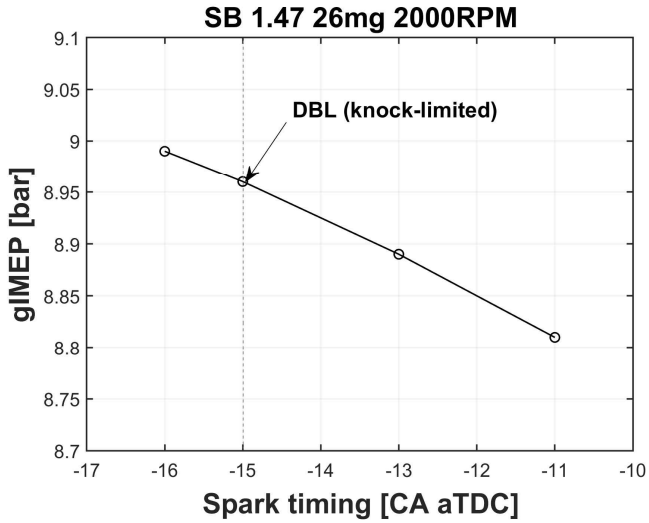

Figure 2.7 Example of gross IMEP data corresponding to the conditions of figure 2.6 (SB 1.47, 26mg of fuel rate and 2000 RPM)

2.2.1 Determination of knock-limited operation and its characteristics

It is widely-used approach to measure the knock characteristics by using in-cylinder pressure data [18, 70-72]. In this study, pressure oscillation induced by harsh autoignition (leading to 'knock' sound) was mainly used to determine knock characteristics. It should be mentioned that detecting pressure oscillation is highly affected by location of pressure transducer [73] because of the characteristics of pressure oscillation modes [74, 75]. This will be comprehensively mentioned in the chapter 3.1.1.

The knock oscillation frequency can vary in different chamber shapes. The frequency of pressure oscillation was described in eq. 2.17.

$$f = \frac{\bar{a}}{2\pi}\sqrt{\left(\frac{\mu^{*}_{\lambda,m}}{B/2}\right)^{2} + \left(\frac{\pi g}{Z_0}\right)^{2}} \qquad \text{eq. 2.17}$$

Here, $\mu^{*}_{\lambda,m}$ is the mth root of the first derivative of Bessel's equation ($J'_{\lambda}(\mu^{*}_{\lambda,m}) = 0$), where each parameter is ordered as (m = 1, 2, …) and (λ = 0, 1, …). λ is the number of the circumferential mode, m is the number of radial mode, and g is the axial mode number. $\bar{a}$ is the sound speed where the assumed temperature (2500K) and gas composition of complete combustion products were used, B is the length of bore size, and Z_0 is the instantaneous height between piston surface and lower surface of cylinder head at the knock onset timing, assuming disc shape cylinder. Considering 81 mm as the bore size and 1.4 of polytropic coefficient, the first six pressure oscillation modes of the used engine

in this study were plotted in figure 2.8, which implies the importance of the location of pressure transducer.

It is also noted that the frequency-based analysis should be considered to understand the pressure oscillation with various SB ratio conditions (i.e. various bore sizes with constant displacement volume). For this, the theoretical frequencies of the pressure oscillation modes were calculated by solving the eq. 2.17 and listed in tables 2.1 with various SB ratio conditions. It should be noted that the allocated frequencies for each oscillation mode are different for each SB ratio attributed by different bore size. These results were quantified in figure 2.9. In this figure, the normalized power spectral densities for each SB ratio were shown, which was derived from experimental data of knocking combustion. As expected, lower bore shape leads to a higher knock frequency. From these results, it can be explained that incorrect signal filtering may cause unexpected attenuation of the knocking signal. If, for example, a low cut-off frequency of the bandpass filter is located around the computed frequency corresponding to the first circumferential mode (approximately 6-8 kHz), the magnitude of bandpass-filtered pressure can be biased by the SB ratio condition. In addition, for example, a high cut-off frequency of the bandpass filter can be limited by the high resonance frequency related to the geometry-related issues such as mounted method of pressure transducer [73] or such space inside the cylinder where a resonance can occur. Considering these aspects, 4-28kHz bandpass filter was used to evaluate the pressure oscillation induced by knock phenomena of which examples from randomly chosen cycles were shown in figure 2.10 and figure 2.11. Determination of the knock cycle was processed by using the maximum oscillation value of bandpass-filtered pressure (called MAPO) – if the peak-to-peak filtered pressure exceeds certain threshold (0.5 bar in this study), the cycle was determined as a knock cycle[13]. With this criterion, the cycle shown in figure 2.10 was determined

[13] This method was also known as TVE (Threshold Value Exceed) method [70].

as knock cycle; the other shown in figure 2.11 was not. In case of knock cycle shown in figure 2.10, the onset timing was expressed as circle (~16.9 CA aTDC), which was explored and determined by using the method suggested in Cho et al. [71] which had been modified from the previous studies.

For the determination of knock-limited operation, spark timing is the most important parameter. Here, with the criterion described above, knock-limited operation was defined based on the spark timing corresponding to the condition that 'knock incidence' exceeds a certain value for total individual cycles of the relevant operating condition, where the definition of knock incidence was listed in eq. 5.1.

$$Knock\ incidence = \frac{N_{knock}}{N_{total}} \times 100\ [\%] \qquad \text{eq. 2.18}$$

Here, N_{knock} means total number of knock cycles in the relevant operating condition, and N_{total} means total number of cycles. In this study, 10% of knock incidence was selected as a criterion of knock-limited operation.

Three questions related to these criteria should be discussed, which were listed below.

1) Is it appropriate to select **0.5 bar** as a threshold of knock intensity that determines whether relevant cycle is knock cycle or not?

2) Is it appropriate to select **10%** of knock incidence as a 'knock'-limited operation? – correlation between knock incidence and intensity

3) Are those criteria suitable to compare the knock characteristics of each SB ratio?

First, threshold of knock intensity was discussed. With many studies which used the same method (MAPO TVE) for the determination of knock occurrence, usual values of the threshold were around 1-2 bar of filtered pressure [76-78], all of which were higher than the threshold used in this study (0.5 bar). Consequently, the criterion used for this study was relatively weak knock criterion, which was intentionally chosen because of the large amount of cycles logged for the knock-related experiment. In order to compare the knock characteristics of each SB ratio condition while removing stochastic behavior of knock phenomena as much as possible, 5000 cycles logging processes were conducted, which needs lots of time. Since engine failure can be induced in the process of experiment for a long time – for example, about 20 minutes was required to log 5000 cycles of 1500 RPM operation (including logging process) – while generating a knock, heavy knock operation with the threshold up to usual value was not able to be conducted. Furthermore, the experimental results related to knock characteristics by these large amounts of data were found out to give us a clear tendency without a stochastic (i.e. not ordered) behavior which will be mainly covered in chapter 6. Therefore, the first question was found to be clear.

Second, threshold of knock incidence was discussed. It should be noted that in the method of knock incidence used in this study, the degree of MAPO value was only considered to determine whether it exceeded the threshold value or not. Therefore, proper logic was required to prove the positive correlation between knock incidence and widely used intensity parameter. The figure related to this question from the reference [71] was redrawn in figure 2.12, where the GDI and PFI data were the experimental data used in this study and the reference [71], respectively. The value used in y-axis was called ISPO (integral of signal pressure oscillation) or SEPO (signal energy of pressure oscillations) [79], calculated by eq. 5.1 from the same reference.

$$ISPO = \int_{\theta_0}^{\theta_0+\Delta\theta} P_{filt}^2 \, d\theta \qquad \text{eq. 2.19}$$

Here, ISPO is one of the knock intensity metrics that used frequently in engine research, based on the pressure data. It was found in figure 2.12 that no matter what data were used, positive relation with strong correlation ($R^2 \sim 0.9779$) was made between knock incidence and ISPO. Since the correlation between ISPO and other parameters used for knock intensity metrics was found to be good [80], It can be concluded that knock incidence is a good parameter that represent the magnitude of knock at relevant condition.

Third question is the most important quest in this work. One can claim that even if same standards for knock occurrence (1st question) and knock incidence (2nd question) were used for all engine conditions (e.g. SB ratio, tumble ratio), the resultant knock data can be different. For example, despite same knock incidence applied for two different conditions of SB ratio, relevant knock cycles can result in different tendencies, in terms of average and/or distribution of knock intensity. However, this should be understood as dependent results to be investigated, not a situation that need to be controlled. Even though averaged knock intensity (e.g. ISPO) was replaced as a standard of knock-limited condition, rather than knock incidence, same circumstance will occur – only the order of parameters changes (controlling knock incidence to investigate the difference of averaged knock intensity among all conditions, and vice versa). Therefore, the answer to the third question will be comprehensively described with the essence of the experimental results in chapter 6.

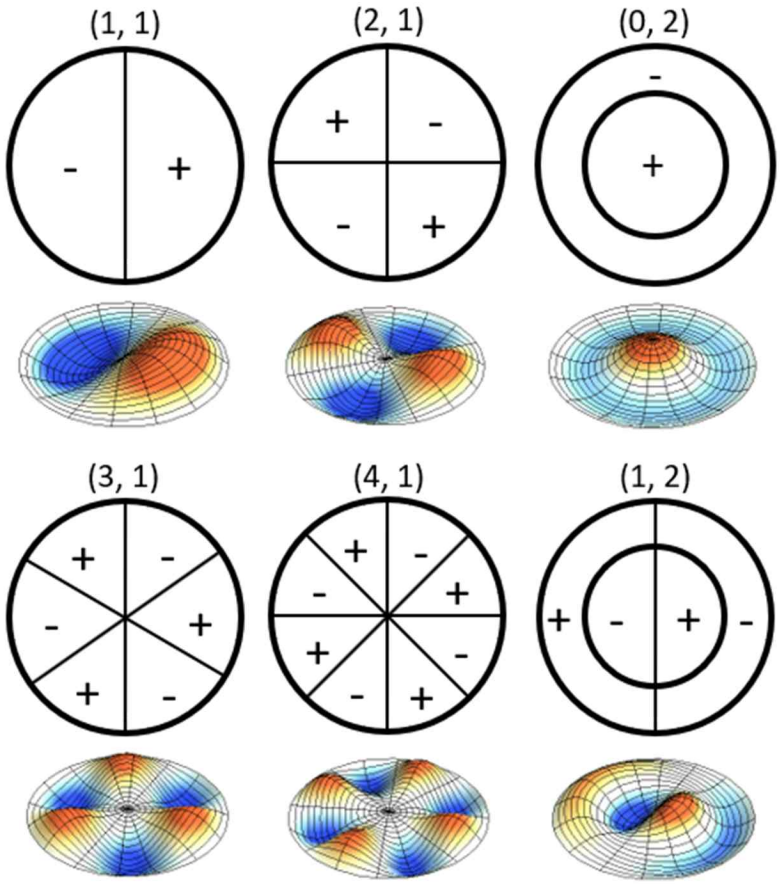

Figure 2.8 First six pressure oscillation modes of pressure wave (redrawn from [71])

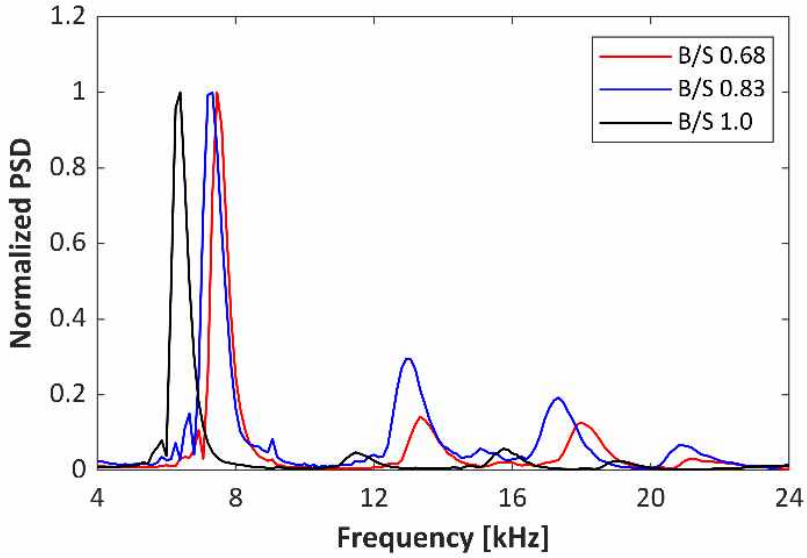

Figure 2.9 Normalized power spectral density of pressure profile with knock occurrence for three different SB ratio (redrawn from [98])

Table 2.1 Theoretical frequencies of the pressure oscillation modes under three SB ratios [98]

Oscillation mode (λ, m)		1st (1,1)	2nd (2,1)	3rd (0,2)
$\mu^*_{\lambda m}$		1.841	3.054	3.832
Frequency [kHz]	SB 1.0	6.58	10.92	13.70
	SB 1.2	6.99	11.59	14.54
	SB 1.47	7.49	12.42	15.58

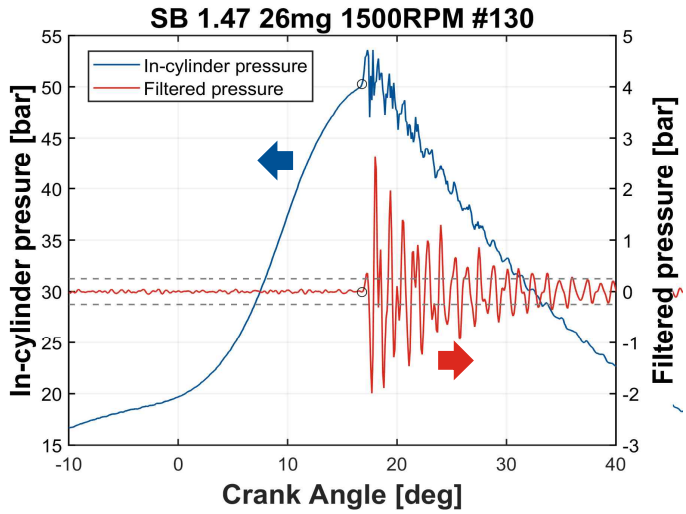

Figure 2.10 Example of in-cylinder and filtered pressure data of knock cycle (SB 1.47, 26 mg of fuel rate, and 1500 RPM, #130 cycle of total 5000 cycles experiment)

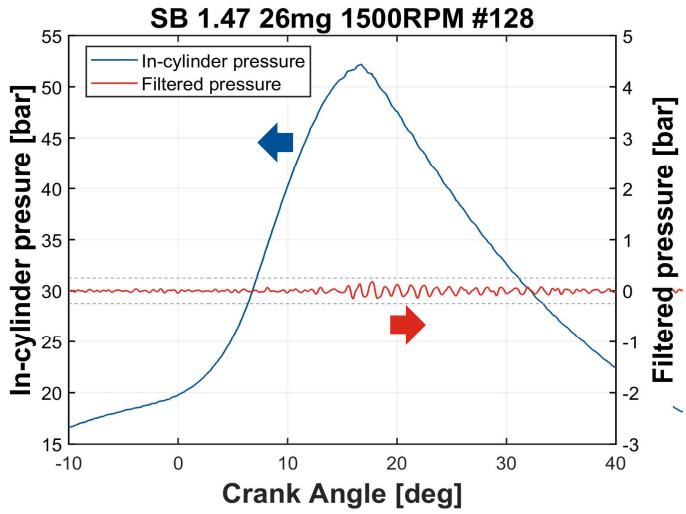

Figure 2.11 Example of in-cylinder and filtered pressure data of non-knock cycle (SB 1.47, 26 mg of fuel rate, and 1500 RPM, # 128 cycle of total 5000 cycles experiment)

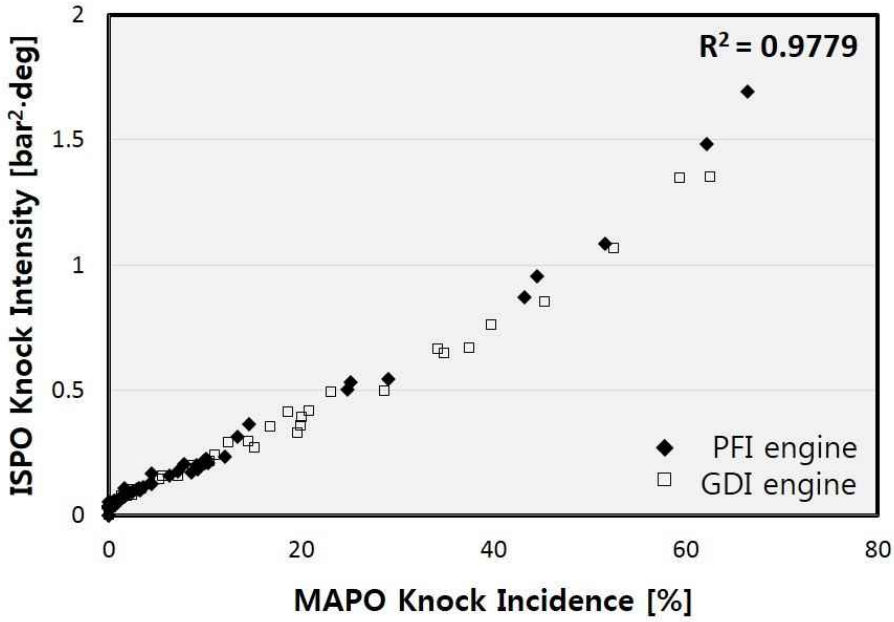

Figure 2.12 Comparison of MAPO knock incidence and ISPO knock intensity, redrawn from [71]

2.2.2 Limitation of knock analysis – averaging process

The major difficulty to conduct knock-related study is its stochastic behavior. The examples related to the issue were plotted in figure 2.13. Many studies dealt with knock-related simulation used unburned mass fraction as a represent value of knock intensity in simulation [81]. It can be indirectly proved by the notion used in many studies related to pre-ignition phenomena [82, 83] – abnormally strong knock intensity occurs with pre-ignition phenomenon, where the unburned mass fraction was theoretically unity. Although the notion mentioned above was known to be empirically correct, however, almost no correlation was achieved between unburned mass fraction and MAPO, shown in figure 2.13 with its R^2 was lower than 0.1. It can be explained by the random distribution of hot spot inducing autoignition – even if the same unburned mass and volume remains at the same crank angle, the existence and size of hot spots can be distributed randomly, depending on the results that were performed before the relevant timing. Therefore, random distribution of MAPO values for same unburned mass fraction can occur, shown in figure 2.13. One thing should be noted that the tendency expressed as a solid line in figure 2.13 implies positive correlation between unburned mass fraction and MAPO, despite bad R^2. Therefore, it can be interpreted as a random distribution but with a specific tendency related to the empirical notion. Kim et al. [76] investigated these issues by displaying MAPO values for each section of unburned mass fraction, redrawn in figure 2.14. In the method from the reference, the section of unburned mass fraction was chosen to allocate similar number of cycles for each section. Based on the results of this method, aforementioned behavior predicted by empirical point of view can be proved – log-normal distribution was detected for each section and clear tendency by moving its distribution toward right (direction of increment in MAPO) was found.

In this work, same method suggested by [76] was also used. In the case of selecting a parameter used as a basis for dividing a section, unburned mass fraction and initial flame speed were chosen, where the reason of selecting the latter will be covered in chapter 6. The example of averaging process with divided sections was shown in figure 2.15, which showed good correlation compared to that expressed in figure 2.13.

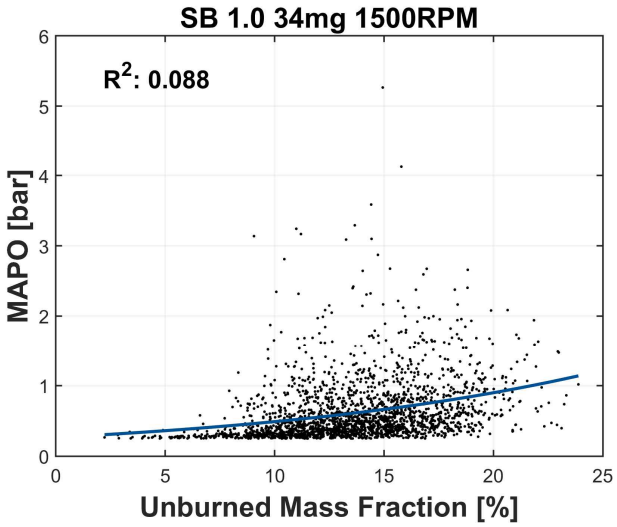

Figure 2.13 Example of the stochastic knock behavior (SB 1.0, 34 mg of fuel rate, 1500 RPM)

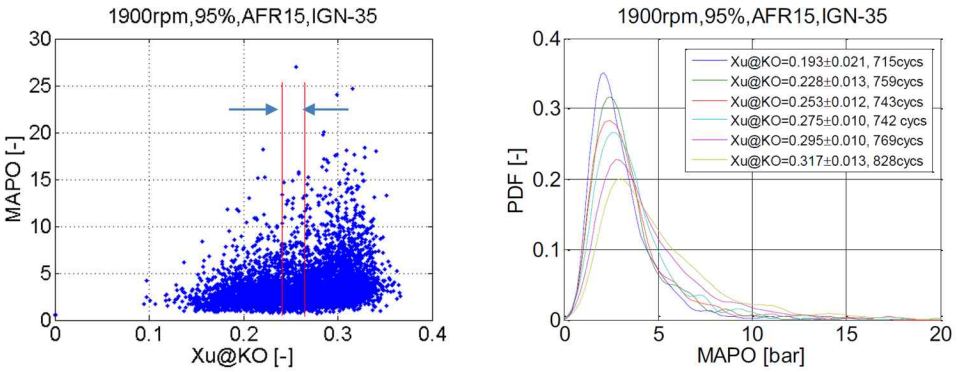

Figure 2.14 Example of section-divided averaging method redrawn from [76]
(a): Guideline for averaging method by unburned mass fraction
(b): Results of averaging method

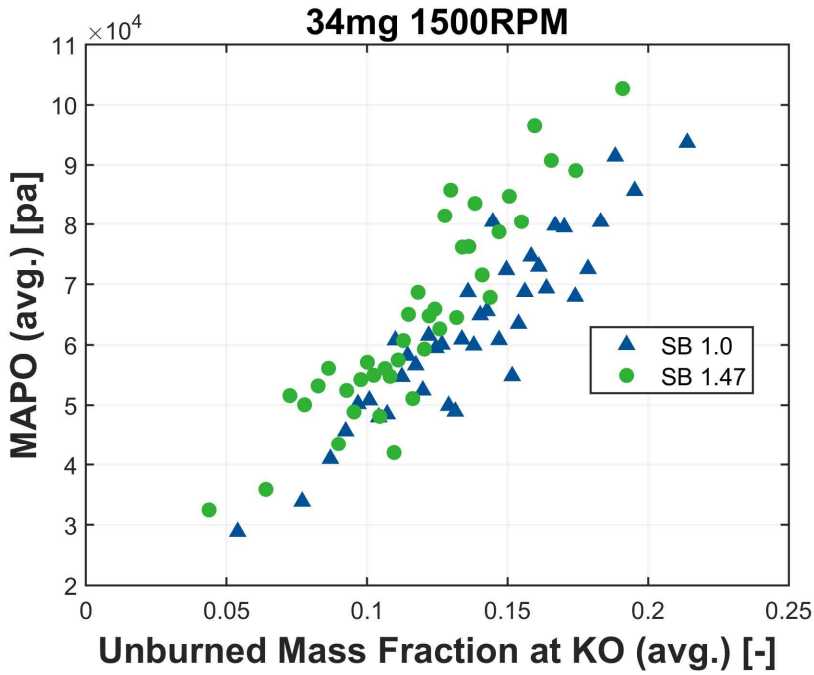

Figure 2.15 Example of the result of averaging method (SB 1.0 and 1.47, 34 mg of fuel rate, 1500 RPM)
x-axis: averaged unburned mass fraction at knock onset
y-axis: averaged MAPO by each section of unburned mass fraction

2.3 0D simulation of SI engine operation

In general, there are two purposes for simulation studies to be used – one is to correlate existing experimental data so that the phenomena which cannot be seen from the experimental results can be predicted. The other is to independently investigate specific phenomenon by controlling factors that cannot be controlled and/or constrained in real experiments. In this study, the latter one was chosen as a main purpose of conducting simulation study to supplement the existing experimental data.

2.3.1 Basic information

As will be mentioned in the simulation section in chapter 5 and 6, the main purposes of the simulation process were summarized as two ways.

1) The effect of heat transfer on the energy balance and exergy destruction in closed duration – related to chapter 5

2) Quantification of work loss due to the different characteristics of knock phenomena for each SB ratio condition – related to chapter 6

It should be noted that considering the purposes, gas exchange process was not modeled in the simulation – only compression and expansion stroke with combustion process were considered.

For the details of the model, conducted was 0D based, two-zone based modeling which was modified from the previous study [84]. MATLAB software and Cantera toolbox [53] were used as main tools of simulation. In order to obtain thermodynamic properties for each crank angle and autoignition-related

properties for each temperature and pressure condition, detailed gasoline surrogate mechanism [85] was used. Same conditions of engine geometries in the experiment were used such as stroke, bore, connecting rod and compression ratio, except for certain topics related to knock issues in chapter 6. The details of simulation conditions were listed in table 2.2.

Basic assumptions of simulation process were listed below (each term was denoted as A1, A2, A3, and A4)

1) IVC and EVO timing were set to intake BDC (-180 CA aTDC) and expansion BDC (180 CA aTDC), which were different from the actual conditions in the experiments. Even if the same crank angle is set for the important valve timing (e.g. IVC timing) and the displacement volume and (nominal) compression ratio are constant for each SB ratio, instantaneous volume can be different for each SB ratio, which induces difference in actual compression and expansion ratio. It is attributed by the difference of the ratio of stroke and connecting rod caused by packaging issue.

2) The composition of intake mixture, comprised of stoichiometric mixture of PRF91.5 with air and residual of which amount was brought from the relevant experimental condition, was used as an initial condition of mixture and unburned gas composition during combustion process. In addition, the composition of complete combustion products relevant to the intake mixture was used as a burned gas composition.

3) For heat transfer estimation, Hohenberg [86] heat transfer correlation was used to evaluate convective heat transfer coefficients for unburned and burned zone, where the formula was listed in eq. 2.20 and eq. 2.21. In addition, adiabatic process was also used.

$$H(\theta) = 130\,P(\theta)^{0.8}\left(S_p + 1.4\right)^{0.8} V(\theta)^{-0.06}\,T(\theta)^{-0.4} \qquad \text{eq. 2.20}$$

$$S_p = 2(S)(RPM)/60 \qquad \text{eq. 2.21}$$

Here, the units of each parameter were listed; H [W/m^{2}K], P [bar], S_p [m/s], V [m3], and T [K]. It should be noted that only velocity term ($S_p + 1.4$) induced by Reynolds number [18] was cycle-averaged value with using mean piston speed.

4) Only combustion-related reaction (mass transfer from the unburned zone to burned zone), predicted by Wiebe function, and heat transfer were considered. That is, autoignition and dissociation which can occur in the unburned and burned zone, respectively, were not applied to simulation.

For the simplicity of simulation with satisfaction of its purposes, Wiebe function, a well-known function which can properly simulate combustion phasing in real SI engine, was used, where the formula was listed in eq. 5.1 [18].

$$y_b(\theta) = M\,FB(\theta) = 1 - exp\left[-a\left(\frac{\theta - \theta_0}{\Delta\theta}\right)^{m+1}\right] \qquad \text{eq. 2.22}$$

Here, θ_0 is spark timing, $\Delta\theta$ is the total combustion duration and the values of a and m are suggested to 5 and 2, respectively, corresponding to actual operation [18]. It should be noted that if the definition of $\Delta\theta$ is related to the spark timing (i.e. start from the spark timing to certain point), a can be derived automatically. Thus, this function has two free variables. In this work,

different approach related to the coefficients in Wiebe function was conducted, which was described below.

1) $\Delta\theta$ was defined as initial burn duration (denoted as IBD) of which definition is the period from spark timing to CA10. According to this,

$$a = -bg\ (1 - 0.1) \qquad \text{eq. 2.23}$$

was derived.

2) After that, main burn duration (denoted as MBD) of which definition is the period from CA10 to CA70 and initial burn duration was used to calculate the m coefficient, where the related equations were listed below.

$$0.7 = 1 - exp\left[-a\left(\frac{IBD + MBD}{IBD}\right)^{m+1}\right] \qquad \text{eq. 2.24}$$

$$m = \frac{bg\ [bg\ (1 - 0.7)/bg\ (1 - 0.1)]}{bg\ [(IBD + MBD)/IBD\ ]} \qquad \text{eq. 2.25}$$

It should be noted that when the variables used for calculation are determined (in this case, IBD and MBD), coefficient m and combustion phasing ($MFB(\theta)$) do not change – only a and $\Delta\theta$ are changed. The reason for usage of CA70 as a main parameter for MBD is that most cases of knock onset timing in the experiments were located after CA70. Because the pressure equilibrium assumption for entire cylinder is broken after knock occurs, this approach is reasonable.

Details of the determination of thermodynamic properties were described below, many of which were referred from the reference [84]. First, the energy conservation (1st law of thermodynamics) was applied to both the unburned and burned zone which were listed in eq. 2.26 and eq. 2.27, respectively, followed by the equations corresponding to each term used in eq. 2.26 and eq. 2.27.

$$0 = \frac{dm_b}{dt} h_u + \frac{dQ_u}{dt} + P\frac{dV_u}{dt} + \frac{dU_u}{dt} \qquad \text{eq. 2.26}$$

$$\frac{dm_b}{dt} h_u = \frac{dQ_b}{dt} + P\frac{dV_b}{dt} + \frac{dU_b}{dt} \qquad \text{eq. 2.27}$$

$$\frac{dQ_u}{dt} = H_u A_u (T_u - T_{wall}) \qquad \text{eq. 2.28}$$

$$\frac{dQ_b}{dt} = H_b A_b (T_b - T_{wall}) \qquad \text{eq. 2.29}$$

$$\begin{aligned} \frac{dm_b}{dt} &= m_{cycle} \frac{dx_b}{dt} \\ &= m_{cycle} \frac{d\theta}{dt} \left[exp\left(-a\left(\frac{\theta - \theta_0}{\Delta\theta}\right)^{m+1} \right) \frac{a}{\Delta\theta^{m+1}} (\theta - \theta_0)^m \right] \end{aligned} \qquad \text{eq. 2.30}$$

Using ideal gas law ($PV = m\,RT$) and mass conservation during closed duration, another governing equation can be obtained for unburned and burned zone.

$$\frac{dP}{dt}V_u + P\frac{dV_u}{dt} = \frac{dm_u}{dt}R_uT_u - \frac{m_uR_uT_u}{MW_u}\frac{d(MW_u)}{dt} + m_uR_u\frac{dT_u}{dt} \quad \text{eq. 2.31}$$

$$\frac{dP}{dt}V_b + P\frac{dV_b}{dt} = \frac{dm_b}{dt}R_bT_b - \frac{m_bR_bT_b}{MW_b}\frac{d(MW_b)}{dt} + m_bR_b\frac{dT_b}{dt} \quad \text{eq. 2.32}$$

$$dm_u + dm_b = 0 \quad \text{eq. 2.33}$$

Noted that the second terms of RHS for eq. 2.31 and eq. 2.32 were removed due to the A4. In addition, volume constraint caused by engine operation was required for each crank angle.

$$V_u + V_b = \frac{m_uR_uT_u + m_bR_bT_b}{P} = V \quad \text{eq. 2.34}$$

Using all the equations from eq. 2.26 to eq. 5.1, final form of governing equations related to the important thermodynamic properties were obtained.

$$\frac{dT_u}{dt} = \frac{1}{m_u c_{p,u}}\left(\frac{dP}{dt}V_u - \frac{dQ_u}{dt}\right) \qquad \text{eq. 2.35}$$

$$\frac{dT_b}{dt} = \frac{1}{m_b c_{p,b}}\left(\frac{dP}{dt}V_b - \frac{dQ_b}{dt} + \frac{dm_b}{dt}(h_u - h_b)\right) \qquad \text{eq. 2.36}$$

$$\frac{dP}{dt} = \frac{\left\{\frac{dm_b}{dt}\left[\frac{R_b}{c_{p,b}}(h_u - h_b) - R_u T_u + R_b T_b\right] - \left[\frac{R_u}{c_{p,u}}\frac{dQ_u}{dt} + \frac{R_b}{c_{p,b}}\frac{dQ_b}{dt}\right] - P\frac{dV}{dt}\right\}}{\left[V - \frac{R_u}{c_{p,u}}(V_u) - \frac{R_b}{c_{p,b}}(V_b)\right]}$$

eq. 2.37

Table 2.2 Detailed conditions used for 0D simulation

Fuel		PRF 91.5 (same RON with gasoline for exp.)
Valve timing*		IVC at -180 CA EVO at 180 CA
Combustion model		Wiebe function
Reaction mechanism		Detailed gasoline surrogate mechanism [85]
Heat transfer		Hohenberg [86] or Adiabatic
Initial condition (i.e. IVC)	Pressure	1 bar
	Temperature	380 K
	Residual mass fraction	7%
Geometries		Relevant conditions from exp. (i.e. three SB ratio and same compression ratio)

*Only compression and expansion strokes were conducted.

2.3.2 Autoignition determination – Livengood-Wu integration model

In order to predict the knock onset timing in SI engine simulation, used was Livengood-Wu integration model [87] of which equation was listed below.

$$\int_{t=t_0}^{t_{onset}} \frac{1}{\tau_{ig}\,(T,\ P,\ x, \ldots)}\,dt = 1 \qquad \text{eq. 2.38}$$

Here, τ_{ig} is the ignition delay at relevant temperature, pressure, and composition. With an empirical approach by engine and RCM experiments, many of previous studies had investigated the relationship between the value of τ_{ig} and relevant parameters such as temperature, pressure, octane number [88], equivalence ratio [89], cooled EGR fraction [90], and (internal) residual mass fraction [91]. Instead of this, mechanism-based ignition delay was also used as an input of Livengood-Wu model [92], due to its simplicity. Since the main fuel for the simulation in this work was PRF 91.5 comprised of iso-octane and n-heptane of which information related to the elementary reaction and its rate was well-defined, the latter way was used. In order to conduct a preliminary calculation of ignition delay corresponding to relevant temperature, pressure, and residual mass fraction, used was constant volume reactor model from the reference [84].

In figure 2.16, calculated ignition delay was plotted with various temperature and pressure conditions. The unit of ignition delay expressed at iso-ignition delay curve is millisecond. The intervals of temperature and pressure were set to 5 K and 1 bar, respectively, and 2D spline interpolation was conducted to find the ignition delay corresponding to the temperature and pressure values at the relevant crank angle. The residual mass fraction was determined from the relevant

experimental data of which fuel rate (i.e. load) was similar to that of simulation conducted.

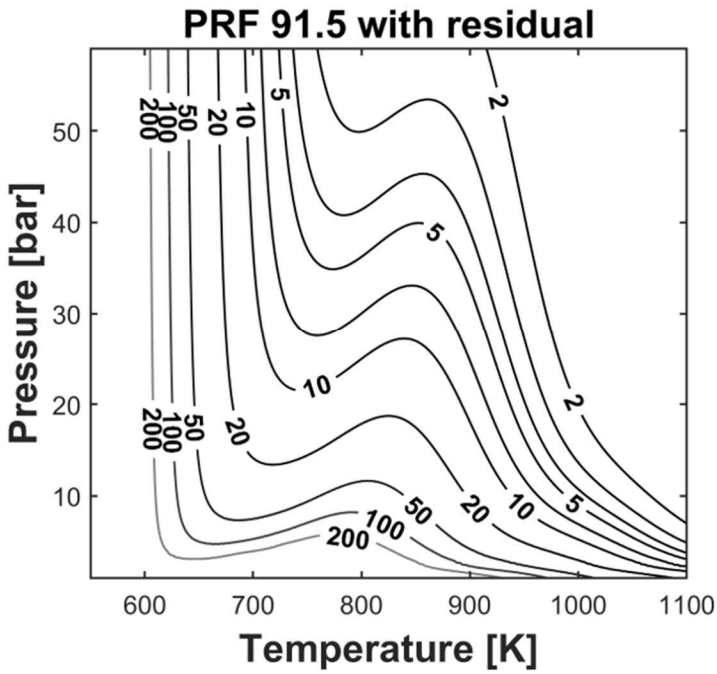

Figure 2.16 Ignition delay map from constant-volume chamber simulation. The value at each iso-ignition delay line means ignition delay with millisecond unit.

2.3.3 Determination of knock-limited condition

The most cases of 0D SI engine simulation, including the one used in this study, assumed steady operation and homogenous conditions for each zone (mixture, temperature and, of course, pressure). Therefore, two things highly related to actual knock phenomena cannot be predicted. First, knock incidence used to define knock occurrence in the experiments cannot be directly predicted, since the cyclic variation, which is the main source of stochastic knock behavior [76], cannot be predicted in usual 0D simulation. Second, knock intensity caused by pressure oscillation cannot be predicted – when the autoignition occurs in the simulation, all the mixture inside the unburned zone reacts spontaneously, corresponding to enormous super-knock situation in real engine operation which was not the scope of this work – knock condition related. In general, knock phenomena corresponding to the experiments were arose by the autoignition from hot spot in the unburned zone, where the heat release speed of the autoignition was too fast to equilibrate pressure with other mixture, i.e. pressure oscillation [30]. Therefore, with an assumption of homogeneity mentioned above, knock intensity cannot be estimated.

Because of this, indirect prediction of knock intensity was achieved before [81] by using, for example, unburned mass fraction or related term, as mentioned in chapter 2.2.2. However, many of these were not directly validated by experimental data – only trends inferred from the theoretical and empirical view were added to establish 'simulated' knock intensity for conducting their simulation. Therefore, with a solid validation by the experiments conducted in this study, new concept of knock intensity was suggested and used to analyze and limit the simulation process, which will be comprehensively mentioned and investigated in chapter 6.

Chapter 3. Experimental Apparatus

3.1 Experimental configuration

3.1.1 Single cylinder engine

In this work, single cylinder, direct-injected spark ignition engine of which design is based on the Ricardo hydra single-cylinder research engines [93] was used. Since the experiment processes included delicate knock measurements and the data analyzing process of small difference among the various SB ratios, all the setup devices should be installed carefully. In addition, one can claim the possibility of assembly error which is able to occur when the geometry is changed from one condition to another. Since a lot of parts should be replaced – around 36 parts of moving system such as crankshaft, connecting rod, and piston, 38 parts of crank case assembly such as timing belt tensioner, 9 parts of cylinder block assembly such as shim plate and liner – for just one change of geometry, the assembly rule was formulated such as tightening torque for shim plate, timing belt assembly. Through several references [73, 94-96], the important issues related to the measuring and parameters setting processes were able to be applied to the engine design and experiment. In this section, only hardware-related (i.e. engine) design issues were reviewed. The details of other issues such as data acquisition and treatment will be mentioned in chapter 3.2.

In order to accurately measure the in-cylinder pressure data, especially in case of knock-related measurement, the pressure transducer was installed at the biased position toward the front of the engine [73]. Single spark plug was located at the center of combustion chamber, as similar to mass production modern

engines. Side-mounted fuel injector, located at the side of intake valve, was used to mainly obtain charge cooling effect for knock mitigation [18]. The flow path of engine coolant was designed to pass the cylinder head and cylinder block separately, where each path was controlled independently. The oil path was built in the crankcase and cylinder head to lubricate the rotating pars such as crankshaft and camshaft. Between the throttle and intake manifold, a plenum was installed to minimize the pressure wave inside the intake manifold. The intake port and angle of valve position was designed to get enhanced flow motion (usually described as tumble motion in SI engine) of the state-of-the-art mass production engine, where around 1.2 to 1.5 was the value of tumble ratio defined from [97]. The details of cylinder head tumble ratio corresponding to various SB ratio conditions will be covered in chapter 3.1.3.

The CVVT system was installed in the engine system to estimate the effect of valve timing (both intake and exhaust) which will be comprehensively covered in chapter 4. In order to apply the state-of-the-art strategies for high-efficient SI engine, LIVC operation (also known as Atkinson cycle, which is not proper usage) was adapted by designing long duration of intake camshaft of which duration is set to 280 CA, where the duration of exhaust valve was set to 240 CA. Since the closing and opening event vary simultaneously, attributed to its design, one effect related to various closing timing and the other effect related to various opening timing should be considered at once.

The engine image and description of valve timing variation was plotted in figure 3.1 and 3.2. Also, important values for engine design except displacement volume (covered in chapter 3.1.3) were listed in table 3.1.

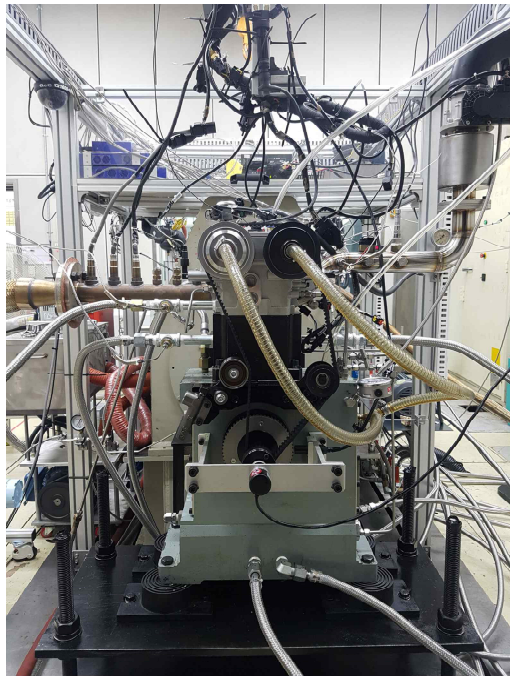

Figure 3.1 Single cylinder DISI engine

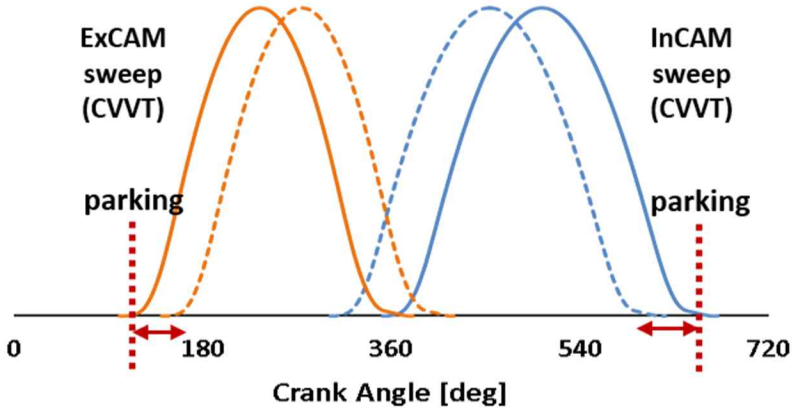

Figure 3.2 Details of CVVT operations

Table 3.1 Details of engine hardware and CVVT

Number of Cylinder		1
Compression Ratio [-]		12 ± 0.1*
Number of Valves		4 (IN 2, EX 2)
Default Valve Timing [CA**]	IVO	-350
	IVC	-70
	EVO	121
	EVC	-359
Max.Valve Lift [mm]	Intake	9.5
	Exhaust	9.5
Moving Range [CA]	Intake	50 (advance from default)
	Exhaust	40 (retard from default)
SOI [CA aTDC]		-315
Rotational Speed [RPM]		1500, 2000

*directly measured. ** 0 CAD at firing TDC

3.1.2 Measurement and test facility

In order to analyze the experimental data, several parameters related to engine performance were measured by many devices. First of all, measured was the temperature at the ambient engine cell, intake manifold, exhaust manifold, oil path, coolant in and out, and supercharger intake port with K type thermocouples. Absolute pressure was measured at intake and exhaust manifold, where the resolution of its acquisition is 0.1 CA, same as in-cylinder pressure. In fact, all pressure data were measured with 0.1 CA resolution with an aid of a 3600 ppr (pulse per revolution) encoder mounted at the front of crankshaft. The intake pressure was measured by using a Kistler type 4045A5 absolute pressure sensor and a Kistler type 4603 piezoresistive amplifier. A Kistler 6056 flush-mounted piezoelectric pressure sensor was used to measure the in-cylinder pressure, and an AVL Indi Micro IFEM was used to amplify the charges measured from the pressure sensor. The in-cylinder pressure, intake pressure and encoder signals from each device were finally measured with AVL INDIMODULE device. For all experiments except knock characteristics analysis, total 300 cycles were logged and ensemble-averaged to calculate the parameters related to engine performance; for knock-related experiment, 5000 cycles were logged. For precise measurement of the fuel flow rate, an OVAL CA001 Coriolis fuel flow meter was used, and the results of the three-minute operation were averaged during data logging process. A HORIBA MEXA-7100 DEGR Exhaust Analyzer was used to measure the composition of main emissions for SI engine, i.e. THC, NOx, and CO, and the other species (CO_2, O_2) in the exhaust gas, which was used to estimate the combustion efficiency. ETAS ES631.1 was used to measure the equivalence ratio of engine mixture, where the equivalence ratio was set to unity for all experimental conditions. The schematic of measuring and controlling devices was plotted in figure 3.3.

The ECU (engine control unit) was modified and used for almost all the experiments to control the valve timing variation by CVVT module, throttle position, fuel injection pressure, rate and timing, and spark timing, with ETAS INCA 7.0 software. Since the resolution of spark timing controlled by ECU was set to 0.75 deg by the gap of target wheel's ticks attached to the front of crankshaft, LabVIEW software with National Instrument cRIO-9039 platform was used to control the spark timing with 0.1 CA resolution and measure the knock incidence and intensity in real time, where the control system had been also used in the previous works [71, 72, 98-100].

190 kW ELIN AC dynamometer was linked through the coupling shaft attached to both dynamometer and flywheel of single cylinder engine. Since the knock characteristics are sensitively affected by the ambient temperature and coolant temperature [71], test cell ambient temperatures were controlled by an air conditioning system, and each coolant (for cylinder head and cylinder block – liner) and oil temperature was also maintained by pump and controller integrated systems. The ambient pressure, highly affected by weather conditions, was set to 1.008 bar ± 0.005 bar. The details of controlled parameters were listed in table 3.2. Also, the measured parameters were listed in figure 3.4.

Finally, tested fuel was Korean gasoline of which octane number is 91.5. The H/C ratio of gasoline was used to estimate the total mass of air inducted successfully, despite lack of information for the composition of gasoline. This information was used to analyze the combustion phenomena inside the cylinder. The details of fuel information were listed in table 3.3.

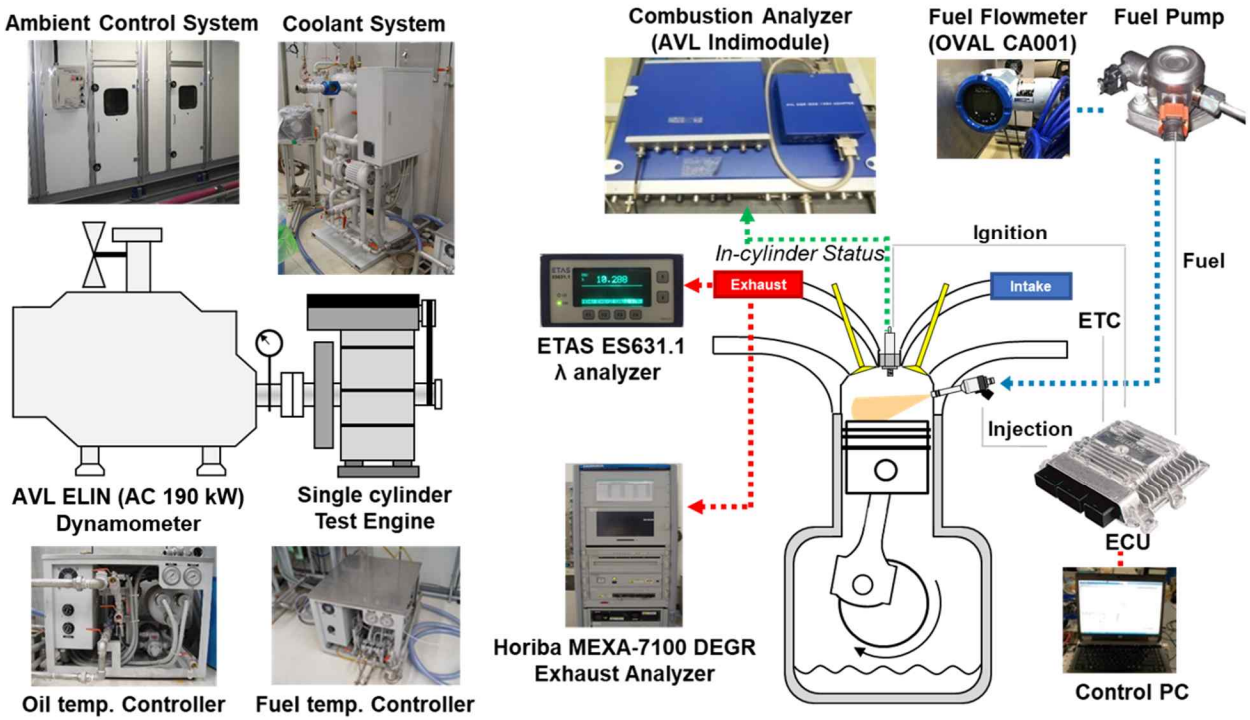

Figure 3.3 Test Facilities for measurement and control processes

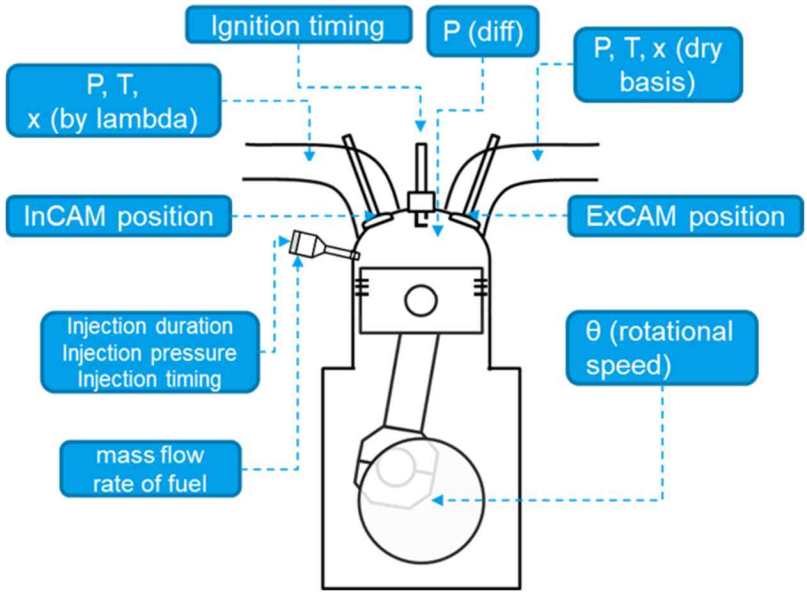

Figure 3.4 Engine parameters measured and controlled in the experiment

Table 3.2 Control target of temperature and pressure in the experiment

Temperature [℃]	Coolant	85 ± 1
	Oil	85 ± 1
	Fuel	30 ± 2
	Ambient	24 ± 2
Pressure	Ambient	1.008 ± 0.005
Relative Humidity [%]	Ambient	50 ± 15

Table 3.3 Information for gasoline used in the experiment

Conventional gasoline	Value	Test Method
H/C ratio	2.064	ASTM D 5291
Density [kg/m^3] @ 15°C	724.5	ASTM D 1298
Research Octane Number	91.5	ASTM D 2699
LHV [MJ/kg]	42.825	ASTM D 240-14
Oxygen [mass %]	1.53	ASTM D 4815
Methanol [mass %]	< 0.05	ASTM D 4815

3.1.3 Experimental conditions – stroke-to-bore ratio, displacement volume, and tumble ratio

As mentioned in chapter 1, approaches to validate the effect of various stroke-to-bore ratios with fixed compression ratio and displacement volume were very complicated but, at the same time, the main novelty of this work. The most intricate thing is to design those requirements with same crankcase and cylinder block. Therefore, the details of varying stroke-to-bore ratio will be reviewed in this chapter.

Five different stroke-to-bore ratios and two different tumble ratios (by different cylinder head) were used in this work. The summary was listed in table 3.4. Since the main goal of the study is to identify independently the effects of changes in SB ratio, the following variables were controlled either by hardware or by experimental methodologies. It is noted that the displacement volume was fixed to 500 cm^3 for five conditions and 593 cm^3 for two conditions by designing custom cylinder head, piston, crankshaft and connecting rod. In order to operate five different SB ratios in the same crankcase, all the piston and crank offsets were fixed at 0, and each absolute height of piston (at TDC) was designed to be the same by adjusting the length of connecting rod which is called 'packaging constraint' – related to the actual process of engine design. Since the actual design of mass production engine is restricted by size of engine room, the sum of stroke and connecting rod is normally limited; if stroke is lengthened, connecting rod should be shortened to maintain their summation. Although it will be mentioned after, this constraint makes remarkable difference in engine performance. In order to maintain same clearance volume for its displacement volume and compression

ratio, piston surface for each geometry condition was made with different bowl. The details of the design were described in figure 3.5 and 3.6.

Total seven conditions were investigated. As described in figure 3.5, those conditions were classified into three groups, as listed below.

1) Basic conditions:
   SB 1.0, 1.2, and 1.47 conditions with same compression ratio (12:1), displacement volume (~500 cm^3), and similar cylinder head tumble ratio (~ 1.35)

2) Changes in displacement volume (referred as Vd in figure 3.5):
   SB 1.19, and 1.42 conditions with same compression ratio (12:1) and similar SB ratio (1.2 vs. 1.19, and 1.47 vs. 1.42) compared to basic conditions

3) Changes in cylinder tumble ratio (referred as Rt in figure 3.5)
   SB 1.2, and 1.47 conditions with same compression ratio (12:1) and displacement volume (~ 500cm^3) compared to basic conditions.

First, 'Basic conditions' contains three different SB ratios (1.0, 1.2, and 1.47) with same compression ratio, displacement volume (~ 500 cm^3), and similar cylinder head tumble ratio. With these, preliminary experiment – valve timing sweep to find the best efficiency – was conducted, which will be comprehensively covered in chapter 4. Second, for 'Changes in displacement volume', higher displacement volume (~ 593 cm^3) compared to that of 'Basic conditions' was applied with same compression ratio and similar SB ratio. The main purpose of this design is to isolate the effect of SB ratio and displacement volume for heat transfer phenomena inside the cylinder, as mentioned in chapter 1. Finally, for 'Changes in cylinder tumble ratio', higher cylinder tumble ratio compared to that

of ‘Basic conditions’ was applied by changing cylinder head, with same compression ratio and displacement volume. Since increasing SB ratio or tumble ratio is related to faster burning rate by enhancing flow characteristics [Filipi] [Nakata], the main purpose of this design is to quantitatively evaluate the degree of increment in thermal efficiency by faster burning rate, caused by SB ratio and tumble ratio.

Here, one thing should be noted. Because of the purpose of efficient design, same cylinder head was shared for certain conditions. The tumble ratio of each cylinder head was estimated by using steady rig facility including superflow bench of Ricardo [101], where the definition and related terms were listed below by referencing [97].

$$N_r = \frac{8M}{\dot{m}V_0B} \qquad \text{eq. 3.1}$$

$$R_t = \frac{L_d \int_{\alpha_1}^{\alpha_2} C_f N_r d\alpha}{\left(\int_{\alpha_1}^{\alpha_2} C_f d\alpha\right)^2} \qquad \text{eq. 3.2}$$

$$L_d = \frac{BS}{n_v D_v^2} \qquad \text{eq. 3.3}$$

In this reference, N_r is called ‘non-dimensional tumble ratio’, where M is the torque value measured at the part of the ‘T-type tumble adaptor’ in steady rig facility, $\dot{m}$ is measured flow rate, V_0 is theoretical intake flow velocity and B is

bore length. Based on this value, the tumble ratio of the cylinder head was evaluated, referred as R_t, where the definition of L_d is listed in eq. 5.1. α_1 and α_2 are IVO and IVC crank angle, C_f is flow coefficient of which value is directly measured in the superflow bench test facility, S is stroke length, n_v is number of intake valves, and finally D_v is intake valve diameter. It is noted that based on the definition mentioned above, R_t is allocated for not only the cylinder head itself but also stroke length; even if the same cylinder was used, R_t can be different for shared conditions in terms of its definition (e.g. SB 1.2 and 1.47 for basic conditions). However, since no piston movement was applied during the measurement of R_t (only in the definition), it was assumed that the different performance caused by the effect of stroke in definition of R_t is the result under the many of control variables (e.g. compression ratio, tumble ratio) so that it should be treated as a part of result, not a control variable.

The cylinder heads used in this work were named by A, B, and C, as described in figure 3.7. Here, cylinder head A and its tumble ratio was designed and estimated based on the SB 1.0 condition (bore 86 mm). In the case of cylinder head B, SB 1.47 condition (bore 75.6 mm) was set to its criterion for design and the tumble ratio. It is noted that the values of tumble ratio for cylinder head A and B were intentionally set to similar degree (~ 1.35), in order to conduct 'basic conditions' experiment with tumble ratio as a control varible. Finally, cylinder head C was designed based on the same bore size of cylinder B (bore 75.6 mm), but its tumble ratio was enhanced compared to that of cylinder head B, by using different specification of intake port design.

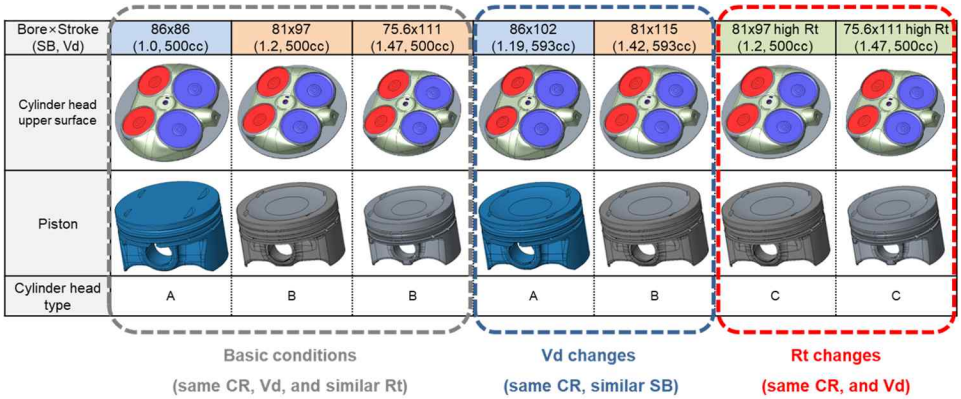

Figure 3.5 Total geometry conditions for the experiment

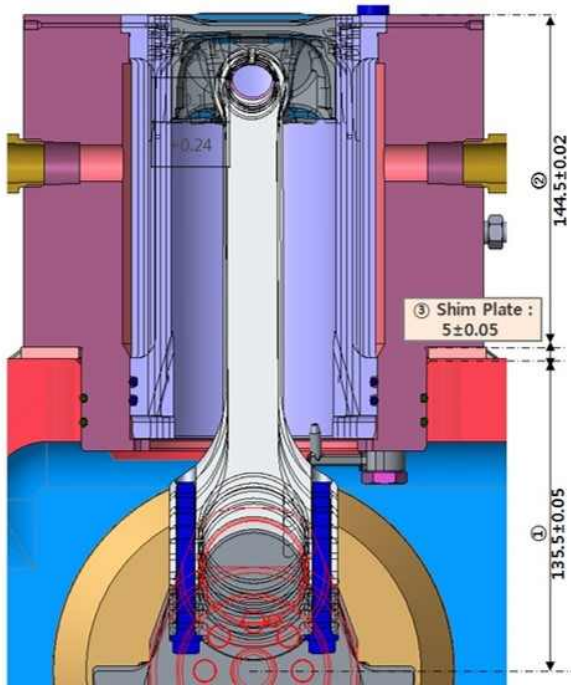

Figure 3.6 Details of the design related to packaging constraint

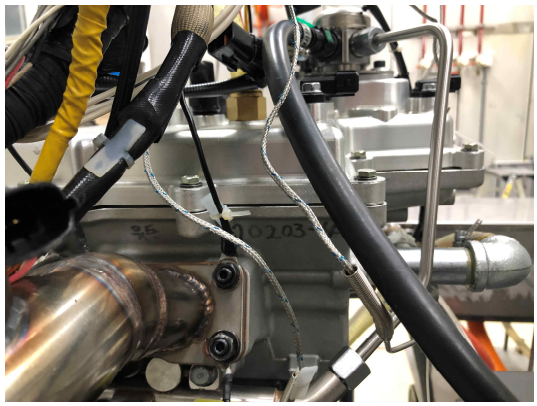

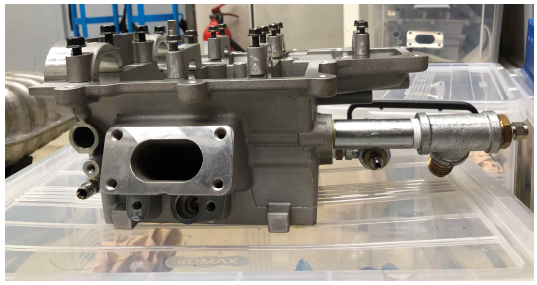

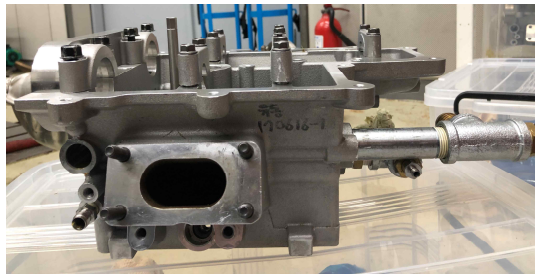

Figure 3.7 The cylinder heads (upper: A, middle: B, lower: C)

Table 3.4 Detailed information of stroke-to-bore ratio and Rt conditions

SB ratio [-]	1.00	1.20	1.47	1.19	1.42	1.20	1.47
Bore [mm]	86	81	75.6	86	81	81	75.6
Stroke [mm]	86	97	111	102	115	97	111
Connecting Rod [mm]	211.65	207.65	199.15	203.65	197.05	207.65	199.15
Displacement [cm^3]	499.6	499.8	498.3	592.5	592.6	499.8	498.3
Cylinder Head	A	B	B	A	B	C	C
Tumble ratio of cylinder head [96]	1.36	-	1.34	-	-	-	1.58

3.2 Approach on the reliability of data acquisition and analysis

As mentioned in chapter 3.1, the data from the experiments have very small difference for each other, which needs very accurate experimental setup, methodologies and data analysis. In this chapter, the processes conducted for reliable data acquisition and analysis will be covered.

Based on the references [73, 94-96] mentioned earlier, reviewed and listed below were the key things for reliable data acquisition and treatment for engine experiment, especially including knock-related conditions.

- In order to accurately measure the knock phenomena, crank angle resolution of at least 0.2 deg for in-cylinder pressure data acquisition should be needed [95]. In this work, 0.1 deg was set as the crank angle resolution of in-cylinder pressure data. For reference, around 10 deg of resolution was enough to obtain reliable nIMEP data [95].

- Since an in-cylinder pressure transducer normally used in lab-scale experiment is based on differential pressure sensing technic, it is required to reference accurate absolute pressure (called 'pegging' process) obtained by several techniques – absolute intake pressure signal and polytropic method [96]. In this work, absolute intake pressure was used to reference in-cylinder pressure data. In the process of pegging the differential pressure value of the in-cylinder pressure sensor, a flow stall was assumed before and after the intake BDC 2 CA, and the average value of the intake manifold pressure at this range was assumed to be equal to the cylinder pressure. Since the pegging process showed

significant effect on the calculation of combustion phasing [94], at least 150 cycles and 1 CA resolution were recommended, where 300 cycles (or 5000 cycles for knock-related situation) and 0.1 CA resolution were applied in this work.

- Since knock phenomena have very stochastic behavior, reported by many works [72, 73], it is important to obtain many cycles for minimizing such stochastic-related results; minimum 1000 cycles were suggested for knock experiments [73]. In this work, 5000 cycles were logged for knock-focused experiments of which results will be mainly covered in chapter 6. For the other experiments including knock-free and knock-related conditions, 300 cycles were logged. However, before the final logging process of knock-related condition, at least 1000 cycles were observed to find whether the ignition timing is knock-limited or not.

- In order to prevent knock-induced transducer resonance, a pressure transducer for measuring in-cylinder pressure should have very high natural frequency over 100 kHz [73]. Also, flush-mounted in-cylinder pressure transducer (i.e. no clearance volume between the tip of transducer and combustion chamber) was suggested to remove unintended pressure oscillation related to high frequency region.

As described, the process related to measure in-cylinder pressure is the most important thing for data acquisition. Here, covered was the process to minimize the error induced from several effects including daily weather, valve timing, and details of data acquisition process.

First, daily weather, especially ambient temperature and humidity, can affect the knock characteristics. Since knock phenomena is very delicate phenomena – only 0.1 deg change in spark timing can result in 1-3 % changes in knock

incidence, ambient temperature and humidity were controlled by air condition system of engine test cell, where the controlled range was previously listed in table 3.2.

Second, during the process of camshaft assembly, valve timing can be slightly biased, because of assembly error – reproducibility issue. Since the same camshaft set (intake and exhaust) was used for all experiments, the signal oriented from the structure of camshaft was used to clearly determine exact valve timing. In the figure 3.8, structure of camshaft used in this work was plotted. Here, the part related to the phase of camshaft (called 'half-moon part' in this work) was highlighted in this figure. In detail, the CMPS mounted at the cover of cylinder head measures the absolute position of half-moon part and outputs voltage signal related to the position, plotted in figure 3.9, where the falling signal was highlighted. As referencing this falling signal with certain valve timing (e.g. falling signal of intake camshaft at -162 CA aTDC is related to IVC timing at 110 CA aBDC), assembly error related to valve timing can be removed. One thing should be noted that due to the same reason – reproducibility, the pole value of each valve timing – 0 (parking) and -50 (fully advanced) for intake valve timing and 0 (parking) and +40 (fully retarded) for exhaust valve timing – may not be reproduced, which can be confirmed by absolute half-moon signal mentioned above. The maximum error which can occur during assembling process of valve-related parts was empirically found to be around ± 2 crank angle. Thus, in the univariate experiment, mainly covered in chapter 4, the valve timing was changed within the range reduced by 5 crank angle at both poles – i.e. total 10 crank angle was reduced from the original moving range listed in table 3.1.

Finally, details of pressure referencing process related to TDC calibration were covered. After each assembly process, TDC position should be set by detecting gap between Z pulse timing from encoder and peak pressure timing of

motoring process. The motoring process related to TDC calibration was conducted at cold motoring conditions where 30 Celsius was set as the coolant and oil temperature. The rotational speed was set to 2500 RPM (practically the highest speed of single cylinder engine without any balancing shaft), considering the error caused by blow-by and any stochastic behavior in heat transfer [TDCaju]. In addition, it was assumed that the difference between peak pressure timing and actual TDC timing (called 'thermodynamic loss angle' [TDCaju]) was set to 0.3 CA for all experiments, where the peak pressure timing occurs firstly, followed by actual TDC timing caused by the heat transfer during motoring process. The value of 0.3 CA was determined by preliminary 3D CFD simulations (not the scope of this work), where the difference of the value among different SB ratios was around 0.05 CA of which amount is lower than crank angle resolution of the experiment. It should be noted that the conditions for motoring process to calibrate TDC timing causes significant changes of engine performance, briefly summarized in table 3.5 – only 0.3 deg error in TDC calibration causes about 1.6 % (rel.) of error in nIMEP calculation. Therefore, for all experiments, TDC calibration process was strictly applied, with same rule mentioned above.

Figure 3.8 Camshaft and the ‘half moon’ part

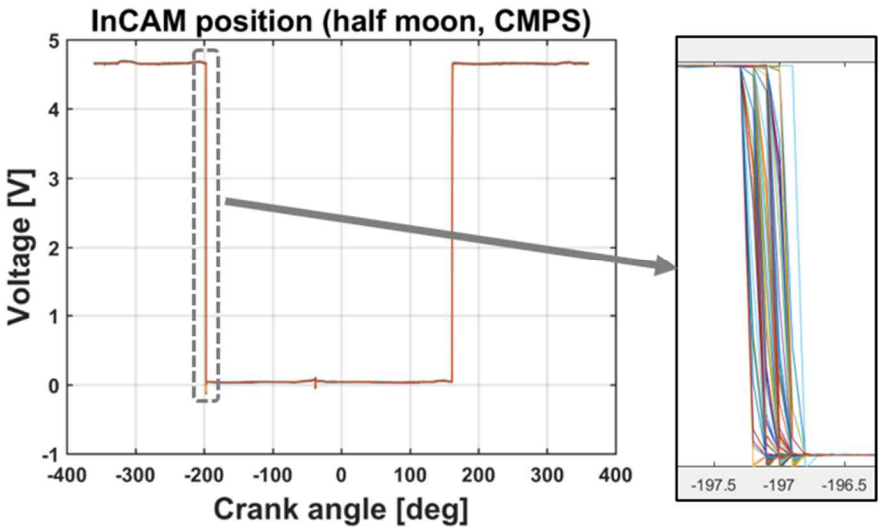

Figure 3.9 CMPS signal derived from absolute position of half-moon part

Table 3.5 Summary of the effect of error in TDC calibration

TDC drift	IMEP [bar]	Difference (%, rel.)
origin	4.5090	-
0.1 deg	4.4848	-0.536%
0.3 deg	4.4363	-1.61%

Chapter 4. Preliminary Experiment – Variable Valve Timing and the Best Efficiency Point

In order to conduct the comparison among all the specifications described in chapter 3.1.2, it is necessary to analyze the results of comprehensive operating conditions for each specification. Based on this, exceeding amount of experiments was performed at each engine load and rotational speed to search the valve timing condition at which the best efficiency was exploited.

In this chapter, firstly, the schemes used for searching were reviewed. From widely-used strategy (i.e. DoE) to full factorial experiment were covered to thoroughly find the best efficiency point. After that, experimental results with various valve timing were presented and discussed for the 'basic conditions' of three SB ratios – 1.0, 1.2, 1.47. With the data and theoretical contents, the valve timing relevant to the best efficiency for each engine load and rotational speed was determined. Finally, same approaches into other specification – varying displacement volume and tumble ratio – were briefly reviewed.

One thing, related to the whole experimental data, should be noted that for the calculation of work from cylinder, net work (including all the strokes – intake, compression, expansion, and exhaust) and gross work (including only two strokes – compression and expansion) were used as a reference of engine performance for N/A and supercharged operation, respectively [98, 100, 102] – i.e. pumping work was not considered in supercharged operation. It was decided by the fact based on thermodynamics that work from supercharger is unintentionally considered during the calculation of total net work. Because of this, pumping work corresponding to the sole result from engine operation cannot be measured. Therefore, for all N/A experiments, net work was used to calculate related-

parameters such as IMEP (nIMEP) and efficiency (net indicated efficiency). Likewise, gross work was used to calculate related-parameters such as IMEP (gIMEP) and efficiency (gross indicated efficiency).

4.1 Scheme for valve timing variation

4.1.1 Univariate search process

First, univariate process for searching best efficiency were reviewed. The essence of this approach is to minimize the experimental process by pre-investigating (i.e. thought experiment) the effect of varying sole manipulated parameter (e.g. intake valve timing) theoretically. For an experiment of which target conditions are low load (e.g. nIMEP 4.5 bar), relatively low speed (e.g. 1500 RPM), for example, fully retarded exhaust valve timing (i.e. increasing actual expansion ratio and valve overlap) will be the condition of the best efficiency by several reasons listed below.

1) Due to the low load condition, intake pressure should be lower than pressure in atmosphere, approximately 0.6-0.7 bar, causing significant pumping loss. Thus, increasing the duration of valve overlap may augment the hot residual gas remaining in the cylinder, causing higher intake pressure to satisfy the required amount of air to be inducted for stoichiometric condition. Because of this, pumping loss will be reduced, being able to be concluded that retarded EVC timing can improve the efficiency at low load condition.

2) It is the essence of non-conventional valve timing strategies (e.g. LIVC, EIVC) to make actual compression and expansion ratio different. One

misconception which may occur should be revised that higher compression ratio itself does not significantly increase the efficiency of engine operation[14] [103] – relevant higher expansion ratio itself does, provided that sufficient temperature and pressure are achieved around TDC to conduct the combustion successfully. Thus, retarded EVO timing can improve the efficiency by exploiting additional expansion work which was destined to destroy by blowdown process, provided no significant loss in efficiency by simultaneously retarded EVC timing[15].

A similar process can be performed in other conditions. Through these processes, it is possible to predict the valve timing that can maximize the efficiency in a relevant operating condition. It should be noted that the only region being ambiguous to choose the predicted valve timings was N/A high load (almost WOT) condition, where the knock occurred but its degree was found to be different for each SB ratio – at the supercharged region, operation with fully retarded intake valve timing[16] (around parking position) and moderately retarded exhaust valve timing showed the best efficiency for all conditions[17].

[14] Whereas higher compression ratio itself can contribute to the improvement of efficiency by reducing exergy destruction – the higher compression ratio is, the higher temperature and pressure are, which can reduce exergy destruction mainly attributed to the decrement in fuel combustion-related exergy destruction [102].

[15] This can occur in high load condition, because increased hot residual gas can lead to higher knock occurrence, causing additional retard in spark timing

[16] Whereas, advanced intake valve timing was normally chosen for highly supercharged operation of real driving situation, not for the efficiency, but the performance. In the real engine operation, supercharged condition is usually required temporarily for very high load. Therefore, only torque matters so that required is advanced intake valve timing with highly supercharged and significantly retarded.

[17] First, for intake valve timing, advance strategy causes increment in actual compression ratio, causing severe knock. Therefore, spark timing should be retarded too much so that the efficiency is reduced. Thus, LIVC with more charging (i.e. increased intake pressure) was found to be good for the efficiency. Second, for exhaust valve timing, fully retarded operation can cause increment of in-cylinder pressure at exhaust stroke, resulting in high pumping loss.

The details of univariate experiment were listed below.

1) With holding the exhaust valve timing to the best efficiency-expected position, variation of intake valve timing was conducted to achieve relevant load (nIMEP or gIMEP) with spark timing of MBT or KLSA. For reference, MBT timing was defined based on CA50 value. Before the experiments, the CA50 for relevant MBT operation was pre-measured for each load, rotational speed, and SB ratio, showing similar range of general operation; 6-8 CA aTDC [18]. It was found that the values were mainly affected by load condition, not the SB ratio condition.

2) The intake valve timing showing the highest efficiency was chosen for variation of exhaust valve timing.

3) From 1) and 2), the intake and exhaust valve timing at which the highest efficiency was achieved was determined for relevant condition of load and rotational speed.

One can claim that this approach may not take into account interactions between each parameter – intake and exhaust valve timing. Although that claim was theoretically right, the results showed that thanks to the pre-investigating process, the operating points determined by univariate condition were not different from those derived by other methods that can consider the interactions physically, such as DoE and full factorial (i.e. complete enumeration) methods which were covered in following chapters.

4.1.2 Design of experiment (DoE) process

For the development process of new engine for mass production, Design of Experiment, called DoE, is widely used [104, 105], thanks to its efficiency in

terms of economic and engineering views. The basic implication of DoE is to understand the interactions of the input variables, specified by DoE process, through the specific interpolation method based on the randomly selected experimental data. That is, it is the core of the DoE process to find out the trend of the objective variable (target variable such as efficiency, emissions) fairly by using only randomly selected conditions rather than searching the whole condition by full factorial experiment.

The DoE-based analysis for the best efficiency point had been conducted [100], using some of experiments conducted by same experimental condition in this study. The detailed procedure was listed below.

1) 15 points (InCAM, ExCAM, and SOI[18]) allocated by the DoE program were investigated experimentally.

2) The results from this 15-point experiment were inputted into the DoE program, and then the program provided the "expected" optimum point based on its distinctive curve-fitting method. In executing the DoE, the ASCMO made by ETAS Inc. was used.

3) In addition, DoE experiment with 15 points and an additional four pairs was conducted. The additional four pairs, which were the pole points of (intake and exhaust valve timing), were used to complement an issue that might occur owing to the inevitable drawback of the curve-fitting method.

Total three different experiments in finding the highest efficiency were conducted and these results were compared at two different load conditions

[18] The SOI variation was not the scope of this work – only considered in the example of DoE process mentioned in this chapter (mainly treated in the previous work [99]).

(nIMEP 4.5 bar and 6.5 bar) with same rotational speed (2000 RPM). Each experiment was named as case A, B, and C of which details were listed below.

A) DoE experiment with 15 points (allocated by DoE program)

B) DoE experiment with 15 points and additional 4 points (InCAM and ExCAM pole points)

C) a series of univariate sweep experiments (InCAM, ExCAM, and SOI sweep, sequentially)

The necessity of case B should be noted – due to the curve fitting procedure of DoE process, the value of objective function (i.e. efficiency) may not be estimated correctly under the conditions corresponding to the pole values of the input variables (i.e. intake and exhaust valve timing). Thus, the DoE process of case B was performed by adding the experimental data, corresponding to the pole values of the input variables, to the 15 DoE test conditions.

The relevant results were expressed in figure 4.1. It was noteworthy that the addition of four pole points improved DoE's efficiency calculation. Interestingly, the point for the highest efficiency with DoE from 15 experimental points was not the actual highest point at the given load. Although it was possible to increase the number of DoE experiments to theoretically achieve better results, it might be more reasonable to add a small number of experiments (i.e. pole conditions) based on the empirical experiences in the field calibration. It was also noted that the expected highest efficiency as well as the input variables from 19 points DoE was very similar to that of univariate sweep experiment. With these results, it can be concluded that univariate experiment with pre-investigating process can find the best efficiency point at least low load condition (i.e. no knock occurs). The

detailed conditions and results of these three different experiments were summarized in table 4.1 and table 4.2.

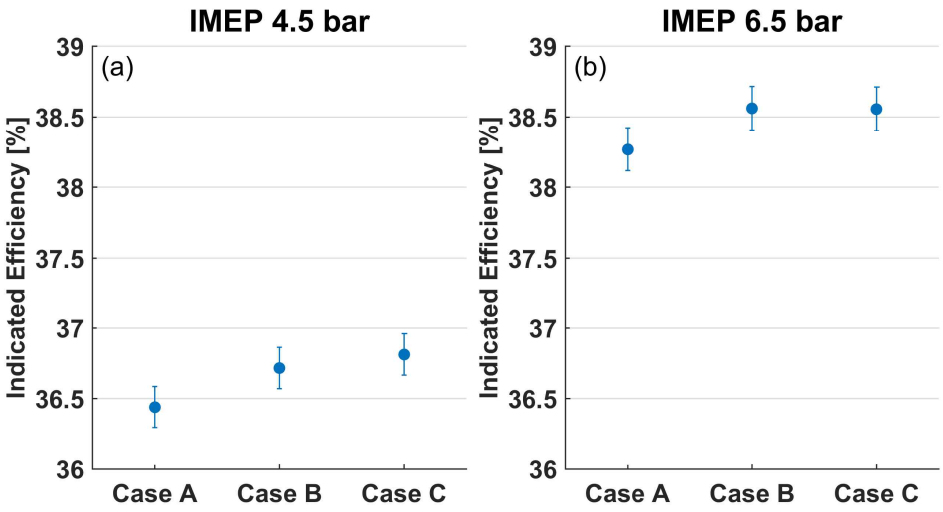

Figure 4.1 Experimental results of maximum efficiency point using various methods (nIMEP 4.5 bar 2000 RPM, 6.5 bar 2000RPM), redrawn from [100]

Table 4.1 Summary of input variables and efficiency for various methods (nIMEP 4.5 bar, 2000 RPM)

IMEP 4.5 bar	InCAM [CA]	ExCAM [CA]	SOI [CA aTDC]	NIE [%]
DoE 15pts	-45.5	39.0	-328.4	36.44
DoE + extreme 19pts	-48.8	40.0	-317.1	36.72
Sweep exp.	-50.0	40.0	-315.0	36.81

Table 4.2 Summary of input variables and efficiency for various methods (nIMEP 6.5 bar, 2000 RPM)

IMEP 6.5 bar	InCAM [CA]	ExCAM [CA]	SOI [CA aTDC]	NIE [%]
DoE 15pts	-39.5	35.0	-320.6	38.27
DoE + extreme 19pts	-47.3	38.3	-318.0	38.56
Sweep exp.	-50.0	40.0	-315.0	38.56

4.1.3 Full factorial (complete enumeration) process

Even though the arguments of interactions became clear for low load operation, uncertainty about the effect of interactions in other operating conditions (i.e. mid-load and supercharged load) still existed. Thus, full factorial (i.e. complete enumeration) experiments were conducted for low (nIMEP 4.5 bar), middle (nIMEP 8.5 bar), and high (GIMEP 10.5 bar) load conditions with same rotational speed (2000 RPM). For this, selected were total 15 points of experimental conditions consisting of the combination of InCAM and ExCAM positions, shown by red dots in figure 4.2. Based on the efficiency results at these points, contour plotting process with linear interpolation was conducted, plotted in figure 4.3, 4.4, and 4.5. Brief explanation related to the results were listed below.

First, for low load (nIMEP 4.5 bar, N/A) operation plotted in figure 4.3, same tendency with the results mentioned above was detected – it was the condition of fully advanced intake valve timing and fully retarded exhaust valve timing that the net efficiency showed the highest value (leftmost and uppermost region). One thing deserves additional explanation that at the parking position of exhaust valve timing (i.e. lowermost region), LIVC operation (i.e. rightmost) showed higher efficiency than fully advanced intake valve timing operation (i.e. leftmost), mainly attributed by pumping loss – since the valve overlap was shortened by fully advanced (parking) exhaust valve timing, only LIVC operation with higher intake pressure can reduce the pumping loss. Although this tendency also came out at the fully retarded exhaust valve timing (i.e. uppermost region), the degree was too low as to exceed the efficiency of fully advanced intake valve timing[19].

[19] This tendency may be specific issue of single-cylinder engine of which manifold structure is necessarily different from that of mass production multi cylinder engine.

Second, for middle load (nIMEP 8.5 bar, N/A) operation plotted in figure 4.4, interesting regions were shown; 'not operable' and 'MBT region'. These were commonly attributed by different burning rate from each SB ratio. Above all, at the right-side region (retarded intake valve timing), inducted air was reduced by re-exhalation from BDC to late IVC, limiting the maximum air and fuel rate under stoichiometric operation. In addition, since the burning rate of SB 1.0 condition was normally slower than that of other SB ratio conditions (this will be discussed later), sufficient gross work to achieve nIMEP 8.5 bar was resultantly not extracted during combustion, causing wide 'not operable' region. In addition, only the conditions of SB ratio 1.2 and 1.47 were able to be operated with MBT condition in some sections, attributed by their faster burning rate compared to that of SB ratio 1.0 case. It should be noted that faster burning rate does not mean high knock resistance; in certain aspects of knock characteristics, faster burning rate may aggravate knock characteristics, which will be covered on chapter 6. Instead, due to the faster burning rate, target load (nIMEP 8.5 bar) was able to be achieved with less amount of fuel and air, causing overall lower pressure and temperature during compression stroke. From this reason and the lack of time to be auto-ignited (caused by shorter burn duration), knock was mitigated, resulting in MBT operation. The details related to the issues mentioned here will be re-investigated in chapter 4.2 with several parameters.

Third, for high load (gIMEP 10.5 bar, supercharged), monotonous trends were found, which was also predicted by the results from univariate method; LIVC with retarded exhaust valve timing showed the highest efficiency. It should be noted that since pumping loss was not considered, conditions for fully retarded exhaust valve timing showed the best 'gross' efficiency. However, as mentioned above, fully retarded operation can lead to higher pumping loss which, unfortunately, cannot be measured properly in this configuration. The details related to the issues will be also explained in chapter 4.2.

With this approach, the main objective of this chapter – to find the valve timing for the best efficiency – was accomplished for now. That is, the final valve timing related to each load condition can be summarized, where the details were listed in table 4.3. It should be noted that rotational speed did not significantly affect the determination of final valve timing. Thus, only load condition was the main variable of table 4.3. Since the experimental results of same fuel rate will be considered in the next chapter, the values of fuel rate relevant to each load were also listed together. All the experiments related to remaining chapters were conducted with fixed valve timing in the table.

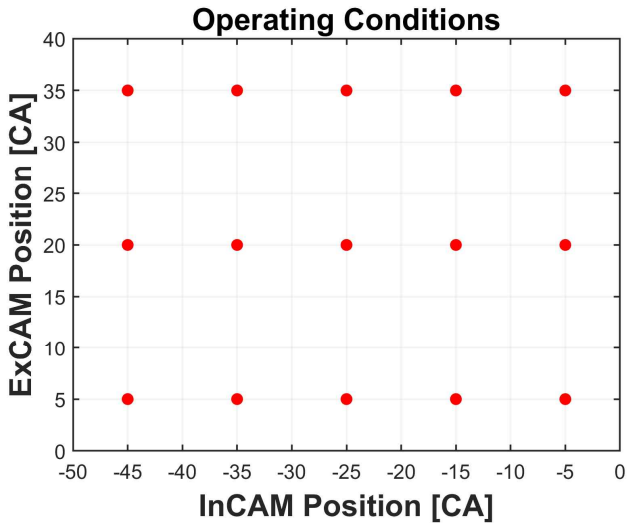

Figure 4.2 Operating points for complete enumeration experiments

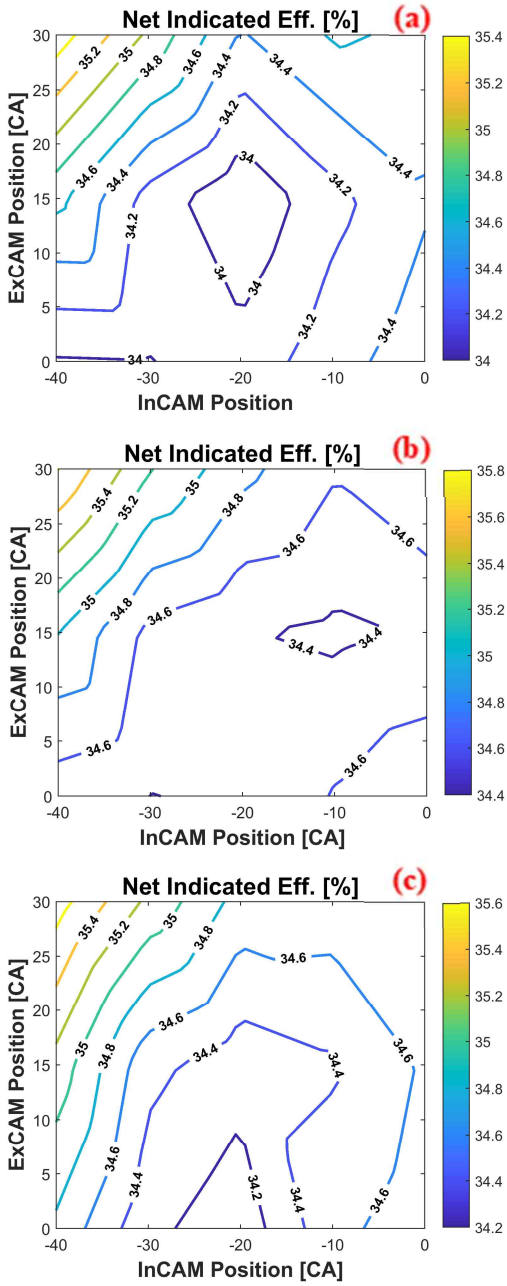

Figure 4.3 Net efficiency results of complete enumeration process for nIMEP 4.5 bar, 2000 RPM
(a: SB 1.0, b: SB 1.2, c: SB 1.47)

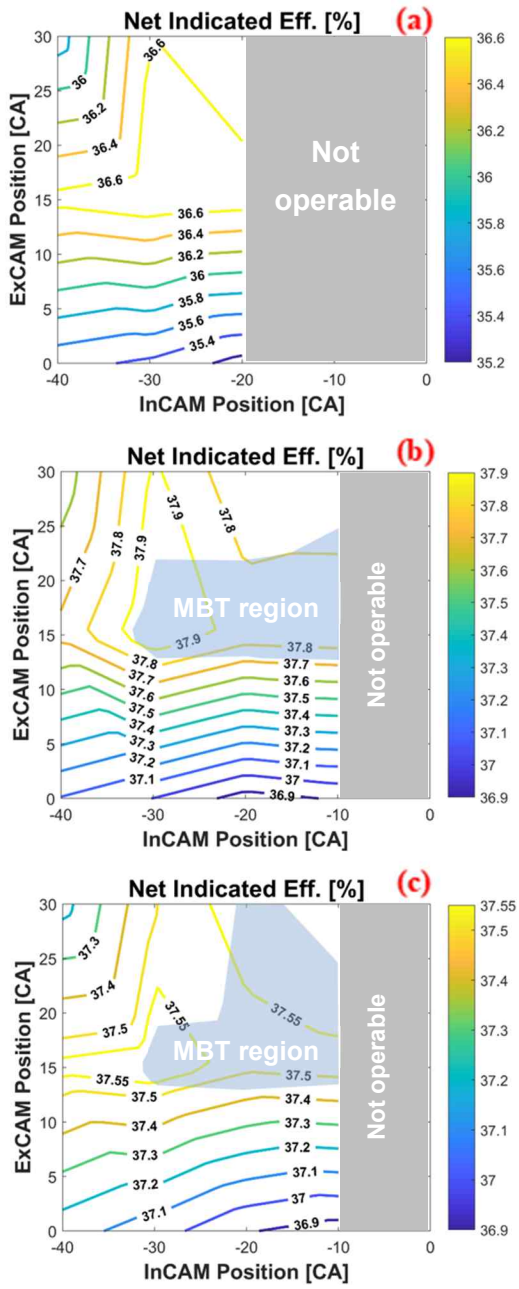

Figure 4.4 Net efficiency results of complete enumeration process for nIMEP 8.5 bar, 2000 RPM
(a: SB 1.0, b: SB 1.2, c: SB 1.47)

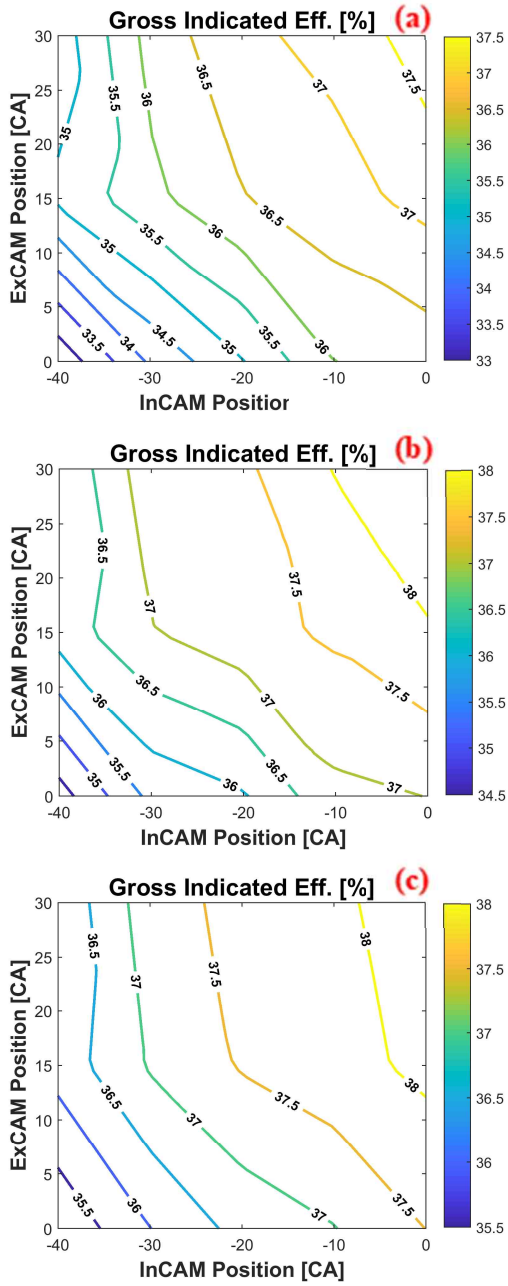

Figure 4.5 Gross efficiency results of complete enumeration process for gIMEP 10.5 bar, 2000 RPM
(a: SB 1.0, b: SB 1.2, c: SB 1.47)

Table 4.3 Valve timing positions for each experiment related to chapter 5 and 6

Valve timing (IN / EX)	Same load experiments (IMEP)		
	nIMEP [bar]		gIMEP [bar]
	4.5 (13-14 mg/cyc)	8.5 (26-28 mg/cyc)	10.5 (32-38mg/cyc)
SB 1.0	45 adv. / 35 rtd.	35 adv / 20 rtd.	5 adv. / 35 rtd.
SB 1.2			
SB 1.47			
SB 1.19		25 adv. / 35 rtd.	-
SB 1.42		45 adv. / 35 rtd	-
SB 1.2 (high Rt)		25 adv. / 20 rtd.	15adv. / 20 rtd.
SB 1.47 (high Rt)			25 adv. / 20 rtd.

Valve timing (IN / EX)	Same fuel experiments (mg/cyc)				
	14	20	26	30	34
SB 1.0	45 adv. / 35 rtd.	45 adv. / 35 rtd.	45 adv. / 5 rtd.	10 adv. / 35 rtd.	10 adv. / 35 rtd.
SB 1.2					
SB 1.47					
SB 1.2 (high Rt)					
SB 1.47 (high Rt)					

4.2 Experimental results of preliminary valve timing sweep operation

The investigation on the results of valve timing variation was conducted with various parameters (not just efficiency) for the 'basic conditions' – three SB ratio (1.0, 1.2, 1.47) with same displacement volume and compression ratio, and similar tumble ratio. Even though the best points for each valve timing were already concluded by the efficiency results presented in previous chapter, detailed investigation was inevitably needed to find the reason why the points were selected. Therefore, several parameters related to not only efficiency but also other important issues such as emissions, flow characteristics (e.g. volumetric efficiency and pumping loss) were also used for this chapter. Noted that the results of intake valve timing sweep were mainly plotted in several figures because of its complexity compared to those of exhaust valve timing sweep. If needed, figure data in the previous chapter (complete enumeration) were mentioned and used to explain the effect related to exhaust valve timing sweep.

One thing should be noted that the range of error was applied such as efficiency-related parameters – net indicated efficiency, exhaust heat loss, cooling loss, and combustion efficiency – and emissions. Since many of the experimental data which will be introduced in the following chapters (5, 6) were the same as those in this chapter, the errorbar was only shown in this chapter, with relevant mention if necessary.

4.2.1 Low load operation

Low load operation (~ nIMEP 4.5 bar) was investigated with two conditions of rotational speed (1500 and 2000 RPM). It should be mentioned that all the experiments of low load condition were conducted under MBT operation with no knock occurrence, where the CA50 was located around 6-7 CA aTDC. First, the experimental results of 1500 RPM cases were plotted in figure 4.6, 4.7, and 4.8, with large number of parameters. With these, detailed investigation was covered to supplement the results expressed in the previous chapter.

Due to the larger amount of residual mass fraction with advanced intake valve timing, it was shown that NOx emissions were decreased as intake valve timing was advanced, as mentioned in chapter 2.1.1 as an example. This can be supplemented by the results of initial flame speed, showing decrement with advanced intake valve timing attributed by increased residual mass fraction. It should be noted that due to the several parameters such as residual mass fraction, initial and main flame speed for SB 1.47 were not so fast compared to those for SB 1.2, which is the opposed to the common sense for SB ratio. It should be noted (and will be mentioned again in chapter 5 and 6) that the volume profile under the 'packaging constraint' may cause slow initial flame speed for SB 1.47, due to its large volume with same crank angle around TDC position. This results in low temperature and pressure around spark timing, causing slow laminar flame speed which is mainly affected by temperature. Therefore, initial flame speed, with crank angle-based time scale, can be decreased (i.e. slow) for higher SB ratio.

Another unexpected behavior was UHC and CO emissions for high SB ratio (1.47), shown in figure 4.6-(c) and (d). In general, UHC emissions were proportional to bore size which is a key parameter to define crevice volume (ring land crevice) [18]. Therefore, one can easily predict that UHC emissions will be the highest for SB 1.0 case, which was shown clearly. However, this notion was not able to be applied for the case of SB 1.2 and 1.47, showing slightly higher

UHC emissions for SB 1.47. It can be explained by two ways. First, peak pressure can be higher and SB 1.47, causing higher pressure and, resultantly, mass in the crevice volume. However, as shown in figure 4.7-(c), peak pressure of SB 1.47 was not high, attributed by unexpectedly slow burn duration and high residual mass fraction. Thus, the other way should be reviewed, which is related to the volume profile mentioned earlier; since the rate of volume change was the highest in SB 1.47, flame propagation can be affected by the reduced temperature caused by volume expansion. Because of this, incomplete oxidation from initial fuel (gasoline) to the complete combustion products (i.e. H_2O and CO_2) may occur, resulting in higher UHC emissions. This contention can be supplemented by the results of CO emission, shown in figure 4.6-c. Here, the CO emissions for SB 1.47 were higher than those of SB 1.2. In general, CO-to-CO_2 oxidation can be achieved above certain temperature conditions [106]. The fast rate of volume expansion, however, may decrease the flame temperature too fast to complete the final oxidation process of hydrocarbon fuel (i.e. CO-to-CO_2 reaction). Therefore, it can be suggested that the unexpected emissions data be attributed by the fast volume expansion rate of high SB ratio condition.

Final issue is related to the efficiency-related parameters, shown in figure 4.8. One thing should be noted (also will be importantly mentioned in chapter 5) that the exhaust loss showed higher tendency for SB 1.47 condition – this trend was also shown in almost all experimental results, regardless of the operating conditions. In general, confined to the same engine configuration, exhaust loss is mainly dependent on the combustion phasing – if the combustion ends quickly and/or spark timing is advanced, exhaust temperature and, resultantly, exhaust loss will be reduced. Thus, considering the facts that SB 1.47 did not show the slowest flame speed, and the spark timing was mostly advanced, it was not expected result. Meanwhile, it can be supplemented by the data shown in figure 4.8-a, where the internal energy extraction was plotted. Even if the initial

condition (i.e. properties at IVC timing) was similarly tuned to achieve same load, the internal energy extraction, defined as equation 4.1, was shown to be the lowest at SB 1.47 condition.

$$\Delta U = U_{IVC} - U_{EVO} \qquad \text{eq. 4.1}$$

Thus, it can be concluded that due to the lower extraction of internal energy with similar initial condition and same work produced, exhaust loss was destined to become larger for SB 1.47 condition. This will be comprehensively investigated in chapter 5, so for now, accepted were the results without further explanation. Considering all the parameters related to the efficiency – exhaust loss, emissions related to the incomplete loss, PMEP, the efficiency was not improved by achieving higher SB ratio (i.e. 1.47), saturated at the moderate SB ratio (i.e. 1.2), shown in figure 4.8-c.

Specific parameters chosen for further explanation about RPM issue were reviewed with the case of 2000 RPM, same load (~ nIMEP 4.5 bar). First of all, widely known matters related to variation of RPM was checked, where the relevant data were shown in figure 4.9 and 4.10. As easily expected, cooling loss per a cycle was reduced because of a decrease in time. According to this, exhaust loss was slightly increased, where the unexpected tendency mentioned earlier (large amount in SB 1.47 condition) also appeared. In addition, PMEP and net indicated efficiency showed same behavior with those in 1500 RPM case – only the degree of each value changed. Considering the purpose of this chapter, 2000 RPM cases were considered as a main explanation for other cases mentioned later if no severe discrepancy existed between 1500 and 2000 RPM cases.

One thing should be noted that cooling loss showed not expected tendency for 2000 RPM case. Under the common knowledge, with increasing SB ratio

under the same displacement volume, decreased was SV ratio around firing TDC, which may reduce the area of heat transfer and, resultantly, heat transfer itself. Thus, one can claim that heat transfer will be reduced by increasing SB ratio [57, 58]. This was shown, however, to be not true as considering the results of SB 1.0 and 1.2 for 1500 RPM, and of all the SB ratios for 2000 RPM, presented in figure 4.9. Thus, it can be suggested that the other parameters related to calculation of convective heat transfer should be investigated – convective heat transfer coefficient and temperature difference terms. It will be comprehensively covered in chapter 5.

The exhaust valve sweep data were shown in figure 4.11. With expecting tendency by pre-investigating process, one can easily determine the best position of exhaust valve timing as a fully retarded location. The results of exhaust loss and PMEP can be used understand the reason, shown in figure 4.11-b and 4.11-c. Since the duration of valve overlap with fixed intake valve timing is increased by retarding exhaust valve timing, residual mass fraction was increased, causing increment in intake manifold pressure and decrement in exhaust gas temperature by reducing peak temperature (chemical effect – dilution). In addition, blowdown loss was decreased with retarded EVO timing. Therefore, for low load operation, it will be desirable to use fully retarded valve timing for all conditions in this work.

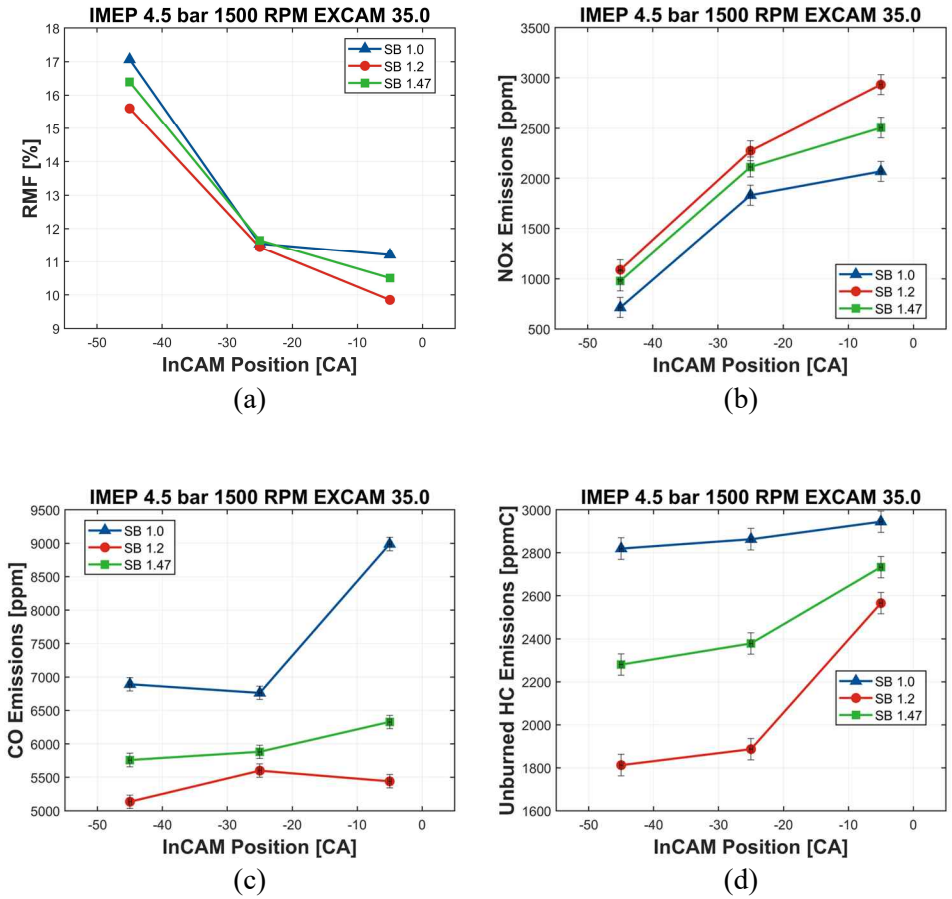

Figure 4.6 Experimental results of intake valve timing sweep for nIMEP 4.5 bar, 1500 RPM, and three SB ratios (1.0, 1.2, and 1.47)
(a) Residual mass fraction
(b) NOx emissions
(c) CO emissions
(d) UHC emissions

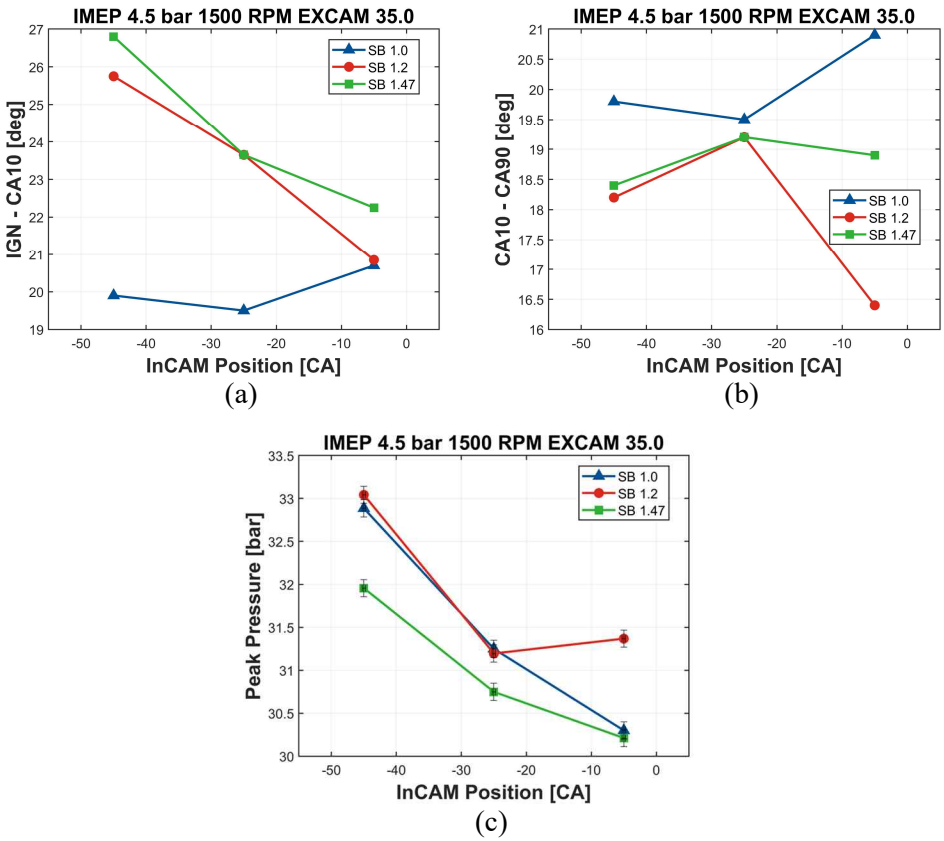

Figure 4.7 Experimental results of intake valve timing sweep for nIMEP 4.5 bar, 1500 RPM, and three SB ratios (1.0, 1.2, and 1.47)
(a) Initial flame speed (ignition to CA10)
(b) Main flame speed (CA10 to CA90)
(c) The maximum in-cylinder pressure

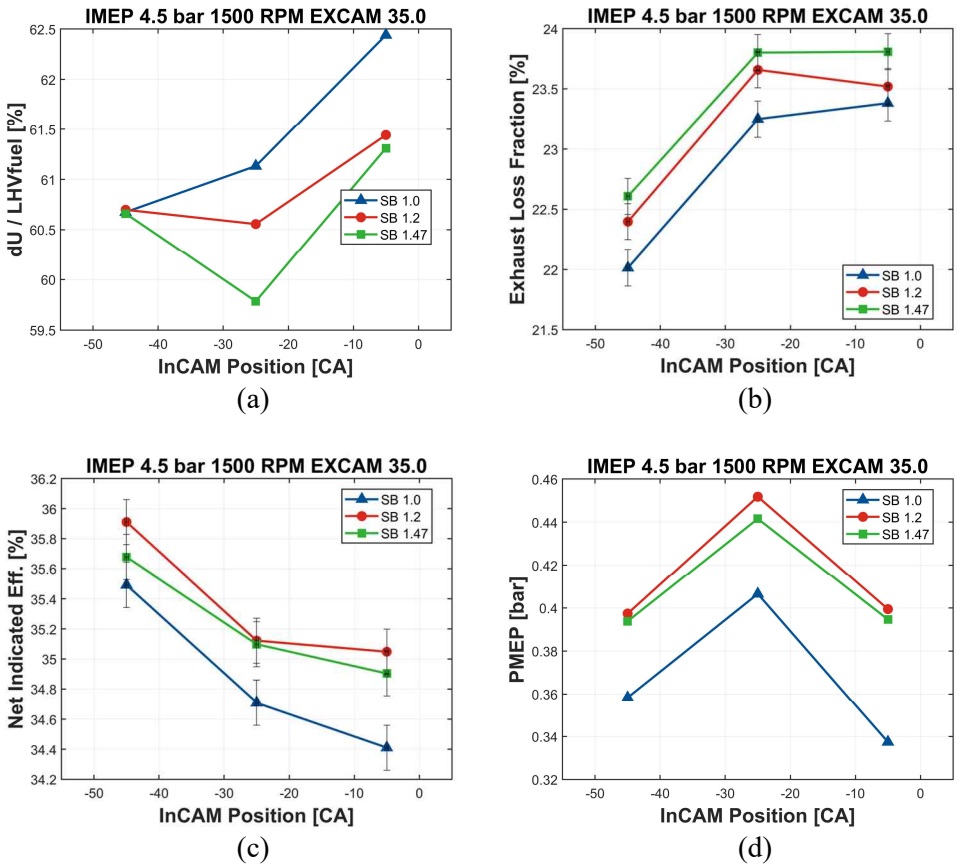

Figure 4.8 Experimental results of intake valve timing sweep for nIMEP 4.5 bar, 1500 RPM, and three SB ratios (1.0, 1.2, and 1.47)
(a) Internal energy extraction normalized by fuel LHV (in closed duration)
(b) Exhaust loss normalized by fuel LHV
(c) Net indicated efficiency
(d) PMEP

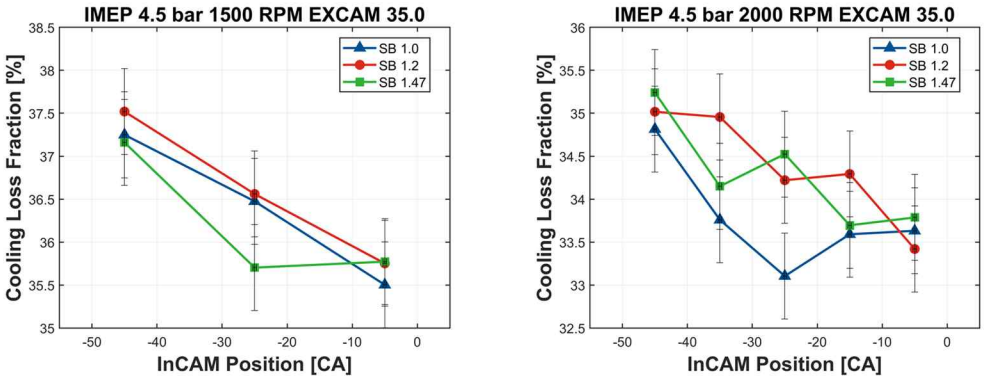

(a) (b)

Figure 4.9 Cooling loss results with intake valve timing sweep for nIMEP 4.5 bar and three SB ratios (1.0, 1.2, and 1.47)
(a) 1500 RPM
(b) 2000 RPM

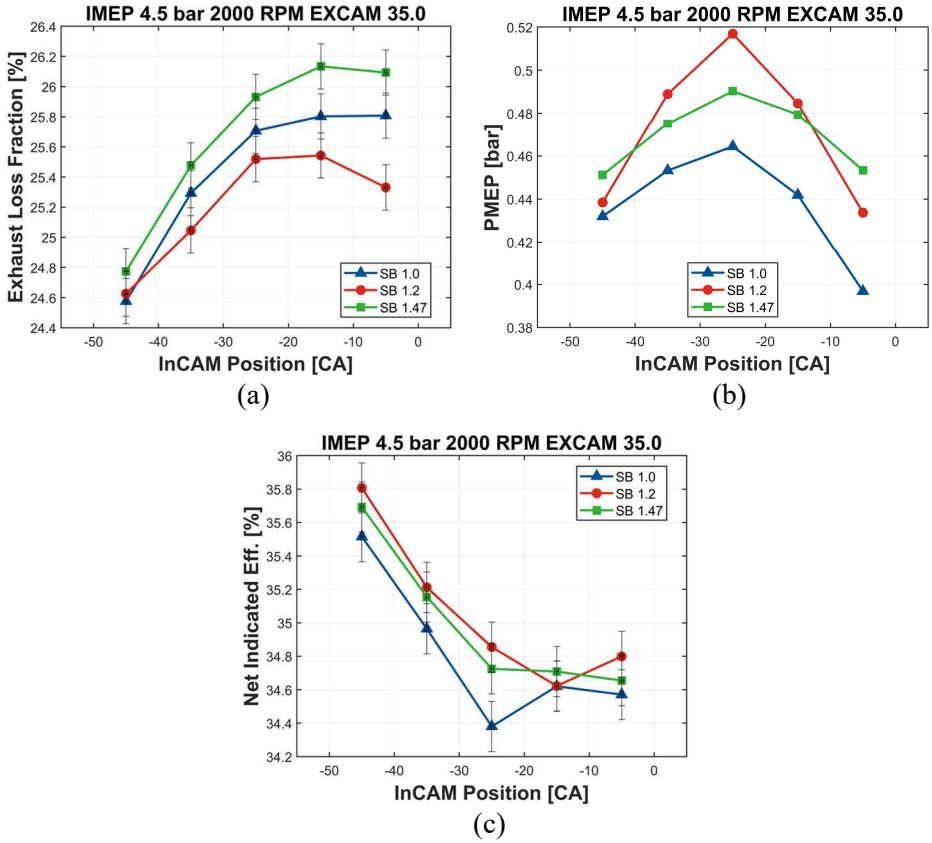

Figure 4.10 Experimental results of intake valve timing sweep for nIMEP 4.5 bar, 2000 RPM, and three SB ratios (1.0, 1.2, and 1.47)
(a) Exhaust loss normalized by fuel LHV
(b) PMEP
(c) Net indicated efficiency

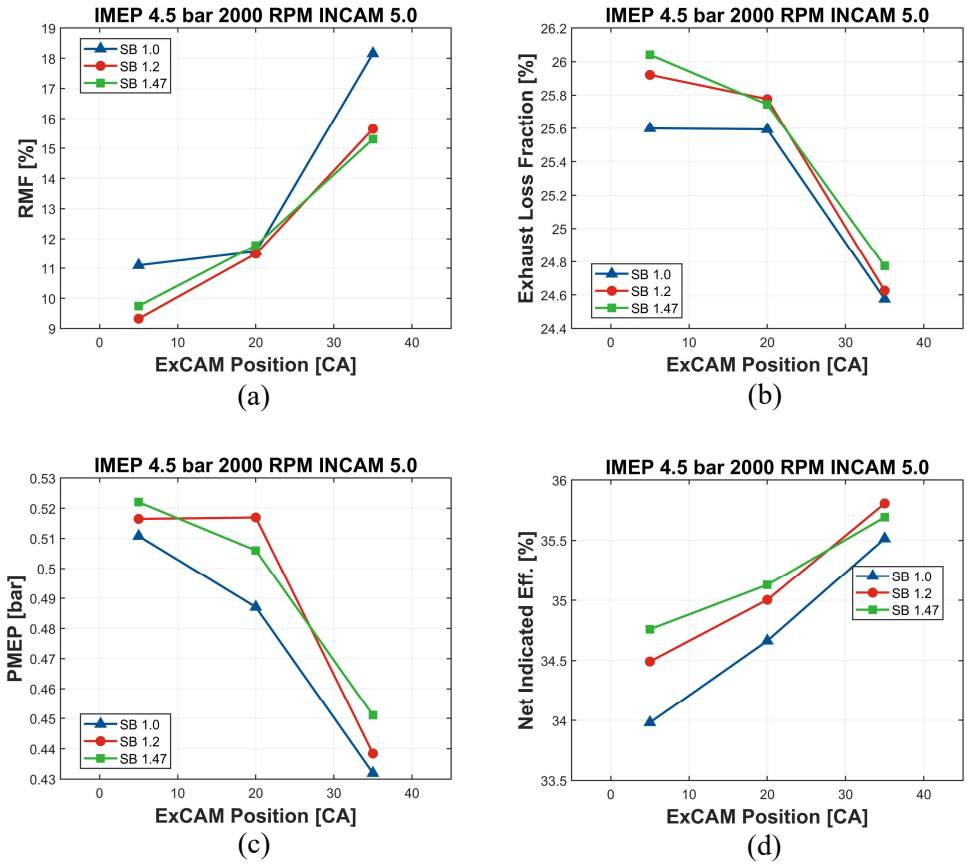

Figure 4.11 Experimental results of exhaust valve timing sweep for nIMEP 4.5 bar, 2000 RPM, and three SB ratios (1.0, 1.2, and 1.47)
(a) Residual mass fraction
(b) Exhaust loss normalized by fuel LHV
(c) PMEP
(d) Net indicated efficiency

4.2.2 Middle load (WOT with N/A operation)

Mid-load operation (~nIMEP 8.5 bar) was investigated with the data of 2000 RPM cases, where the data were shown in figure 4.12, 4.13, and 4.14. ExCAM position was set to 20 (moderately retarded exhaust valve timing) as considering the results shown in figure 4.4. Since knock started to occur in many points under the corresponding load, the main parameters that can affect the efficiency were combustion phasing – i.e. CA50 and burn duration. It should be noted that due to the knock occurrence, main flame speed was re-defined as the duration from CA10 to CA70, where the reason was clearly mentioned in chapter 2.

For emissions data, shown in figure 4.12, similar trends were found in CO and UHC emissions compared to those of low load case. One thing should be noted that peak pressure of SB 1.0 case was significantly lower attributed by spark timing retard for knock mitigation. Considering this result, the highest UHC emissions from SB 1.0 can be concluded to be attributed by large bore size. In addition, with same reason, NOx emissions were decreased, compared to other conditions. Because of decrement in residual mass fraction attributed by higher load and intake manifold pressure, both initial and flame speed of SB 1.47 were fast enough compared to those of other conditions – conforming to the expected notion. Therefore, peak pressure of SB 1.47 was closed to that of SB 1.2, enhancing UHC emissions by increased mass in crevice, in addition to the same effect of faster volume expansion mentioned earlier.

Due to the knock occurrence, combustion phasing may be retarded in many cases, shown by the value of CA50 in figure 4.13-c. As expressed in figure 4.4, SB 1.2 and 1.47 showed partially MBT-operated (CA50 around 8 CA aTDC) results at moderately retarded intake valve timing. It should be noted that considering the difference of PMEP value for each SB ratio, shown in figure 4.13-

c, pumping loss did not significantly affect the net indicated efficiency. Instead, higher cooling loss from SB 1.0 appeared, which follows conventional notion mentioned earlier. Still, higher cooling and exhaust loss were measured for SB 1.47 compared to those of SB 1.2, resulting in lower efficiency shown in figure 4.14.

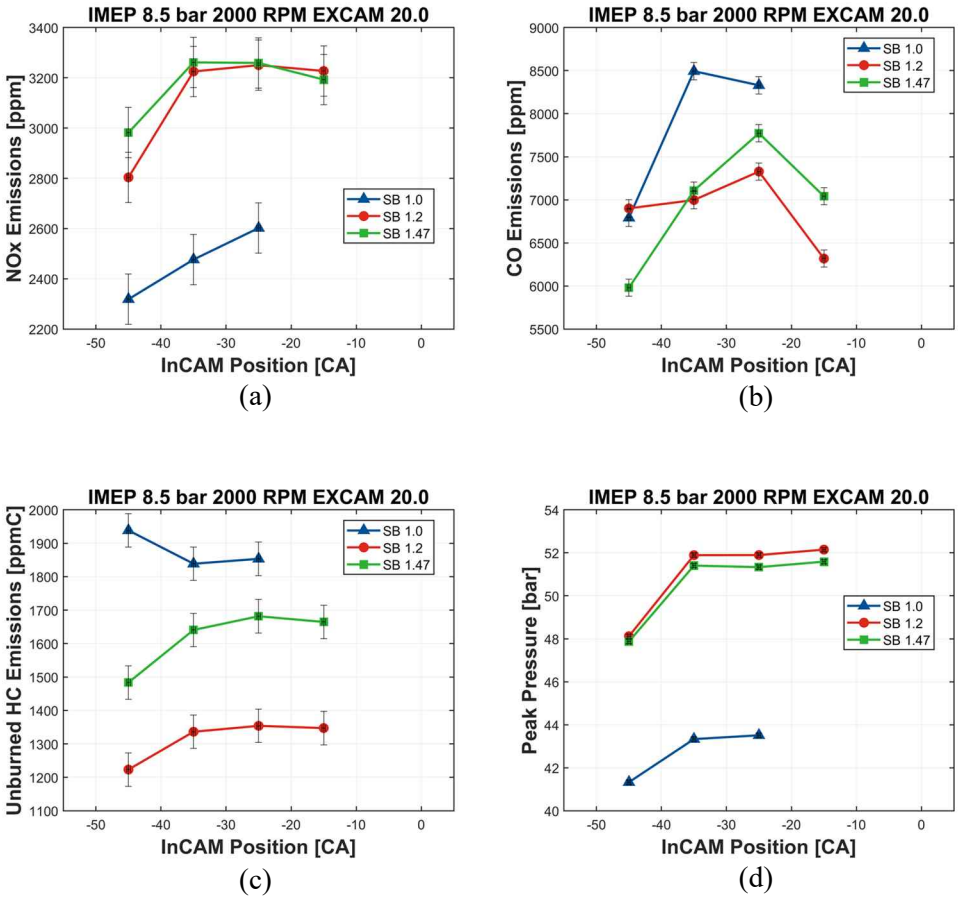

Figure 4.12 Experimental results of intake valve timing sweep for nIMEP 8.5 bar, 2000 RPM, and three SB ratios (1.0, 1.2, and 1.47)
(a) NOx emissions
(b) CO emissions
(c) UHC emissions
(d) The maximum in-cylinder pressure

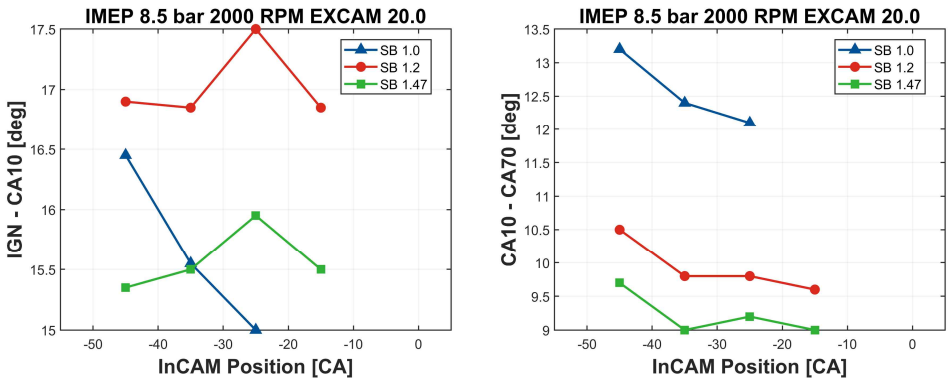

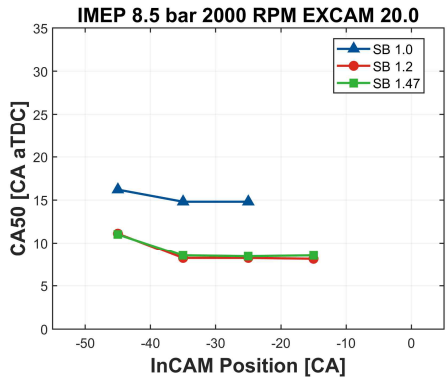

Figure 4.13 Experimental results of intake valve timing sweep for nIMEP 8.5 bar, 2000 RPM, and three SB ratios (1.0, 1.2, and 1.47)
(a) Initial flame speed
(b) Main flame speed (CA10-CA70)
(c) CA50

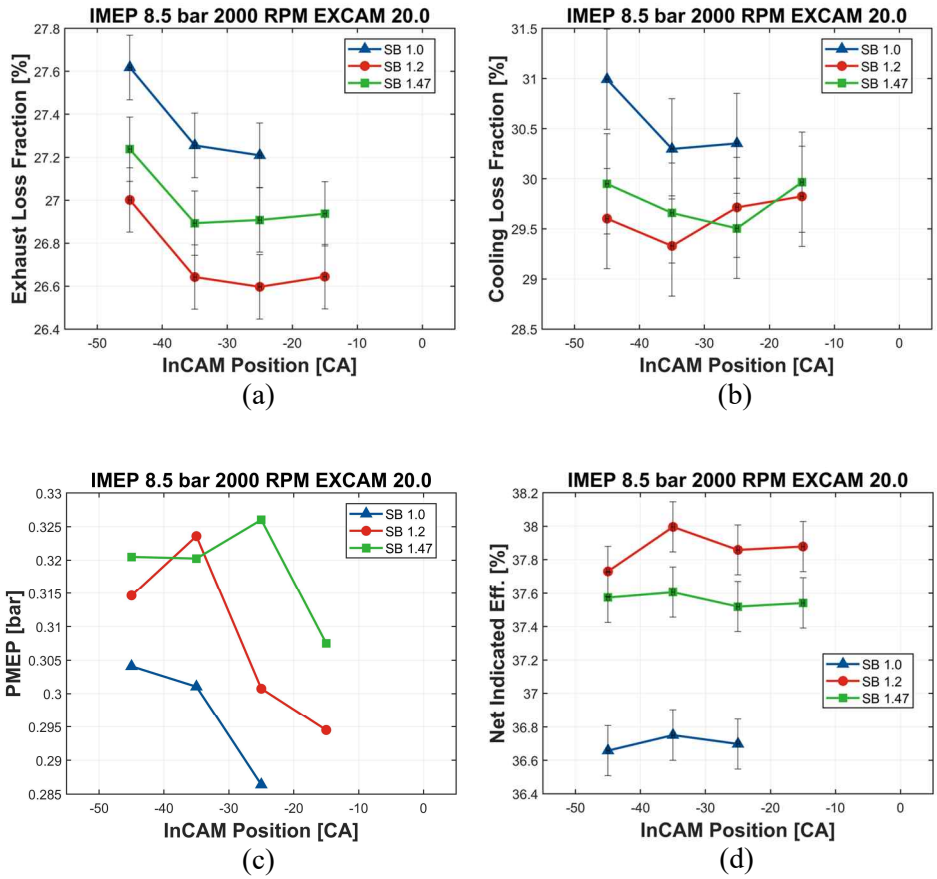

Figure 4.14 Experimental results of intake valve timing sweep for nIMEP 8.5 bar, 2000 RPM, and three SB ratios (1.0, 1.2, and 1.47)
(a) Exhaust loss normalized by fuel LHV
(b) Cooling loss normalized by fuel LHV
(c) PMEP
(d) Net indicated efficiency

4.2.3 High load operation

High load operation with supercharger operation (~ gIMEP 10.5 bar) was investigated with the data of 2000 RPM cases. The relevant data were plotted in figure 4.15, 4.16, 4.17, and 4.18. ExCAM position was set to 35 (fully retarded exhaust valve timing) as considering the results shown in figure 4.5. One can claim that this is not identical with the value mentioned in pre-investigating process (where ExCAM position was 20). This was caused by PMEP of which value was not able to be measured accurately by the reason mentioned above – each gross and net efficiency showed the best results for each ExCAM 35 and 20, respectively. As the gross work was used to evaluate the performance of engine operation for supercharged condition, ExCAM 35 was eventually chosen. For reference, the tendencies for the main parameters except PMEP were not significantly changed for each ExCAM position.

In general, residual mass fraction is not significant for the supercharged (or turbocharged) operation because of high intake manifold pressure[20]. Thus, PMEP did not decrease as advancing intake valve timing, shown in figure 4.15. In addition, supercharged operation with LIVC showed poor volumetric efficiency, resulting in decreased PMEP by high intake manifold pressure (around 1.3 – 1.5 bar).

For emissions data shown in figure 4.16, no significant change occurred compared to those of middle road results. One thing should be noted that peak pressure showed its highest value at SB 1.47 condition for almost every point of

[20] In a mass production multi-cylinder engine, so-called 'scavenging' normally occurs in supercharged (or turbocharged) operation, where the residual is dragged by high pressure intake mixture into an exhaust manifold. This might cause biased level of oxygen measured by lambda sensor due to the oxygen concentration of intake mixture.

intake valve timing, which was related to the overall location of spark timing at this load. Since the load became high, generally retarded was spark timing of which location was near the firing TDC. Because of this, first, peak pressure was extremely decreased as advancing intake valve timing attributed by retarding combustion phasing to avoid knock occurrence, supplemented by CA50 timing data. Second, the difference of the instantaneous volume at spark timing for each SB ratio significantly reduced, diminishing volume effect on the initial flame speed mentioned in chapter 4.2.1.1. Therefore, both initial flame speed and main flame speed became the highest at SB 1.47 condition, resulting in high peak pressure for almost every intake valve timing point. Still, cooling and exhaust loss for SB 1.47 condition was higher than those of SB 1.2, which compensated for the positive effect of fast burning rate and made almost same gross indicated efficiency for SB 1.2 and 1.47 shown in figure 4.18.

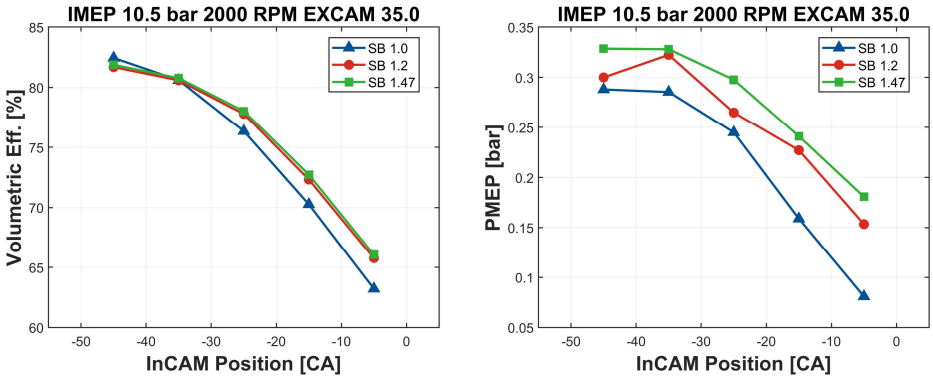

(a) (b)

Figure 4.15 Experimental results of intake valve timing sweep for gIMEP 10.5 bar, 2000 RPM, and three SB ratios (1.0, 1.2, and 1.47)
(a) Volumetric efficiency
(b) PMEP

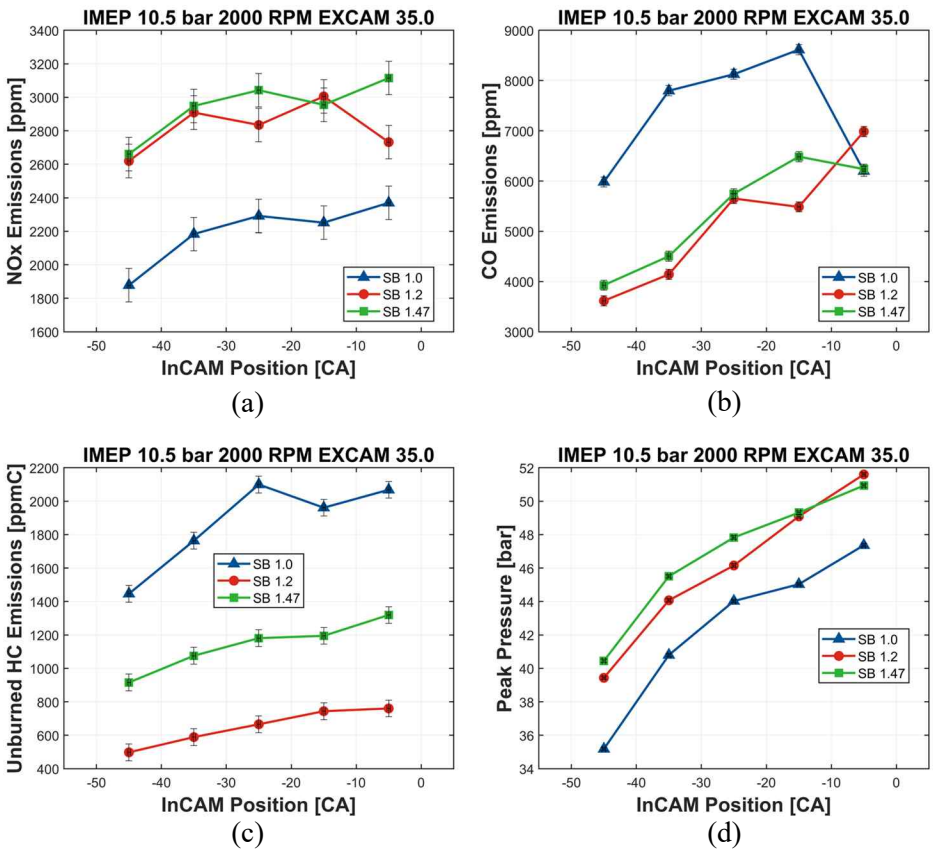

Figure 4.16 Experimental results of intake valve timing sweep for gIMEP 10.5 bar, 2000 RPM, and three SB ratios (1.0, 1.2, and 1.47)
(a) NOx emissions
(b) CO emissions
(c) UHC emissions
(d) The maximum in-cylinder pressure

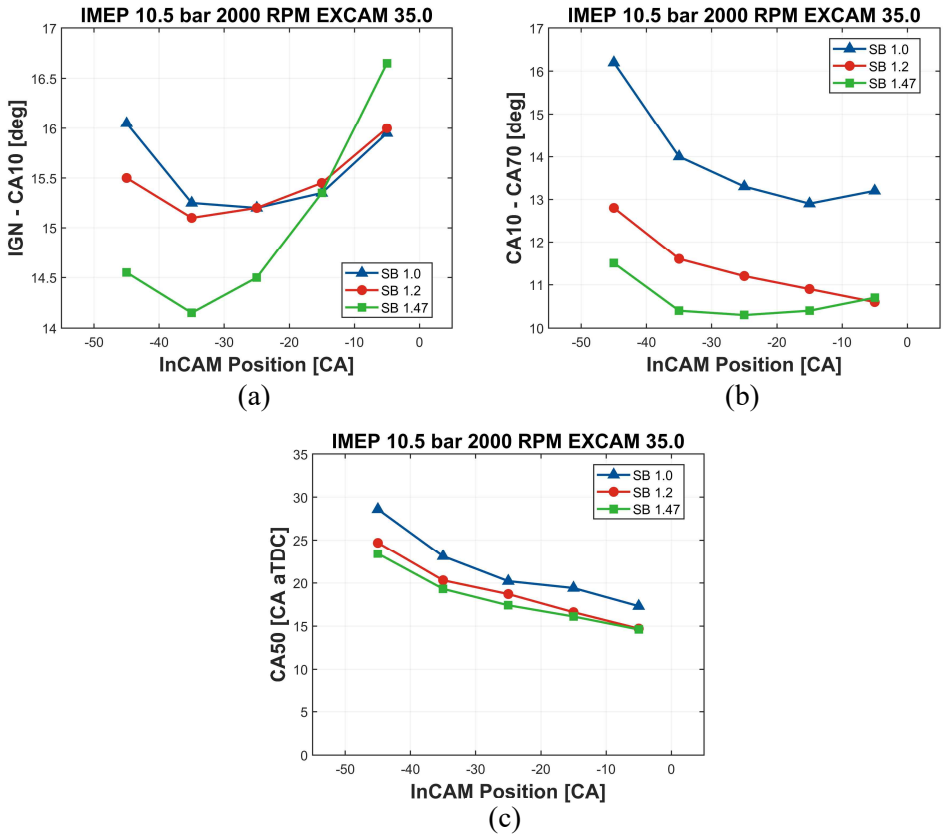

Figure 4.17 Experimental results of intake valve timing sweep for gIMEP 10.5 bar, 2000 RPM, and three SB ratios (1.0, 1.2, and 1.47)
(a) Initial flame speed
(b) Main flame speed (CA10-CA70)
(c) CA50

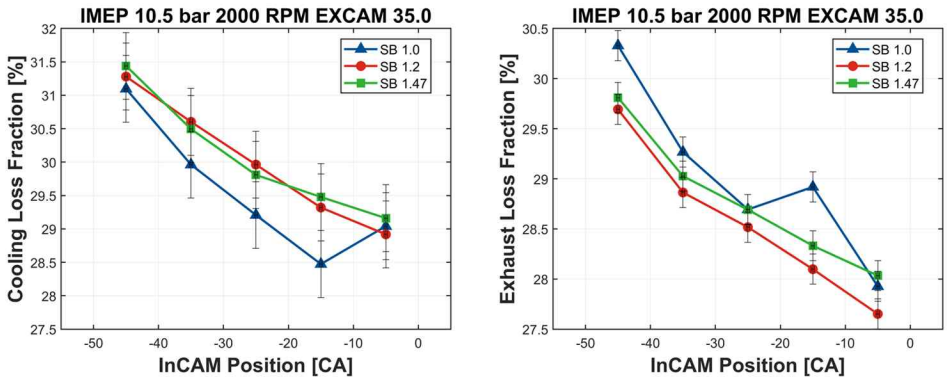

Figure 4.18 Experimental results of intake valve timing sweep for gIMEP 10.5 bar, 2000 RPM, and three SB ratios (1.0, 1.2, and 1.47)
(a) Cooling loss normalized by fuel LHV
(b) Exhaust loss normalized by fuel LHV
(c) Gross indicated efficiency

4.3 Comparison with different displacement volume and tumble ratio conditions

In this chapter, conducted was the validation of valve timing variation for the different displacement volume and tumble ratio conditions. Only low load results of each additional condition were used in this chapter for the effectiveness of discussion, where the sequence was listed below.

1) low load (~ nIMEP 4.5 bar) operation:
   basic conditions (SB 1.0, 1.2, and 1.47) and different displacement volume conditions (SB 1.19, 1.42)

2) low load (~ nIMEP 4.5 bar) operation:
   basic conditions (SB 1.0, 1.2, and 1.47) and different tumble ratio conditions (SB 1.2 high Rt and 1.47 high Rt)

Although the high load operation ($\geq$ nIMEP 8.5 bar) had been also conducted for the additional conditions (i.e. different displacement volume and tumble ration conditions), it was not covered in this chapter with two reasons. First, for different displacement volume condition, it was not the scope of this work to investigate the knock-related characteristics with varying displacement volume – only low load operation with effective amount of heat transfer was covered in this and the next chapter. Second, for different tumble ratio condition, only slight change in valve timing due to the enhanced flame speed was discovered, where no further discussion with valve timing variation for this issue was needed. Here, only efficiency-related parameters were presented in order to check whether the difference of best points for intake and exhaust valve timing existed.

4.3.1 Basic conditions vs. different displacement volume conditions

The experimental data of low load operation were plotted in figure 4.19, 4.20, 4.21, and 4.22, with 1500 and 2000 RPM conditions. ExCAM position was set to 35 (fully retarded) with same reason mentioned in previous chapter. First of all, for the pumping loss, it was shown that the conditions with higher displacement volume (i.e. SB 1.19 and 1.42) had larger pumping loss for almost all valve timing points than the conditions of same bore size for each (i.e. SB 1.0 and 1.2), attributed by relatively small valve diameter compared to increased displacement volume. However, it was inevitable as considering common notion that valve diameter is proportional to its bore size. Therefore, these were not specific results to the current engine setup but a general result that should be fully considered in the process of determining the SB ratio with increased displacement volume. In case of the results of cooling loss, expected behaviors were found – increased displacement volume can make smaller S/V ratio and, resultantly, reduce cooling loss compared to the condition of small displacement volume with similar SB ratio. One thing should be noted that with RPM variation, SB 1.42 showed relatively increased cooling loss compared to other conditions. In addition, for the case of exhaust loss, similar trends were found that higher SB ratio (both SB 1.47 and 1.42) had increased exhaust loss compared to other conditions. Although all the efficiency data showed higher tendency for larger displacement volume conditions, the above-mentioned trends are worth further analysis, which will be covered in chapter 5.

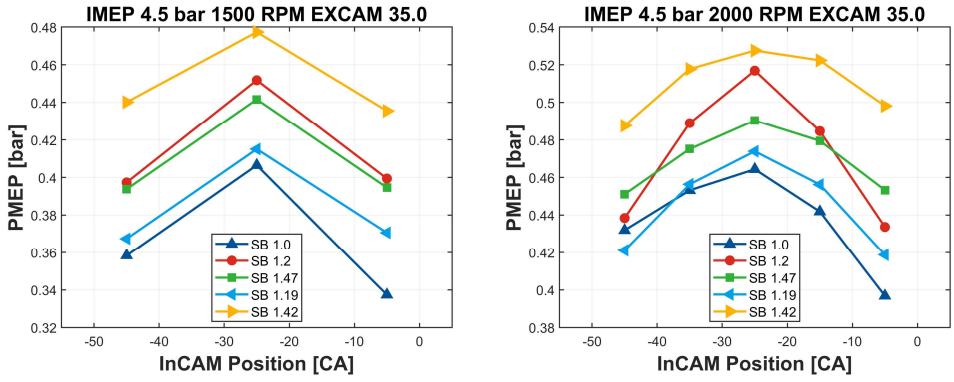

(a) (b)

Figure 4.19 Pumping loss data for intake valve timing sweep with nIMEP 4.5 bar, 1500 and 2000 RPM, and five SB ratios (1.0, 1.2, 1.47, 1.19 and 1.42)
(a) 1500 RPM
(b) 2000 RPM

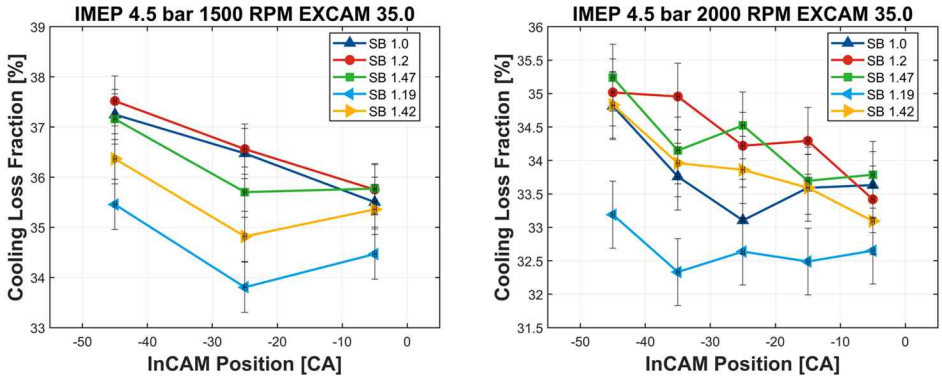

(a) (b)

Figure 4.20 Cooling loss data for intake valve timing sweep with nIMEP 4.5 bar, 1500 and 2000 RPM, and five SB ratios (1.0, 1.2, 1.47, 1.19 and 1.42)
(a) 1500 RPM
(b) 2000 RPM

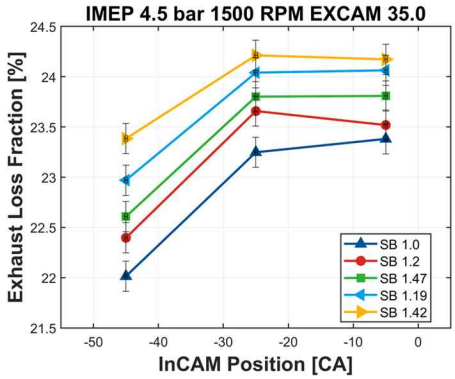

(a)

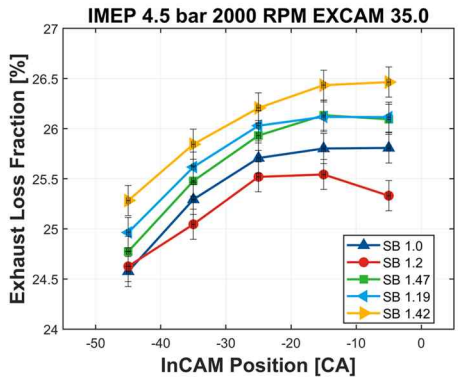

(b)

Figure 4.21 Exhaust loss data for intake valve timing sweep with nIMEP 4.5 bar, 1500 and 2000 RPM, and five SB ratios (1.0, 1.2, 1.47, 1.19 and 1.42)
(a) 1500 RPM
(b) 2000 RPM

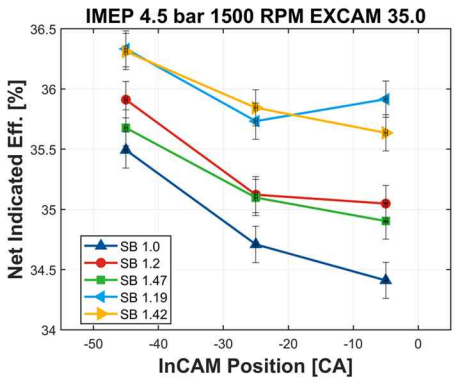

(c)

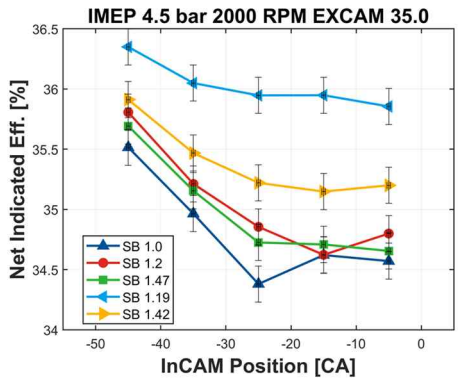

(d)

Figure 4.22 Net indicated efficiency data for intake valve timing sweep with nIMEP 4.5 bar, 1500 and 2000 RPM, and five SB ratios (1.0, 1.2, 1.47, 1.19 and 1.42)
(a) 1500 RPM
(b) 2000 RPM

4.3.2 Basic conditions vs. different tumble ratio conditions

The experimental data of low load operation were plotted in figure 4.23, 4.24, 4.25, 4.26, and 4.27, for 1500 and 2000 RPM conditions. ExCAM position was set to 35 (fully retarded). First, combustion efficiency was discussed, which showed interesting behavior with different RPM and SB ratio. Because of enhanced tumble ratio and, resultantly, flame speed in both initial and main duration[21], both 'SB 1.2 high Rt' and 'SB 1.47 high Rt' conditions showed improvement in combustion efficiency for both 1500 and 2000 RPM, whereas the degree was different – slightly lower increment between SB 1.47 and 'SB 1.47 high Rt' (although the tendency was slightly fluctuated for some points of intake valve timing). This may be caused by fast volume expansion issue mentioned earlier. Second, for the flame speed issue, both initial and main flame speed were increased thanks to the enhanced tumble ratio, except for some points. Because of this, gross work can be extracted sufficiently to achieve relevant load (~nIMEP 4.5 bar) with lower fuel and, resultantly, air mass. According to this small amount of inducted air, higher pumping loss was derived for higher tumble ratio cases, shown in figure 4.25. One can claim that this is demerit of constant nIMEP experiment – in order to achieve same nIMEP, different amount of PMEP was derived which, for certain cases, may not be the focus of the experiment. Thus, another sort of experiment was suggested – same fuel rate experiment of which operating conditions were partially mentioned in table 4.3. Therefore, in the remaining chapters, same fuel rate experiments were also presented except for different displacement volume experiments[22], because the discussion about pumping loss was not the objective of the remaining chapters.

[21] Noted that not all the conditions of valve timing points followed this trend.
[22] Due to the different value of displacement volume, same fuel rate was not suitable to compare the experimental results fairly.

The other things which should be mentioned were both cooling and exhaust loss – especially cooling loss, shown in figure 4.26. Here, the results of cooling loss were shown to be higher for enhanced tumble ratio conditions (i.e. 'SB 1.2 high Rt' and 'SB 1.47 high Rt') of 1500 RPM case, attributed by faster burn duration. This trend, however, did not mean the decrement in efficiency, shown in figure 4.27, thanks to the significant decrement in exhaust loss caused by fast burning rate. However, for the case of 2000 RPM, only 'SB 1.47 high Rt' showed high cooling loss, compared to that of 'SB 1.2 high Rt' of which values were similar to those of SB 1.2 case. Since the heat transfer per a cycle is generally decreased as rotational speed increases due to the lack of time for heat transfer, the results of SB 1.2 can be understood by the general notion mentioned. Therefore, considering different rotational speed, this result can be attributed by the velocity term of convective heat transfer estimation (included in Reynolds number) – that is, due to the high piston speed caused by not only RPM increment but also high SB ratio, 'SB 1.47 high Rt' may have increased h term (convective heat transfer coefficient), resulting in higher cooling loss compared to other cases. For reference, exhaust loss showed same trend – the higher SB ratio, the larger exhaust loss. These will be comprehensively reviewed in chapter 5.

Because of improvement in combustion efficiency and decrement in exhaust loss, as a result, net indicated efficiency was improved for high tumble ratio conditions, shown in figure 4.27 with same position of intake valve timing (fully advanced).

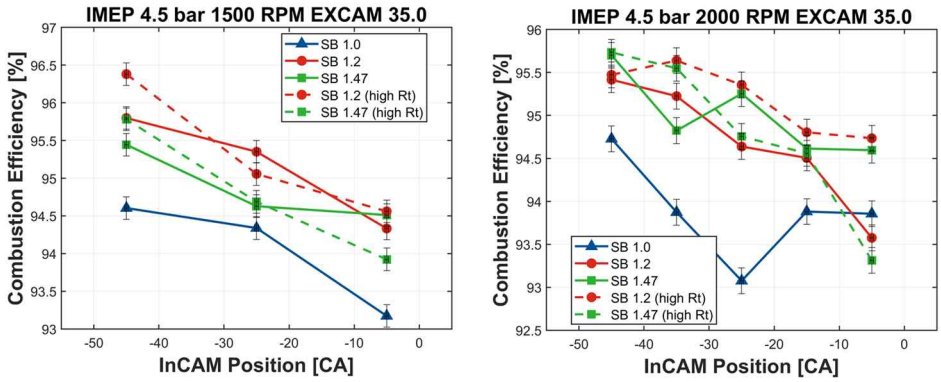

(a) (b)

Figure 4.23 Combustion efficiency data for intake valve timing sweep with nIMEP 4.5 bar, 1500 and 2000 RPM, and five different conditions (SB 1.0, 1.2, 1.47, 1.2 high Rt, and 1.47 high Rt)
(a) 1500 RPM
(b) 2000 RPM

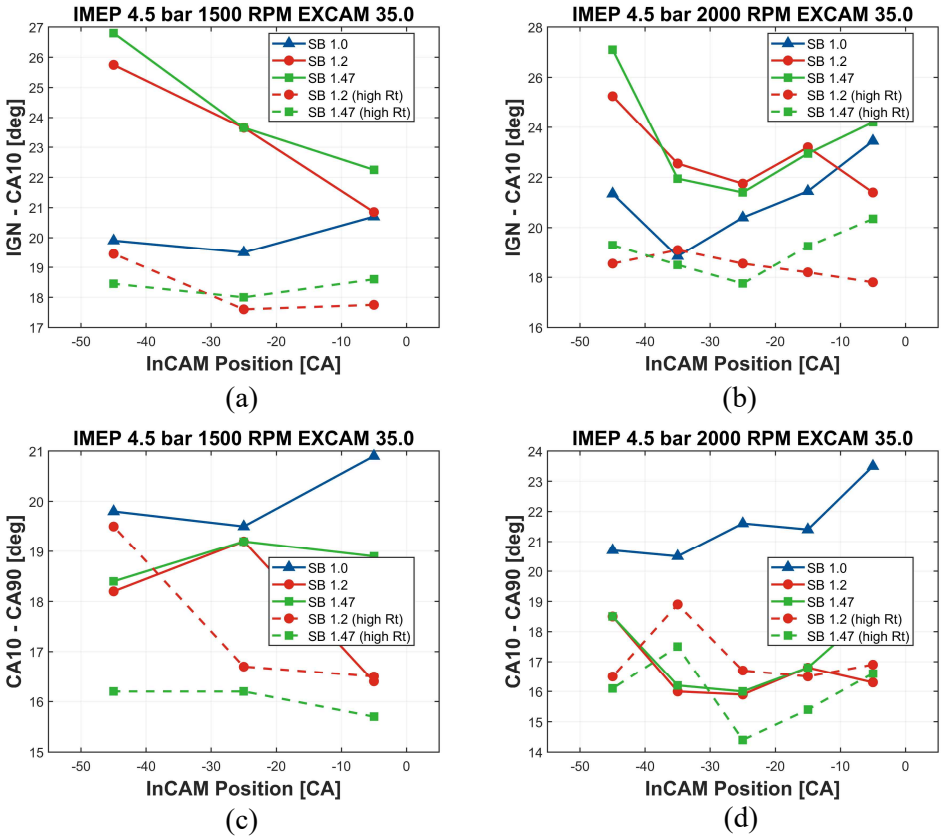

Figure 4.24 Flame speed data for intake valve timing sweep with nIMEP 4.5 bar, 1500 and 2000 RPM, and five different conditions (SB 1.0, 1.2, 1.47, 1.2 high Rt, and 1.47 high Rt)
(a) Initial flame speed for 1500 RPM
(b) Initial flame speed for 2000 RPM
(c) Main flame speed for 1500 RPM
(b) Main flame speed for 2000 RPM

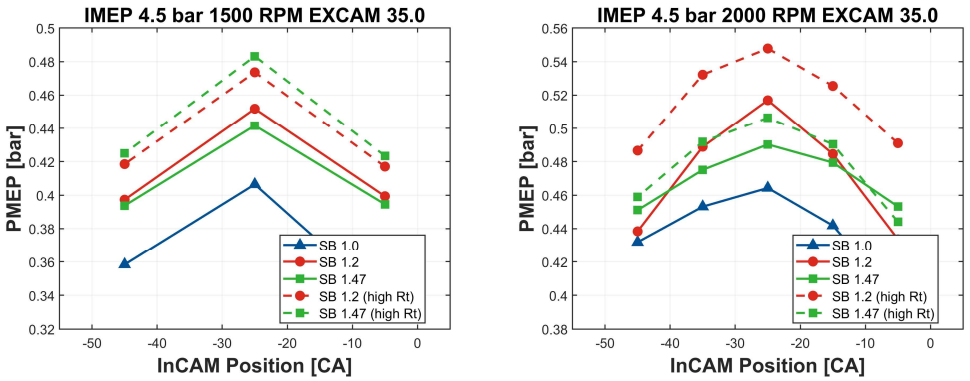

(a) (b)

Figure 4.25 Pumping loss data for intake valve timing sweep with nIMEP 4.5 bar, 1500 and 2000 RPM, and five different conditions (SB 1.0, 1.2, 1.47, 1.2 high Rt, and 1.47 high Rt)
(a) 1500 RPM
(b) 2000 RPM

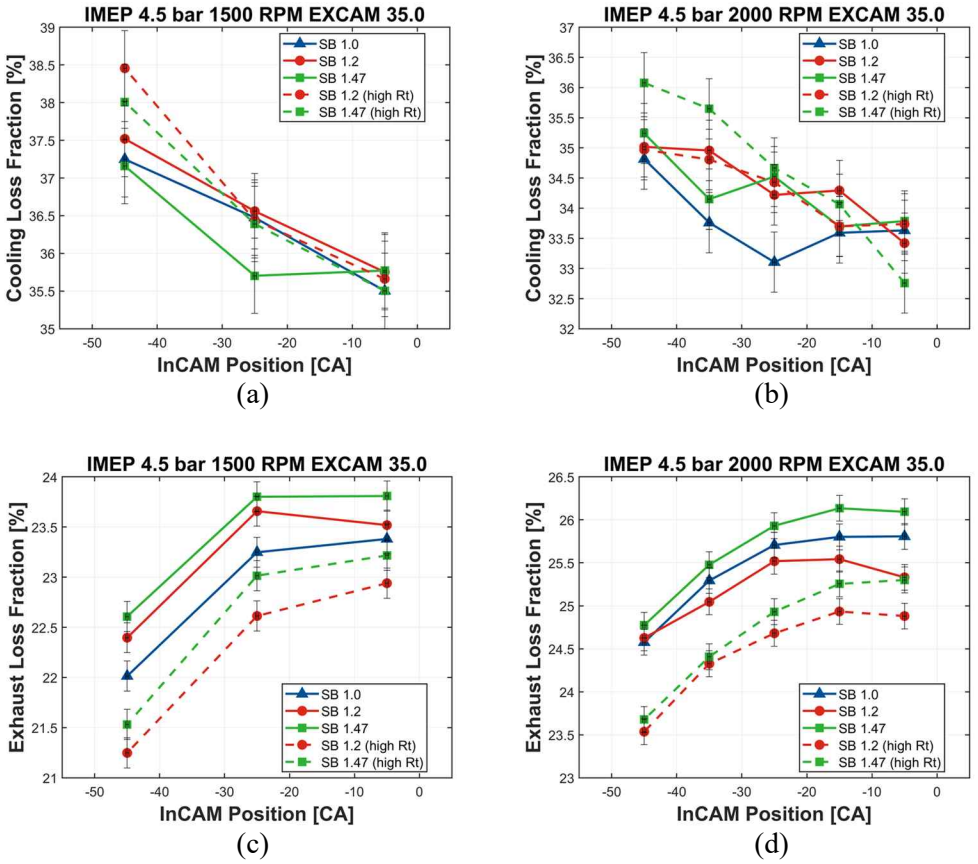

Figure 4.26 Cooling and exhaust loss data for intake valve timing sweep with nIMEP 4.5 bar, 1500 and 2000 RPM, and five different conditions (SB 1.0, 1.2, 1.47, 1.2 high Rt, and 1.47 high Rt)
(a) Cooling loss normalized by fuel LHV for 1500 RPM
(b) Cooling loss normalized by fuel LHV for 2000 RPM
(c) Exhaust loss normalized by fuel LHV for 1500 RPM
(b) Exhaust loss normalized by fuel LHV for 2000 RPM

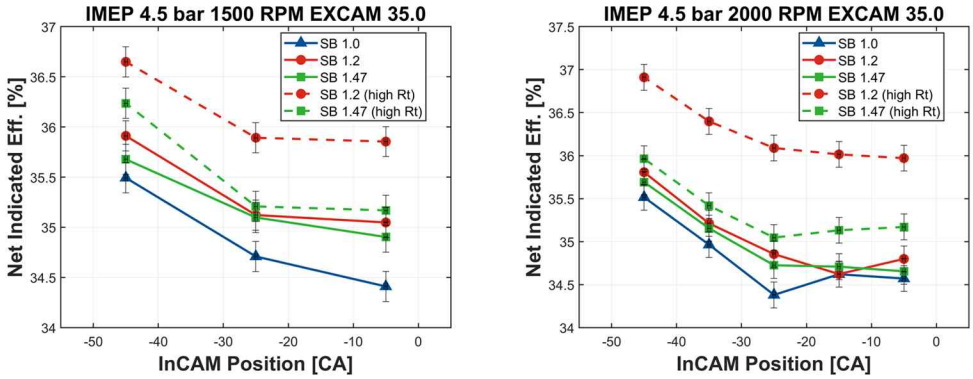

(a) (b)

Figure 4.27 Net indicated efficiency data for intake valve timing sweep with nIMEP 4.5 bar, 1500 and 2000 RPM, and five different conditions (SB 1.0, 1.2, 1.47, 1.2 high Rt, and 1.47 high Rt)
(a) 1500 RPM
(b) 2000 RPM

4.4 Interim summary

In this chapter, plenty of experimental results were briefly investigated to find the relevant valve timing for the best efficiency. Brief summary was listed below.

1) For all experimental conditions including basic three conditions (SB 1.0, 1.2, and 1.47), different displacement volume conditions (SB 1.19 and 1.42), and different tumble ratio conditions (SB 1.2 high Rt and SB 1.47 high Rt), fully advanced intake valve timing with fully retarded exhaust valve timing showed the best efficiency. This point was chosen as the best efficiency point in low load operation, not only for constant load experiment but also constant fuel rate experiment which will be presented in following chapters.

2) In case of middle load operation (~ nIMEP 8.5 bar, N/A WOT), moderately retarded exhaust valve timing with moderately or significantly advanced intake valve timing showed the best efficiency. Whether more advance in the intake valve timing was conducted or not depends on the flame speed and knock resistance of relevant specification.

3) In case of high load operation (~ gIMEP 10.5 bar, supercharged), significantly retarded (closed to the parking position) intake valve timing with moderately or significantly retarded exhaust valve timing showed the best efficiency, no matter how the specification can resist knock occurrence. That is, LIVC operation was found to effectively increase the gross indicated efficiency.

Through this process, many of trends which is unexpected were found such as increased cooling and exhaust loss for high SB ratio. Following chapters will focus on these unexpected issues in detail, which was classified as two issues

6) In terms of the heat transfer, and work and internal energy extraction, which SB ratio can result in the best efficiency for SI engine operation?

7) In terms of the knock characteristics, dominating the efficiency of high load operation, which SB ratio can show high knock resistance?

One issue, and eventually the most important issue in this work is that those two contents are significantly related to burning rate which is eventually the main target for engineers to increase SB ratio from common sense. Therefore, those issues can be re-summarized as listed below.

1) Could the increment in piston speed, which is the biggest factor that enhances burning rate by increasing SB ratio, cause other adverse effects related to engine efficiency?

2) Is the condition of fast burning rate really robust to knock occurrence?

These will be comprehensively covered in the following chapters, respectively.

Chapter 5. Experiment and Simulation – Burning Rate and Thermodynamics in Cylinder

As mentioned in the previous chapter, two important issues were found in the results of preliminary experiments of valve timing variation, as summarized in the final part of chapter 4. Here, the details of cooling and exhaust loss which are directly related to the efficiency of engine operation were investigated, with several techniques of combustion analysis mentioned in chapter 2. With the contents in this chapter, it can be clarified that whether an existing attempt to increase engine efficiency by increasing SB ratio is appropriate in some ways or not effective in other ways.

5.1 Introduction

From the experimental results in the previous chapter, undisputed tendency related to LHV breakdown parameters (i.e. efficiency-related parameters) was able to be found, as listed below.

1) The expected notion – 'due to the reduced SV ratio, cooling loss will be reduced with higher SB ratio condition' – was confirmed to be wrong. The notion was found to be the result of increment in displacement volume with fixed bore size.

2) Exhaust loss was increased with increment in SB ratio regardless of the displacement volume.

3) Combustion efficiency was aggravated with increment in SB ratio, possible attributed to the fast volume expansion during combustion period.

Two things should be noted that the difference of cooling loss did not show monotonous tendency and was not significant. In fact, cooling loss induced during whole cycle is too complicated phenomenon to be easily analyzed by using only bulk motion-based in-cylinder pressure and exhaust temperature, because lots of parameters (such as residual mass fraction, coolant jacket design, materials for engine block, volume profile, flow motion and its intensity related to turbulence, and combustion itself) were inevitably engaged. In addition, attributed by the method of calculating cooling loss (adding every LHV breakdown terms and subtracting the value from fuel LHV, mentioned in chapter 2), it is compelled to have large error range. Nonetheless, even accepting the difficulties, proper analysis with exploiting everything in this work can be and should be followed to explain the reason why the existing notion was not true.

5.2 Heat transfer timing and its effect

In general, heat transfer (cooling loss) during engine operation has the highest value around firing TDC timing, caused by high temperature and convective heat transfer coefficient. It is also associated with the conventional notion that it should be required to reduce SV ratio around TDC timing to diminish total amount of heat transfer. However, with the experimental data and combustion analysis in this study, it was found that the diminution of cooling loss itself is not the only reason to reduce heat transfer rate around TDC timing – the amount of exhaust loss or the remainder of internal energy at BDC (the end of closed duration) timing was also highly affected by the heat transfer rate around TDC timing.

Figure 5.1 showed the in-cylinder pressure experimental data and predicted 'adiabatic' in-cylinder pressure from relevant data, where the data was produced with constant fuel rate (14 mg per cycle, approximately nIMEP 4-4.5 bar depending on the operating condition). In order to estimate adiabatic pressure, in the first place, heat transfer rate for each crank angle was calculated by the method mentioned in chapter 2.1.2, and removed to evaluate the renewed internal energy containing not only the original value but also relevant heat transfer rate. Because of the updated internal energy[23] [98], pressure has to be changed to compensate the changed temperature (by removed heat transfer rate) under same instantaneous volume, called 'adiabatic' in-cylinder pressure. Because of the elimination of heat transfer, the work accumulation must be larger for adiabatic case, as shown in figure 5.1. However, it must be noted that the difference between accumulated work of adiabatic and real case does not have to be the same with the amount of heat transfer rate because internal combustion engine does not convert all types of work from internal energy but only mechanical work (i.e. PdV). Since dV, the difference of volume between adjacent crank angle, was always constant for each crank angle, pressure change due to heat transfer was the only matter that determine the difference between accumulated work of adiabatic and real cases. Furthermore, since the adiabatic case can be regarded as ideal operation, the difference can be considered as 'work loss' due to heat transfer, about not only its amount but also its timing. Considering these, it is not surprising to raise the question – when does a heat transfer affect PdV work generation to the maximum? This can be theoretically resolved by simple calculation with the approach on Otto-cycle operation. For contextual issue, the details of proof was covered in Appendix A, and only the final results of the proof were mentioned in here that

[23] Noted that in the beginning of compression stroke (from IVC to approximately -70 CA aTDC), the heat transfer rate was negative due to the lower temperature of mixture compared to that of cylinder wall so that the adiabatic pressure was lower than original (measured) pressure at certain timing, considering the cumulative effects. After that, it was always higher than measured in-cylinder pressure.

the maximum pressure timing (i.e. TDC timing for Otto cycle) has the maximum effect on the change of PdV work extraction for Otto cycle operation. Therefore, despite the difference between Otto-cycle and real engine operation, it can be postulated that the heat transfer around TDC timing has a significant effect on 'work loss' and, resultantly, real work extraction itself from measured data, because the maximum pressure usually occurs around TDC timing for MBT operation.

In order to investigate these issues further, relevant experimental data were shown in figure 5.2 with simulated heat transfer rate, and figure 5.3 with real heat transfer rate from the case of nIMEP 4.5 bar and 2000 RPM for three SB ratio conditions. Here, presented was the difference between the accumulated work from adiabatic pressure (ideal case) and the accumulated work from semi-adiabatic pressure with only applying the heat transfer rate of pertinent crank angle. Therefore, for certain crank angle, the y value represented the effect of heat transfer rate on the work loss on the crank angle. Firstly, same amount of heat transfer rate (one Joule per deg) was applied for each crank angle, where the relevant data was shown in figure 5.2. Considering the results, no significant difference between the conditions of SB ratio was found with same amount of heat transfer rate for each crank angle. Therefore, it can be postulated that if the difference in work loss occurs, it is only caused by the amount of heat transfer rate for relevant crank angle, not by the geometrical reason[24]. The relevant data were shown in figure 5.3. Here, important results were found that SB 1.47 condition showed the greatest difference in work loss around its peak pressure timing compared to other SB ratios. Therefore, considering the discussions mentioned earlier, it can be postulated that at least for this operating condition (nIMEP 4.5

[24] However, the different heat transfer rate for each crank angle will be undoubtedly caused by different geometries (i.e. SB ratio). Thus, this is not perfectly right postulation.

bar, 2000 RPM), the higher SB ratio, the greater heat transfer rate around its peak pressure timing (near TDC), which is completely opposite to expected results that higher SB ratio will have small amount of heat transfer rate around TDC due to its lower SV ratio. Thus, regarding these results, it was necessary to conduct comprehensive analysis of heat transfer while observing each parameter separately, where the relevant contents were covered in the next chapter.

In order to assure that this tendency appears in the overall results of the experiments, conducted was another approach of which results were shown in figure 5.4. Here, the values in x-axis were the estimated total heat transfer from IVC to EVO timing for each operating point with no knock occurrence, and those in y-axis were the work loss caused by relevant total heat transfer. It should be noted that every knock-free condition conducted in the experiments were plotted together regardless of its operating conditions (e.g. valve timing, rotational speed). Regarding the issues mentioned above, if there is a high fraction of heat transfer occurrence near TDC or peak pressure timing, work loss will be generated significantly even though the same amount of heat transfer occurs. As shown in figure 5.4-b, c, and d, these were presented with a 1st order-fitted curve where the value of slope for each SB ratio condition represented how much work loss occurred with same amount of total heat transfer. It was found that the higher SB ratio, the greater the value of slope – that is, regardless of operating conditions[25], higher SB ratio condition produced more work loss caused by large fraction of heat transfer around TDC (or peak pressure) timing. In other words, with same amount of total heat transfer, higher SB ratio can result in more work loss due to its characteristics of heat transfer rate. However, the work loss itself does not actually appear in the real experiments because it is based on the estimated value of ideal case (i.e. adiabatic operation). Therefore, the related question can be

[25] Noted that the effect of different operating conditions (e.g. valve timing, rotational speed) was indirectly represented as a coefficient of determination (i.e. R^2).

raised as summarized; if the same values of initial internal energy (i.e. same internal energy at IVC timing) and total heat transfer during closed duration, how can this trend be shown in actual data of experiments? It can be resolved by applying 1st law of thermodynamics into the closed duration as listed below[26].

$$U_{IVC} = Q_{IVC-EVO} + \int_{IVC}^{EVO} PdV + U_{EVO} \qquad \text{eq. 5.1}$$

Regarding this equation, the LHS term and first term at RHS were assumed to be same by the assumption of the question mentioned earlier. In addition, since the ideal case of relevant operation was set to be fixed (i.e. uniqueness), the only terms that can be affected by heat transfer timing were remaining two terms – work generation term (second term at RHS) and the remainder of internal energy at EVO timing (third in RHS). Therefore, it can be postulated that the heat transfer timing, which turned out to have a significant effect on work loss, affects total work generation of which form is mechanical work (i.e. PdV) and resultantly, the remainder of internal energy at EVO timing. As a result, the following proposition can be concluded.

- Even if the system input (i.e. temperature, pressure, and composition of the mixture at the start – IVC timing, time per cycle (related to rotational speed), engine geometries (e.g. compression ratio)) and total heat transfer can be assumed to be same, real work generation can be different because it is directly affected by the timing of heat transfer rate of which outcome is represented as system output (i.e. temperature, pressure, and composition of the mixture at the end – EVO timing).

[26] Noted that it is another form of eq. 2.11.

Two data set which can supplement aforementioned proposition and the final conclusion of this chapter were presented in figure 5.5, 5.6, and 5.7. For figure 5.5-a and 5.5-b, the values of x-axis represent the difference between total heat transfer and work loss for each condition, and those of y-axis represent the difference of internal energy between IVC and EVO timing. It is noted that the data in this figure were corresponding to knock-free load conditions. By the tendency presented in this figure, it can be postulated that if the work loss becomes larger with same amount of total heat transfer (i.e. lower x-values), relatively larger amount of internal energy (mainly sensible term) will remain, which was supposed to be used as a source of work extraction or heat transfer during closed duration. In addition to this, as shown in figure 5.5-b, same data with specific marker were presented to distinguish each other. Here, one thing should be noted that as burning rate became faster by increasing SB ratio or tumble ratio, the relevant data showed a tendency to have larger work loss and smaller internal energy extraction. Considering aforementioned contents, it is possible to predict that faster burning speed can affect the heat transfer rate around TDC (or peak pressure timing) so that the tendency occurs. Although this will be covered in detail with relevant experimental data in the next chapter, the relevant results with clear tendency can be obtained as shown in figure 5.6. In this figure, heat transfer during CA10 to CA70 was normalized by total amount of heat transfer during closed duration, correlated with relevant burn duration (from CA10 to CA70) for basic three SB ratio and different tumble ratio conditions with knock-free region (fuel rate under 22 mg per cycle). Here, enhancement in tumble ratio resulted in faster flame speed for both SB 1.2 and 1.47 conditions, whereas the trends of heat transfer showed opposite directions for each case of SB 1.2 to 1.2 high Rt (shown as red arrow) and SB 1.47 to 1.47 high Rt (shown as green arrow). That is, although similar increment in flame speed were conducted by enhanced tumble ratio for both SB 1.2 and 1.47, the fraction of heat transfer during main combustion process (around TDC or peak pressure timing) was higher for SB 1.47

case. Therefore, it can be postulated that if the same amount of heat transfer during closed duration occurred, SB 1.47 may result in higher work loss due to the specific trend shown in figure 5.6. Furthermore, according to the data shown in figure 5.5, it can be easily predicted that the larger amount of internal energy remains, the greater exhaust loss remains if there is no significant heat transfer during exhaust stroke, supplemented by the data shown in figure 5.7, where the whole experimental data including not only the basic conditions (i.e. three SB ratios) but also the conditions of different displacement volume and tumble ratio, for all load (knock-free and knock-related) and rotational speed conditions. Regarding the tendency shown in this figure, it is clear that the more sensible internal energy remains, the greater exhaust loss occurs. Therefore, with all the contents discussed in this chapter, it can be finally concluded that due to the distinguishing timing of heat transfer rate for each SB ratio, not only cooling loss but also exhaust loss, all of which are directly related to engine efficiency, can be differed by the conditions of SB ratio.

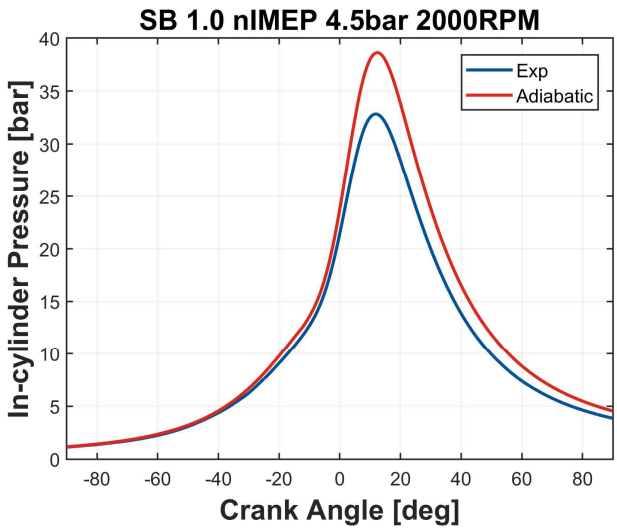

Figure 5.1 In-cylinder pressure profile of the best efficiency condition with SB 1.0, nIMEP 4.5 bar, and 2000 RPM and its adiabatic pressure profile

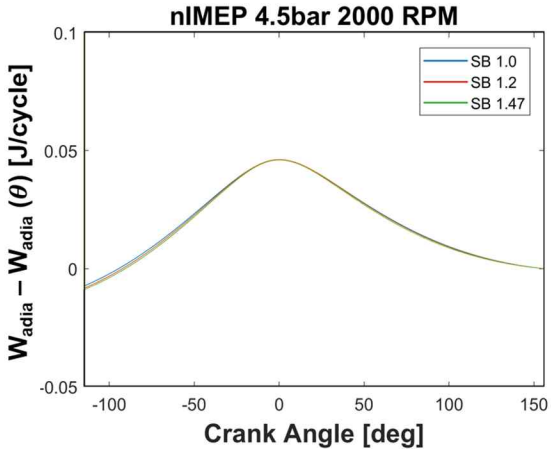

Figure 5.2 The effect of heat transfer timing on the summation of adiabatic work, expressed as subtraction between total adiabatic work and pseudo adiabatic work (nIMEP 4.5 bar, 2000 RPM)

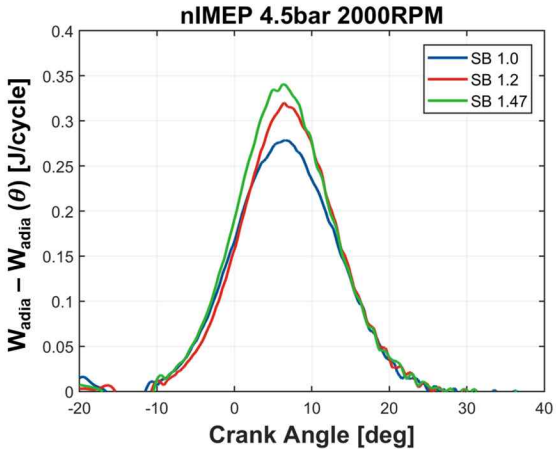

Figure 5.3 The effect of heat transfer timing on the summation of adiabatic work with real heat transfer value at the relevant crank angle timing (nIMEP 4.5 bar, 2000 RPM)

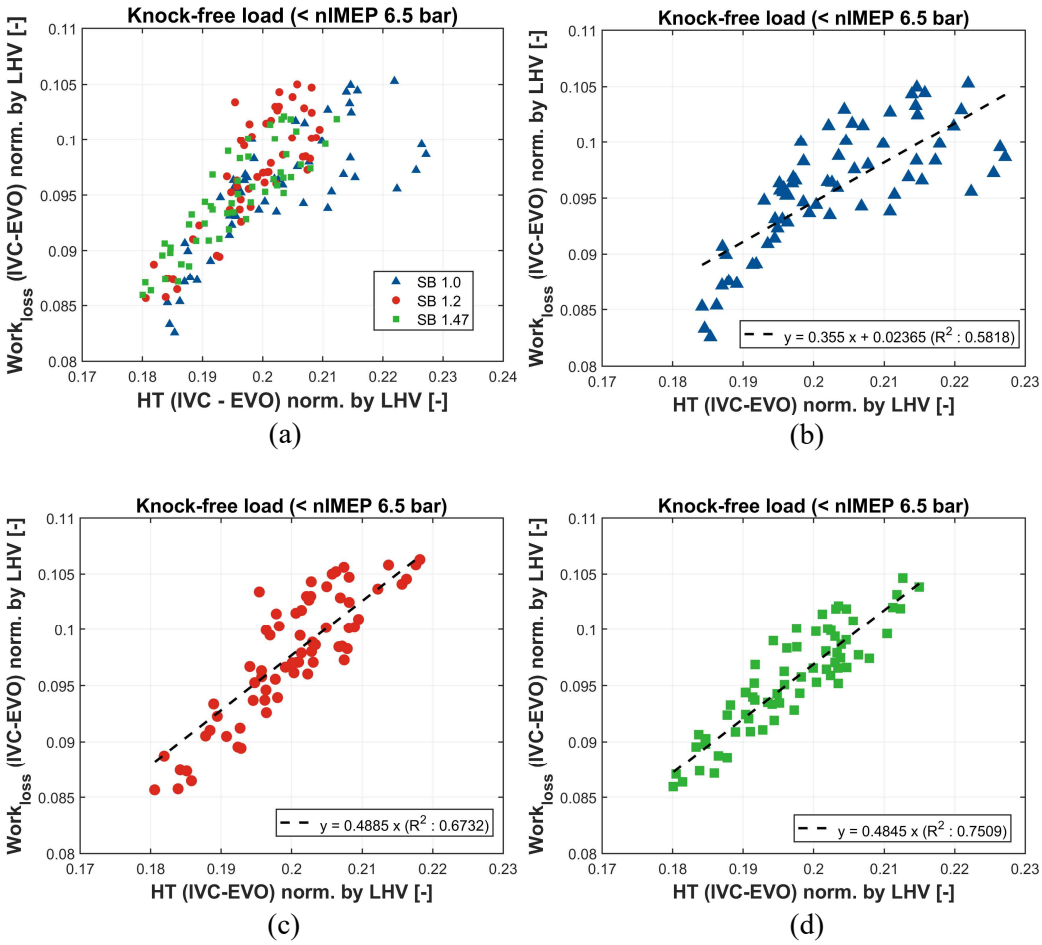

Figure 5.4 Correlation between heat transfer and work loss during closed duration for each SB ratio condition with knock-free data (< nIMEP 6.5 bar), normalized by relevant fuel LHV
(a): all conditions
(b): SB 1.0 with 1st order curve fitting
(c): SB 1.2 with 1st order curve fitting
(d): SB 1.47 with 1st order curve fitting

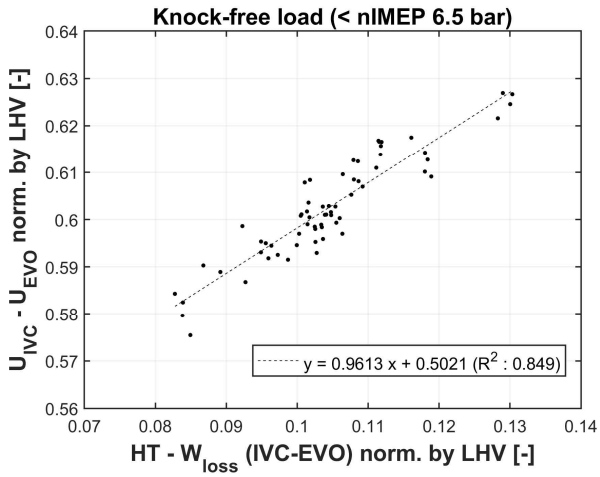

(a)

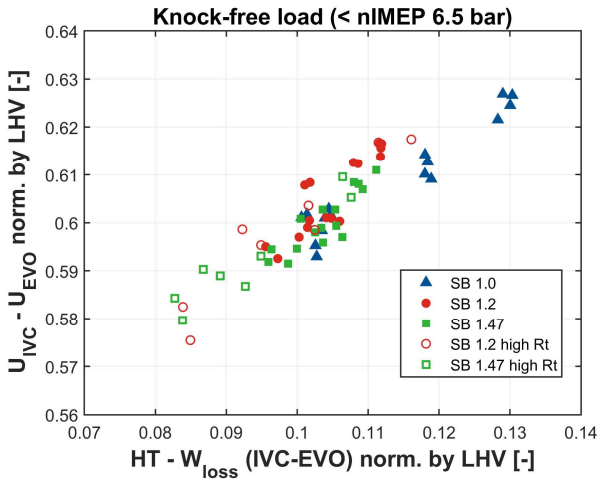

(b)

Figure 5.5 Correlation between the difference between heat transfer and work loss during closed duration and the difference of internal energy from IVC to EVO with knock-free data (< nIMEP 6.5 bar), normalized by relevant fuel LHV
(a) basic three SB ratio with tumble ratio enhanced conditions
(b) same graph with (a) but conditions marked

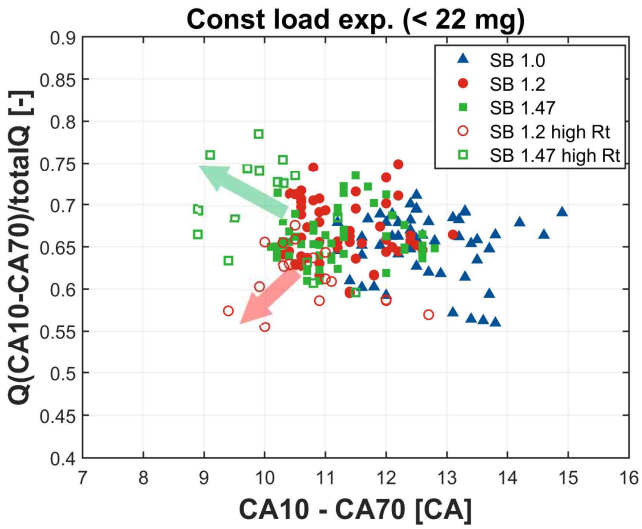

Figure 5.6 Trends of heat transfer during main flame propagation (CA10 to CA70) with relevant burn duration for basic three SB ratio and different tumble ratio, normalized by total amount of heat transfer during closed duration

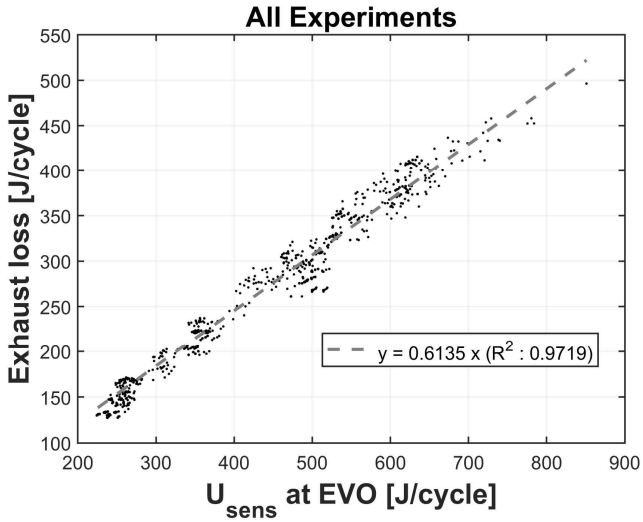

Figure 5.7 Correlation between the remainder of internal energy at EVO timing and exhaust loss for all operating conditions under knock-free operation (including basic three SB ratio, different displacement volume and tumble ratio conditions)

5.3 Experimental Results

Using what was discussed earlier and the experimental data, shown in chapter 4, detailed results were covered in this chapter. Here, the basic conditions mainly used in the previous chapter and other conditions – different displacement volume and tumble ratio – were covered for each sub-chapter. It is noted that the following data were based on the best efficiency point derived in chapter 4. In addition, only low load operation (~nIMEP 4.5 bar, 14-20 mg of fuel rate per cycle) was considered because of the two reasons – firstly, the fraction of heat transfer (among LHV breakdown) is usually considerable in low load operation. In addition, the valve timing corresponding to the best efficiency at low load operation was same for all the conditions.

One thing should be noted that heat transfer rate, which was assumed to be only convective heat transfer term, was analyzed by separation of each term comprising convective heat transfer – the coefficient, contact (wetted) area, and temperature difference. Since the area term was changed by only SB ratio, the remaining two terms were mainly considered for the analysis. The pre-calculated wet area data for pertinent crank angle were plotted in figure 5.8.

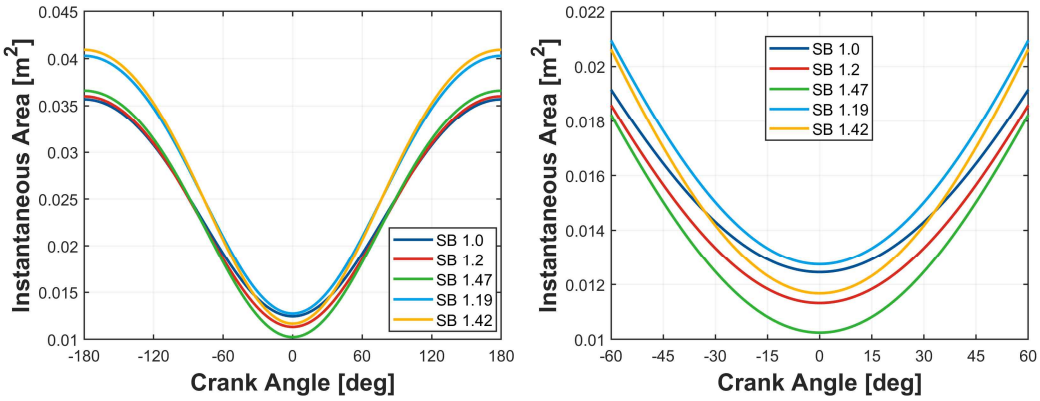

(a) (b)

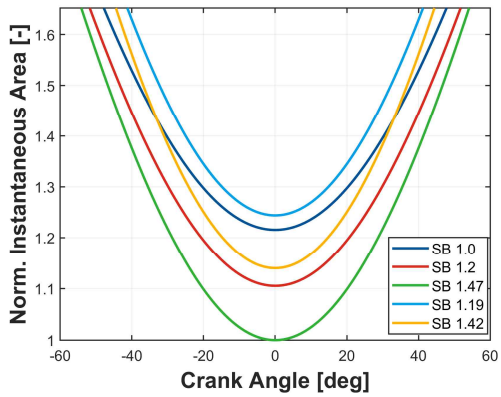

(c)

Figure 5.8 Instantaneous are at each crank angle for basic three SB ratio and different displacement volume conditions.
(a): whole crank angle (compression + expansion stroke)
(b): same with (a) but magnified, targeted to firing TDC timing
(c): same with (b) but normalized by the volume of firing TDC timing for SB 1.47 condition

5.3.1 Basic three conditions with different displacement volume

The experimental data from basic three conditions (i.e. SB 1.0, 1.2, and 1.47) and different displacement volume conditions (i.e. SB 1.19 and 1.42) were covered in this chapter. Because of the difference in displacement volume, the data of same load operation (~nIMEP 4.5 bar) was used instead of same fuel rate, which was mainly used in chapter 5.3.2, where the same displacement volume with different tumble ratio was covered.

Firstly, the experimental data for nIMEP 4.5 bar, 1500 RPM case were plotted in figure 5.9 and 5.10. Here, as mentioned before, convective heat transfer rate was separated by the parameters used to calculate its value – convective heat transfer coefficient, wet area, and mass averaged temperature[27], where the relevant data were presented in figure 5.9. Two things should be noted. First, the summation of each bar in figure 5.10-b was identical to the amount of internal energy extraction by the 1st law of thermodynamics, normalized by relevant fuel LHV. Second, the degree of heat transfer, normalized by fuel LHV, shown in the same figure, was considerably lower than the fraction of cooling loss shown in figure 5.10-c. It implies that a significant amount of heat transfer occurs after EVO timing. Therefore, the tendency of total cooling loss cannot be judged by the fraction of heat transfer during closed duration.

Here, it was found that, firstly, the convective heat transfer coefficient was found to be higher for high SB ratio condition. Because of this, although the area was lower for high SB ratio condition, no significant difference occurred in heat transfer rate. With regard to exhaust loss, both SB 1.47 and 1.42 conditions (i.e. higher SB ratio) showed larger amount compared to that of both SB 1.2 and 1.42

[27] The relevant equation was previously introduced in the equation 2.27 and 2.28 of chapter 2.3.1.

conditions, respectively. While the difference of exhaust loss between SB 1.2 and 1.47 was too low to exceed error bar, that between SB 1.19 and 1.42 was sufficiently high of which tendency was also presented in the internal energy extraction value shown in figure 5.10-b (final height of bar graph, i.e. summation of two bars). For closed duration, slightly higher work generation and lower heat transfer occurred at SB 1.42 condition compared to SB 1.19, while the tendency was compensated by higher pumping loss for SB 1.42, shown in figure 4.19-b and represented as the value of net indicated efficiency in figure 5.10-c. Here, proved was the conventional notion that larger displacement volume can reduce cooling loss, by the value of cooling loss shown in the same figure.

The experimental data for the same load (nIMEP 4.5 bar) with different rotational speed (2000 RPM) were plotted in figure 5.11 and 5.12. First, significant increases in both heat transfer rate and its coefficient were found in SB 1.42 condition, ironically attributed by faster burning rate caused by increased SB ratio. Here, the increase in convective heat transfer coefficient seemed to be attributed by enhanced flow motion related to both increment in SB ratio and rotational speed. In general, increment in rotational speed may cause enhanced convective heat transfer coefficient, whereas the total heat transfer was decreased due to the lack of time for heat transfer. Considering this general case, it can be postulated that too much increment in SB ratio can cause significant growth in convective heat transfer coefficient, which may defeat the effect of decrement in time. In addition, despite the discussion about heat transfer timing and internal energy extraction, excessively large amount of heat transfer occurred so that the internal energy extraction was also higher for the case of SB 1.42 compared to that of SB 1.19. Here, one thing should be noted that despite faster burning rate, increment in SB ratio seemed to not be a good strategy to increase engine efficiency due to the unexpected heat transfer occurrence, which can be supplemented by the decrement of cooling loss from SB 1.2 to SB 1.19.

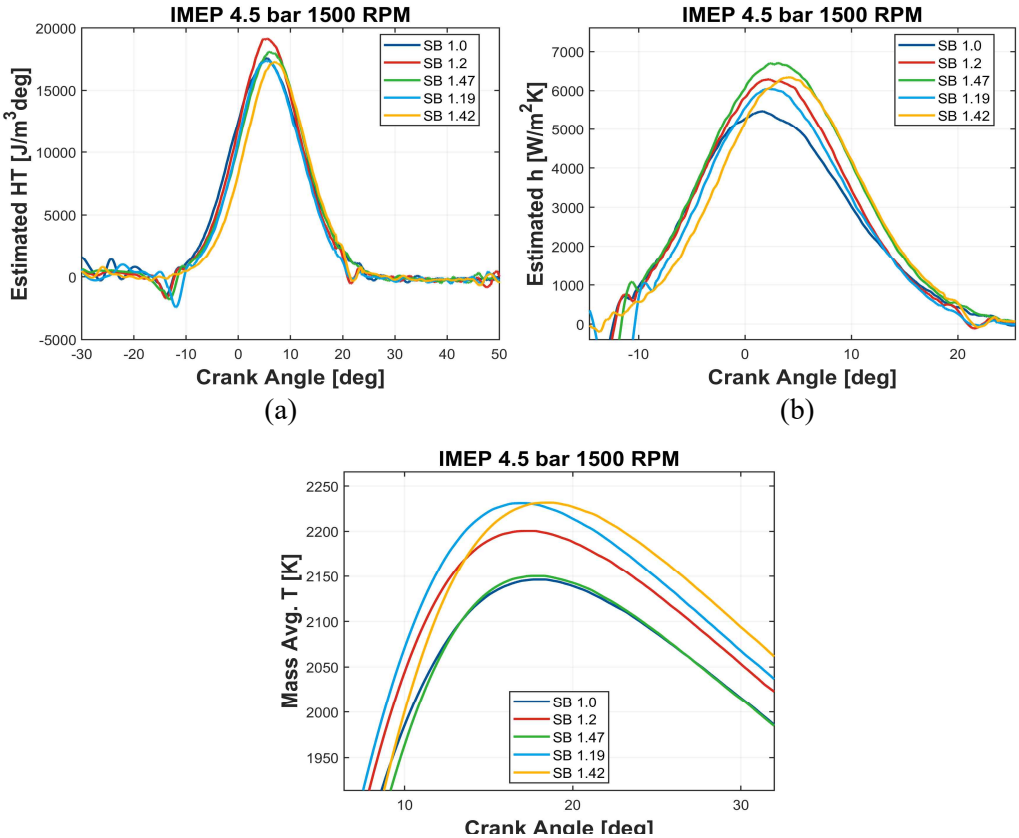

Figure 5.9 Experimental data for basic three SB ratio with different displacement volume (nIMEP 4.5 bar, 1500 RPM with the best efficiency operation)
(a): estimated heat transfer during closed duration
(b): estimated convective heat transfer coefficient
(from single zone approach)
(c): mass-averaged single zone temperature

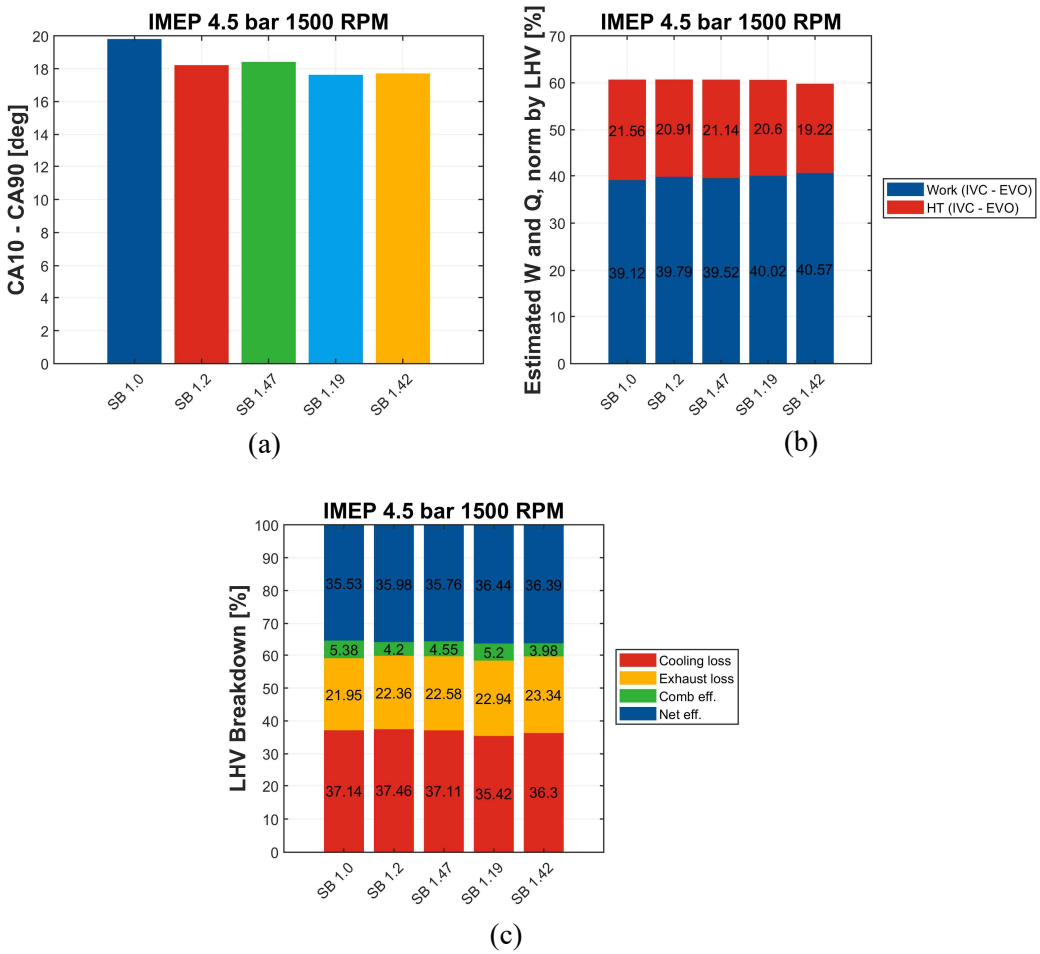

Figure 5.10 Experimental data for basic three SB ratio with different displacement volume (nIMEP 4.5 bar, 1500 RPM with the best efficiency operation)
(a): burn duration from CA10 to CA90
(b): estimated heat transfer and work extraction during closed duration, normalized by relevant fuel LHV
(c): fuel LHV breakdown

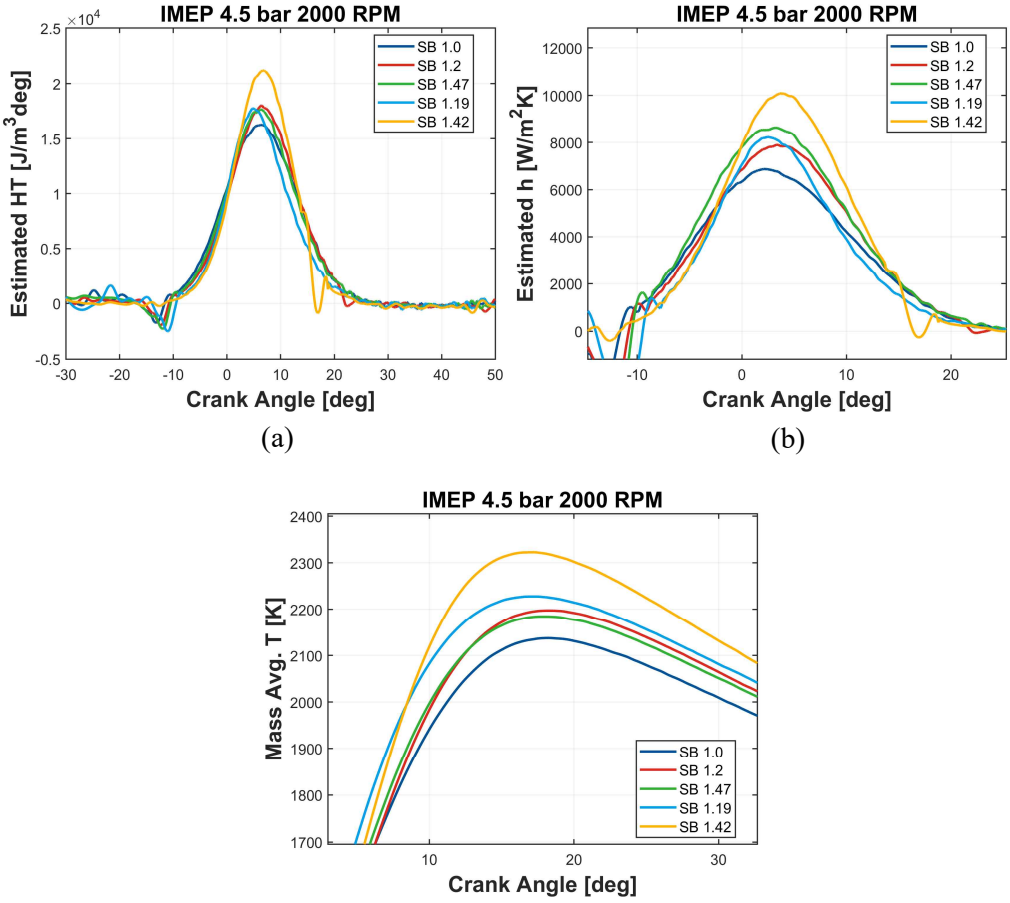

Figure 5.11 Experimental data for basic three SB ratio with different displacement volume (nIMEP 4.5 bar, 2000 RPM with the best efficiency operation)
(a): estimated heat transfer during closed duration
(b): estimated convective heat transfer coefficient
(from single zone approach)
(c): mass-averaged single zone temperature

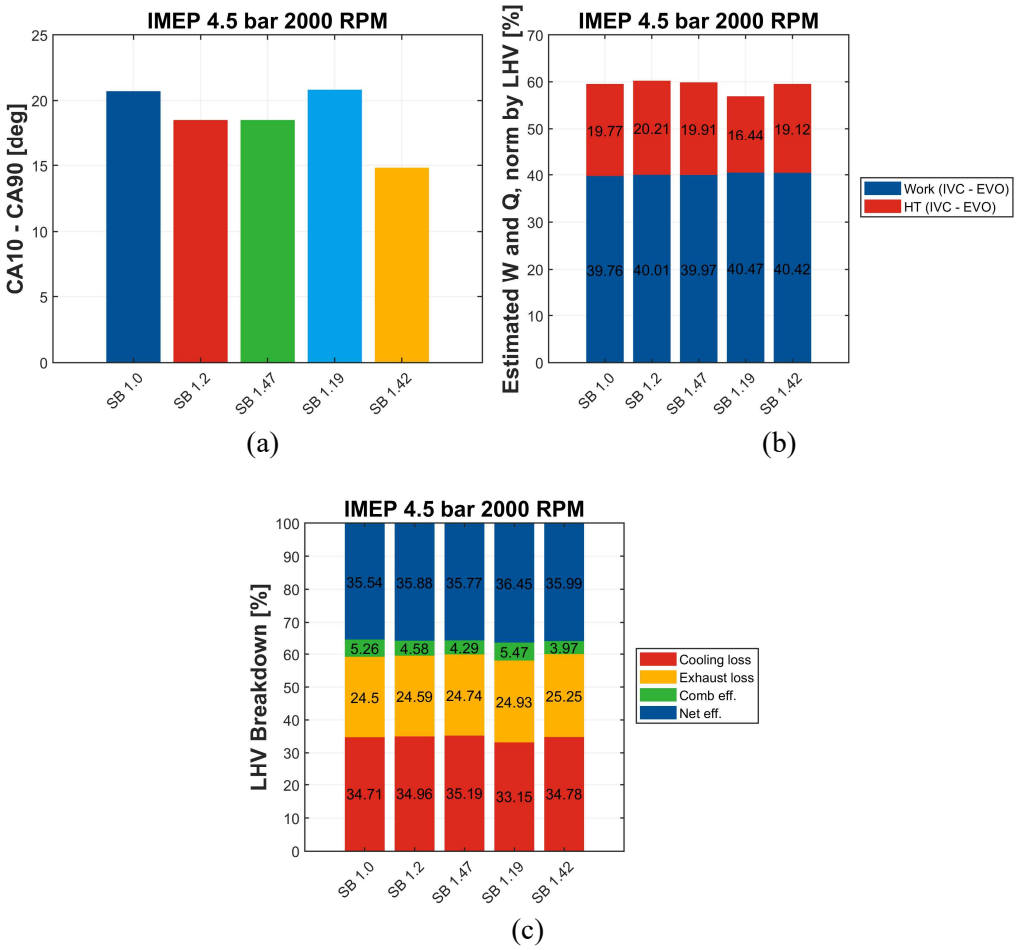

Figure 5.12 Experimental data for basic three SB ratio with different displacement volume (nIMEP 4.5 bar, 2000 RPM with the best efficiency operation)
(a): burn duration from CA10 to CA90
(b): estimated heat transfer and work extraction during closed duration, normalized by relevant fuel LHV
(c): fuel LHV breakdown

5.3.2 Basic three conditions with different tumble ratio

The experimental data from basic three conditions (i.e. SB 1.0, 1.2, and 1.47) and different tumble ratio conditions (i.e. SB 1.2 high Rt and 1.47 high Rt) were covered in this chapter. Here, same fuel rate experiments rather than same load condition were used because the displacement volume of all the conditions were same as ~500cc.

Firstly, the experimental data for 14 mg per cycle of fuel rate and 1500 RPM case were plotted in figure 5.13 and 5.14. Here, in common with SB 1.47 and SB 1.47 high Rt conditions, heat transfer rate around its peak pressure timing was found to be high, mainly attributed by convective heat transfer coefficient as shown in figure 5.13-b. In addition, due to the enhanced flame speed for not only main duration (CA10-CA90) but also initial duration (IGN-CA10), declining tendency was found for exhaust loss and incomplete combustion loss of high tumble ratio conditions (i.e. both SB 1.2 high Rt and 1.47 high Rt). One thing should be noted that despite enhanced burning rate from SB 1.47 high Rt, which can induce the decrement in exhaust loss, the maximum heat transfer rate around peak pressure timing compensated the effect, resulting in almost same amount of exhaust loss compared to that of SB 1.2 high Rt, following aforementioned discussion about work loss and remaining internal energy as supplemented in figure 5.14-b. The main reason of the difference in net indicated efficiency between SB 1.2 high Rt and SB 1.47 high Rt was attributed by the amount of incomplete combustion loss (i.e. combustion efficiency), induced by faster volume expansion as mentioned in chapter 4. Therefore, it can be postulated that at least the specific case, the effect of enhancement in burning rate was defeated by that of the timing of heat transfer rate.

Regarding the results, the experimental data for the same fuel rate (i.e. 14 mg per cycle) and 2000 RPM case were plotted in figure 5.15 and 5.16. Here, interesting changes were detected from high tumble ratio data, where both SB 1.2 high Rt and SB 1.47 high Rt showed higher value of the maximum heat transfer rate around their peak pressure timing compared to those of low tumble ratio cases. Although the enhancement on burning rate compensated the effect caused by increment in the maximum heat transfer rate, which resulted in decreased exhaust loss for high tumble ratio, the effect was inevitably represented as a decrement of internal energy extraction as shown in figure 5.16-b. In addition, confined to high tumble ratio conditions, no improvement in burning rate was detected by increasing SB ratio. Instead, found was the increment in both cooling loss and the maximum heat transfer rate which also resulted in higher exhaust loss compared to SB 1.2 high Rt case. One thing should be noted that the cooling loss was increased for both SB 1.2 high Rt and SB 1.47 high Rt for 1500 RPM case; however, for 2000 RPM case, only SB 1.47 high Rt showed increment in cooling loss compared to that of low tumble ratio case. Therefore, it can be postulated that although the lack of time generally reduces cooling loss in spite of enhanced convective heat transfer coefficient, excessively increasing SB ratio may cause additional increment in convective heat transfer coefficient, which can affect not only exhaust loss but also cooling loss itself.

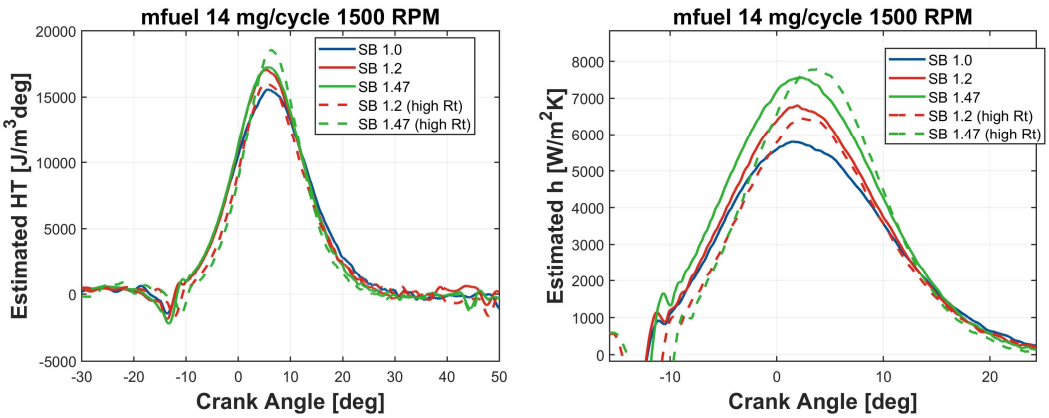

(a)

(b)

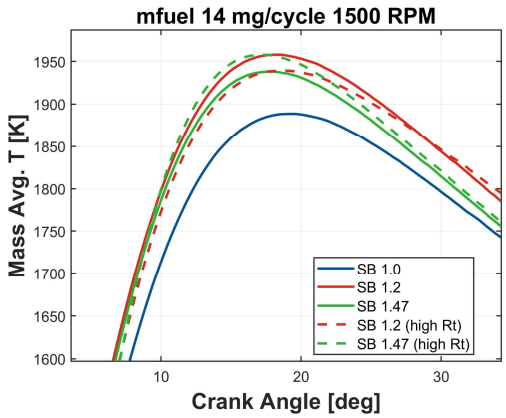

(c)

Figure 5.13 Experimental data for basic three SB ratio with different tumble ratio
(fuel rate 14mg per cycle, 1500 RPM with the best efficiency operation)
(a): estimated heat transfer during closed duration
(b): estimated convective heat transfer coefficient
(from single zone approach)
(c): mass-averaged single zone temperature

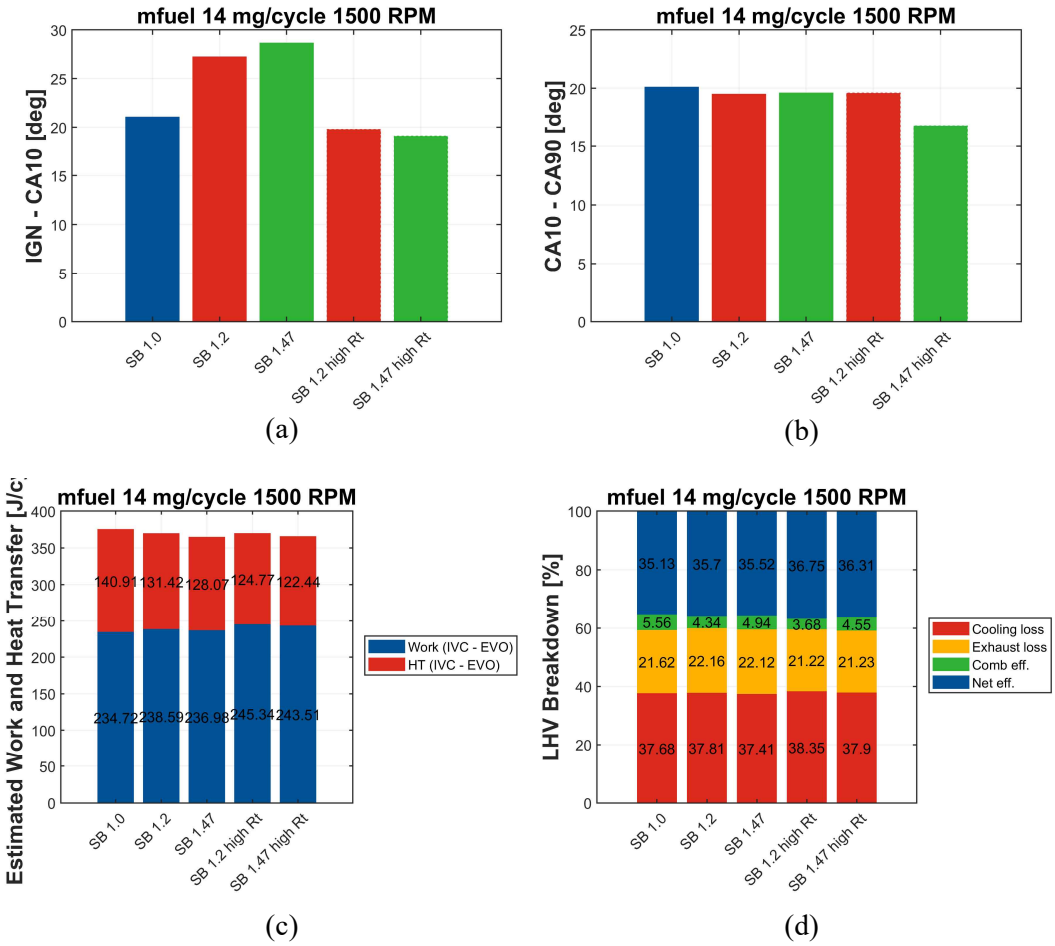

Figure 5.14 Experimental data for basic three SB ratio with different tumble ratio (fuel rate 14 mg per cycle, 1500 RPM with the best efficiency operation)
(a): initial flame speed from spark timing to CA10
(b): burn duration from CA10 to CA90
(c): estimated heat transfer and work extraction during closed duration
(d): fuel LHV breakdown

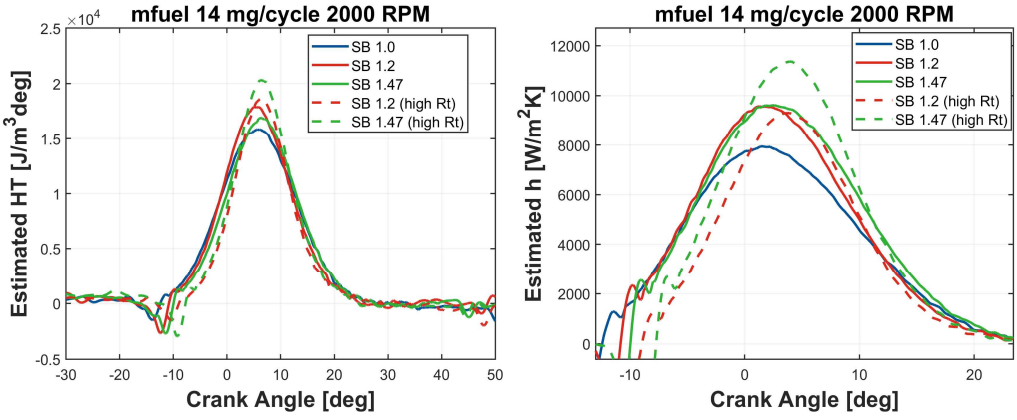

(a)

(b)

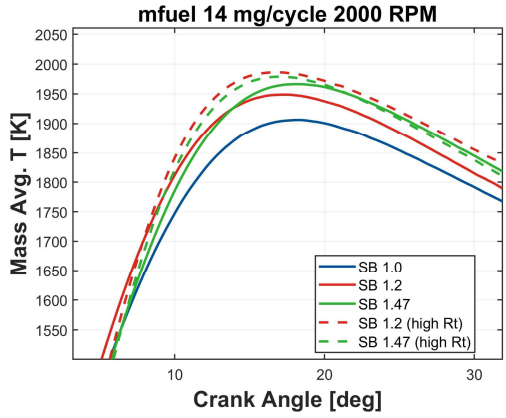

(c)

Figure 5.15 Experimental data for basic three SB ratio with different tumble ratio
(fuel rate 14mg per cycle, 2000 RPM with the best efficiency operation)
(a): estimated heat transfer during closed duration
(b): estimated convective heat transfer coefficient
(from single zone approach)
(c): mass-averaged single zone temperature

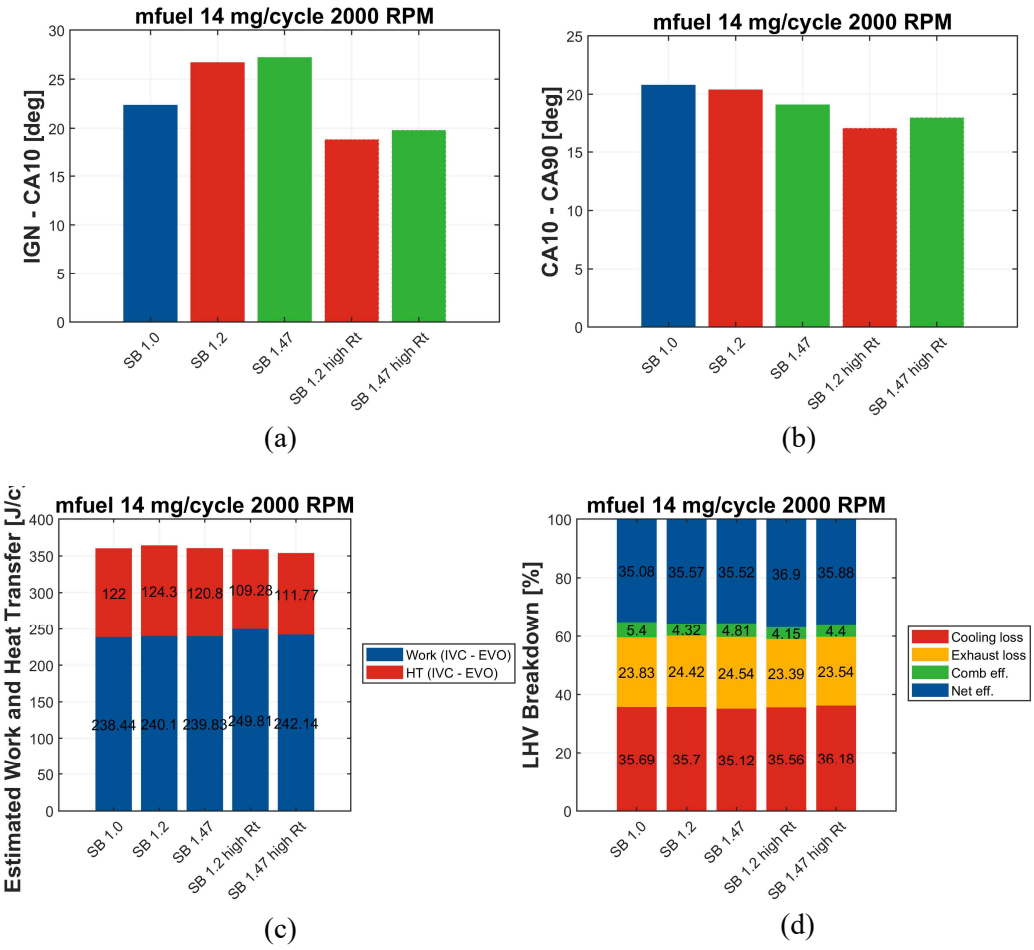

Figure 5.16 Experimental data for basic three SB ratio with different tumble ratio (fuel rate 14 mg per cycle, 2000 RPM with the best efficiency operation)
(a): initial flame speed from spark timing to CA10
(b): burn duration from CA10 to CA90
(c): estimated heat transfer and work extraction during closed duration
(d): fuel LHV breakdown

Chapter 6. Experiment and Simulation – Burning Rate and Knock Characteristics

6.1 Introduction – definition of robustness in knock

As mentioned in chapter 1, gasoline SI engine still, in general, have an issue on knock phenomena in terms of the deficiency on gross work. As many of developments related to SI engine were conducted for mitigating knock occurrence, the definition of 'knock resistance' should be reviewed – What is the definition of a robust SI engine for knock phenomenon? Above all things, operating strategies that can achieve more advance in spark timing will be the first choice to make a robust SI engine since it can increase engine efficiency by adjusting combustion phasing to near MBT operation in knock-related load region. Thus, one can insist that the engine being capable of further advancing spark timing be the robust SI engine for knock. The other also can claim that the engine having fast burning rate be the robust SI engine for knock, within the framework of common notion – faster flame propagation can reduce the time for unburned zone mixture to be auto-ignited and cause knock.

However, the definition can be varied by the reason why we should make a robust SI engine for knock. If one engine can be operated with more advanced ignition timing but cannot generate more work by several reasons (e.g. increased compression work, higher heat transfer), that is not desirable. Furthermore, if another engine can be operated with faster burning rate but cannot increase work by several reasons (e.g. earlier knock-limited combustion phasing), that is also not desirable. By these examples, it can be clearly concluded that the reason for developing knock-robust SI engine is all about nothing but engine efficiency.

Therefore, the definition of a knock-robust SI engine, used in this study, is the engine which generates more work with same input (i.e. fuel rate related to engine load) under the same knock criterion and, of course, knock-related operation (i.e. knock-limited). It should be noted that under this definition, the engine with slower burning rate can be more robust than the one with faster burning rate if the generated work is higher for former one under same knock-limited criterion (e.g. KLSA with 10% knock incidence). In addition, the engine with less advanced spark timing (for KLSA) can be more robust than the one with more advanced spark timing, by the same logic. However, several questions also can be raised such as – can these unexpected behaviors really happen? Does the existing well-known notion about knock-robustness become invalid for this study? If not, why was the certain definition of knock-robustness used in this study? – it is the essence of this chapter to answer those questions.

The main objective of this chapter is to investigate the different knock behavior with several SB ratio conditions. In these processes, classified were the variables that were expected to be different for several SB ratio conditions and were related to the knock characteristics, as listed below with important keywords.

1) Combustion phasing and burning rate:
   relationship between burning rate and knock resistance (robustness)

2) Volume profile under the ‘packaging constraint’:
   the effect of different volume profile for knock occurrence

3) Cylinder shape – especially unburned zone:
   the possibility to generate ‘hot spot’ – the main source of weak and moderate knock

Among these, second one can be easily investigated compared to other issues. The related figures were shown in figure 6.1, 6.2, and 6.3. These data were obtained by 0D simulation with same combustion phasing (-10 CA aTDC of spark timing, 15 CA of duration from spark timing to CA10, 12.6 CA of duration from CA10 to CA70), heat transfer correlation and coefficient (Hohenberg [86] with 1.5 overall coefficient), and thermodynamic properties of IVC (initial) condition with adjusting IVC into BDC timing to remove biased initial volume. The results showed that higher SB ratio had more knock-resisted operation because of overall lower value of L-W integration, attributed by volume expansion rate under the 'packaging constraint'. However, as shown, the degree of effect was found to be relatively small compared to other issues that will be described in the following chapters. Therefore, with large amount of experimental data and detailed simulation[28], other two issues – 'combustion phasing and burning rate' and 'Cylinder shape' – were comprehensively investigated.

[28] The figure of which data was derived by simulation process had been titled as 'Knock Simulation' to avoid confusion whether the data were from experiments or simulation.

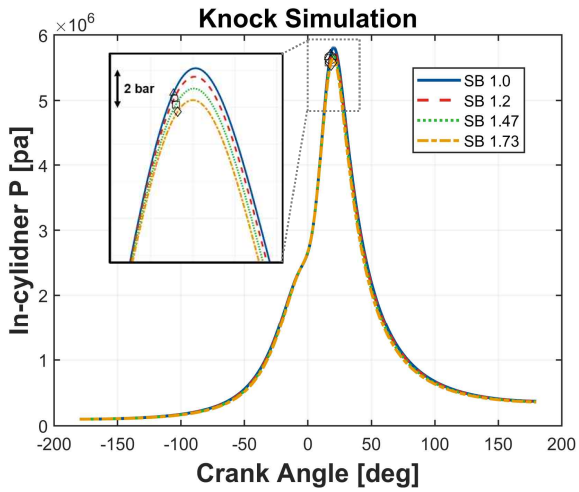

Figure 6.1 In-cylinder pressure data of four different SB ratio conditions (1500 RPM, 1 bar and 380 K with stoichiometric condition at IVC timing) – Simulation data

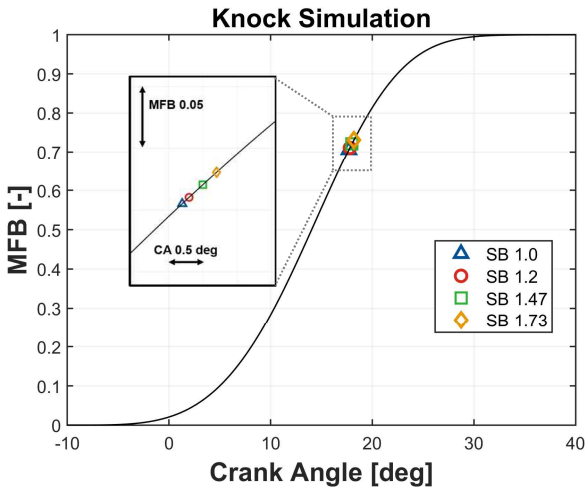

Figure 6.2 MFB and knock onset results of four different SB ratio conditions (1500 RPM, 1 bar and 380 K with stoichiometric condition at IVC timing) – Simulation data

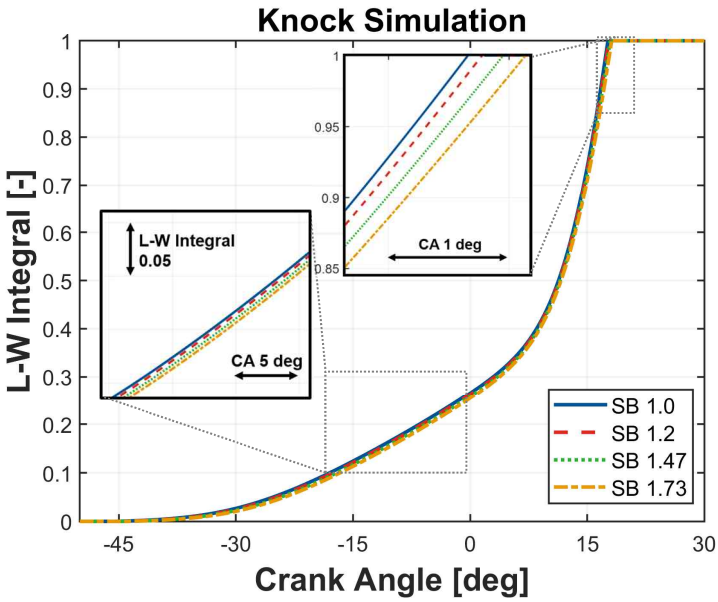

Figure 6.3 Results of Livengood-Wu integration of four different SB ratio conditions (1500 RPM, 1 bar and 380 K with stoichiometric condition at IVC timing) – Simulation data

6.2 Experimental conditions and scheme

In order to investigate the knock characteristics of each SB ratio, further experiments with slightly heavy knock compared to existing knock criterion (i.e. 10% knock incidence) were conducted by varying fuel rate and rotational speed. The details of further experiments were listed in table 6.1. Total three conditions of fuel rate (26, 30, and 34 mg per cycle) and two conditions of rotational speed (1500 and 2000 RPM) were used to conduct the experiments. As shown in table 6.1, total 5000 individual cycles were logged for each case to obtain many cycles with knock occurrence, which can reduce the stochastic behavior of knock phenomena as mentioned in chapter 2 [73]. The valve timing used for the cases of fuel rate 30 and 34 mg per cycle was located at retarded intake and exhaust valve timing, corresponding to the valve timing results of supercharged condition based on the results of chapter 4. One thing should be noted that the valve timing used for the case of fuel rate 26 mg per cycle was slightly different from that of the best efficiency point at WOT, N/A operating condition (i.e. ~nIMEP 8.5 bar) – further advanced exhaust valve timing was used, in order to adjust the duration of valve overlap with similar as that of the cases of 30 and 34 mg per cycle. Since the objective of these experiments was not related to the best efficiency, it can be considered that these manipulations are not important in the analysis of further experiments related to this chapter. Detailed procedure of the experiments was followed.

1) Determine the KLSA of each condition where the knock incidence was found to be 10% of total cycles.

2) Slightly advance spark timing to obtain at least 20% of knock incidence operation.[29]

3) After reaching steady state operation[30], save the data of total 5000 individual cycles consecutively, with same input parameters (e.g. spark timing, rotational speed, and fuel rate).

After obtaining the data, averaging process based on the unburned mass fraction, which was described in chapter 2.2.2, was conducted. Both averaged and raw data from knock experiments were used with the mark (avg. and raw) to be distinguishable.

[29] The valve of final knock incidence may vary with each SB ratio. The only important thing is that the minimum number of knock incidence should be guaranteed to remove the stochastic behavior of knock phenomena.
[30] It was judged by the saturation of exhaust temperature.

Table 6.1 Operating parameters of knock-related experiments

		SB ratio					
		1.0	1.2	1.47	1.0	1.2	1.47
RPM [rev/min]	Fuel rate [mg/cycle]	Spark timing [CA aTDC]			Knock incidence [%]		
1500	26	-4.5	none	-9.5	35.5	none	35.5
	30	-9.5		-12	46.0		42.2
	34	-6.5		-7	43.1		35.4
2000	26	-12	-15.5	-16	48.8	34.3	28.0
	30	-11	-11	-13.7	54.6	30.7	23.9
	34	-7	-6	-9	47.7	23.4	21.6

6.3 Experiment and simulation results

6.3.1 Burning rate on knock intensity

Firstly, plotted was figure 6.4 redrawn from the figure 16 in the previous work [72]. The data from the figure was obtained by the experiment in the similar environment[31][71] as the engine used in this study, where same bore and stroke size, and compression ratio with SB 1.2 case (81mm and 97mm, and 12, respectively) were used. The results showed that the stronger knock (exceeds 1 bar of MAPO) was obtained from the point where the more unburned mass remained at knock onset timing. This result seemed to not deviate from the conventional notion – the more unburned mass fraction, the more strength in knock occurrence. However, it deserves additional discussion that the larger values of MAPO were located at not just lower section (higher unburned mass fraction), but also lower 'left' section (higher unburned mass with 'advanced' onset timing for 'fast' burning cycle), supplemented by the data shown in figure 6.5 redrawn from the figure 15-a in the previous work [72]. That is, the cases with stronger knock occurrence were found to have not only the tendency in faster burn duration, but also larger amount of unburned mass. This result seems to have a slightly different tendency from the conventional idea that faster burning rate is the first strategy to avoid knock occurrence because the unburned mass is consumed faster due to the faster flame propagation. First of all, however, as mentioned in chapter 1, many of recent studies have been focusing on the contradiction of knock and burning rate [48-52]. The main issue which should be mentioned in this study and was mentioned in those references is the two terms of

[31] Same engine test cell, fuel (Korean gasoline), and boundary conditions (e.g. coolant temperature) was used. The main differences were the design of cylinder head (related to tumble ratio), piston shape, and injection type (PFI)..

time reduction – the first reduction term for an unburned gas to be consumed by faster flame speed, causing reduction in time to burn all the unburned zone with flame propagation mode, and the second reduction term for an unburned gas to be auto-ignited earlier by increased temperature and pressure due to the faster flame propagation speed. One thing clearly shown in the figure 6.4 and 6.5 is that the latter reduction – shorten autoignition delay of unburned mixture to be autoignited faster – was more effective than the former so that the knock cycle with faster burning rate had larger amount of unburned mass. This tendency was also valid in the data used in present study, shown in figure 6.6. Regardless of SB ratio condition, same tendencies were found, shown in each sub-figure. Two things should be mentioned – first, because of the effects of direct injection and difference in total number of cycles (10000 in [72]), the onset data plotted as dots were more scattered compared to those of figure 6.4, although the tendency was not collapsed. Second, for higher rotational speed condition (i.e. 2000 RPM), slightly decrement in unburned mass fraction at knock onset was detected with more scattered data. It will be discussed later.

In order to summarized these, presented was the relationship between the 'total' burn duration (initial + main burn duration, i.e. from spark timing to CA70) and duration from spark timing to knock onset timing for each SB ratio condition, shown in figure 6.7 with 1st order curve fitting. From the definition, the slope of fitted curve will be lower than unity if the time reduction from faster flame propagation is more effective than that from shorter autoignition delay caused by relevant pressure and temperature rise, corresponding to conventional notion – faster burning cycle will have retarded knock onset timing with lower knock intensity. However, for each SB ratio condition, the values of each slope were found to be higher than unity, shown in the equations of legends in figure 6.7. Therefore, it can be concluded that SB ratio cannot reverse the tendency. It should be noted that, however, the absolute value of the slope for higher SB ratio (i.e. SB

1.47) was lower than that of other cases. It was attributed by faster burning rate considering further simulation results shown in figure 6.8. The simulation was conducted with fixing all the input parameters (e.g. RPM, fuel rate, spark timing) other than burn duration, defined as the duration from spark timing to CA70[32]. It can be considered that each line is corresponding to individual cycle with different burn rate. Here, the turning point existed around IGN-CA10 10 deg – after that, the relationship between two time reductions was reversed, inducing small amount of unburned mass at knock onset timing by overwhelming effect of extremely fast flame propagation speed. This saturation can be a supplement of gradual slope for SB 1.47 case. One thing should be noted that the pressure rise rate corresponding to the fastest line (IGN-CA10 6 deg) was about 12.1 bar/deg, only by flame propagation (no autoignition included), which is too much higher than the usual high-limit (5 bar/deg, [107]) of engine operation.

Considering these results, the question can be raised; Is the cycle with fast burning rate always robust to knock occurrence? This question should be considered together with the definition of knock-robust SI engine – "engine which generates more work with same input (i.e. fuel rate related to engine load) under knock-related operation (i.e. knock-limited)". That is, even if the cycle with faster burning rate actually causes too severe knock to advance combustion phasing (e.g. CA50) so that the resultant combustion phasing is farther from that of relevant MBT operation compared to the case of slow burning rate, it still can be considered as more robust SI engine in knock only if the work extraction is higher. In order to find the correlation between fast burning and work generation, simple 0D simulation with no heat transfer (i.e. adiabatic process) was conducted, where the results were shown in figure 6.9, with SB 1.0 and 1500 RPM operation. Here,

[32] Noted that only the duration from spark timing to CA10 (IGN-CA10) was changed; the duration from CA10 to CA70 was determined by multiplying 0.75 to IGN-CA10, based on the relevant relationship of experimental data.

used was same knock criterion to determine the KLSA of each operating condition, which will be mentioned later with geometric issues. The simulation data from adiabatic process showed that the cases of faster burning rate show more work generation with advanced CA50. Therefore, if the heat transfer does not reverse the trend shown in figure 6.9, it can be concluded that faster burning rate is still required for knock-robust operation. In this regard, the data of constant fuel experiments for both N/A and supercharging operation were presented in figure 6.10 and 6.11 with different rotational speed and under the same knock criterion (knock incidence 10%), respectively. Here, the striking results were found in variation of both SB ratio and tumble ratio results. From SB 1.2 to SB 1.2 high Rt case, significant increment in both flame propagation speed and efficiency was detected for all conditions with more advanced CA50 timing. However, in case of SB 1.47 condition, only flame propagation speed was increased, whereas both CA50 and efficiency were not improved. One can claim that these results were attributed by heat transfer characteristics which was covered in chapter 5. Although it can be also true, it cannot explain the tendency of CA50 behavior since more heat transfer usually leads to the decrement in the temperature of unburned zone, facilitating more advanced combustion phasing [71]. Considering these results, the answer to the question raised at the start of this column can be; half correct and half wrong. Here, it is reasonable to guess the reason of different tendency for SB 1.2 and 1.47 conditions as a geometric issue since, among all the input parameters, changed was no other than SB ratio only[33]. Therefore, the relationship between SB ratio (engine geometry) and knock occurrence should be further investigated, which is the main issue of the next chapter.

[33] Even the two conditions (SB 1.2 and 1.47, SB 1.2 high Rt and 1.47 high Rt) shared same cylinder head, respectively.

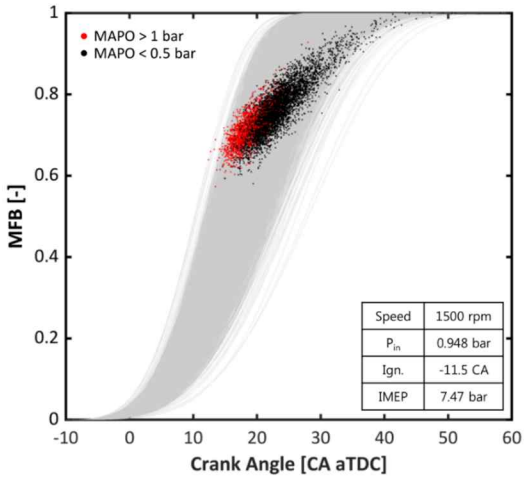

Figure 6.4 Burned mass fraction of 10000 individual cycles with fixed-operating condition with marked MAPO value, redrawn from [72]

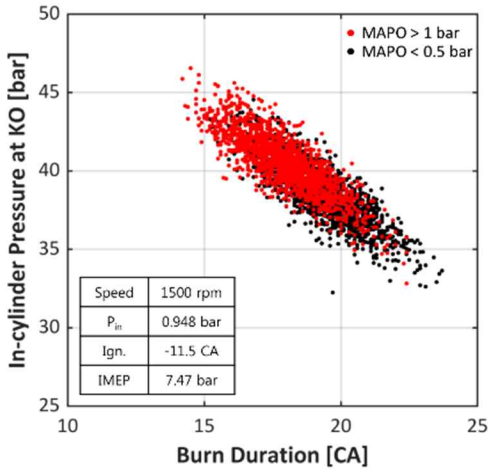

Figure 6.5 Correlation between burn duration and in-cylinder pressure at knock onset timing of 10000 individual cycles, redrawn from [72]

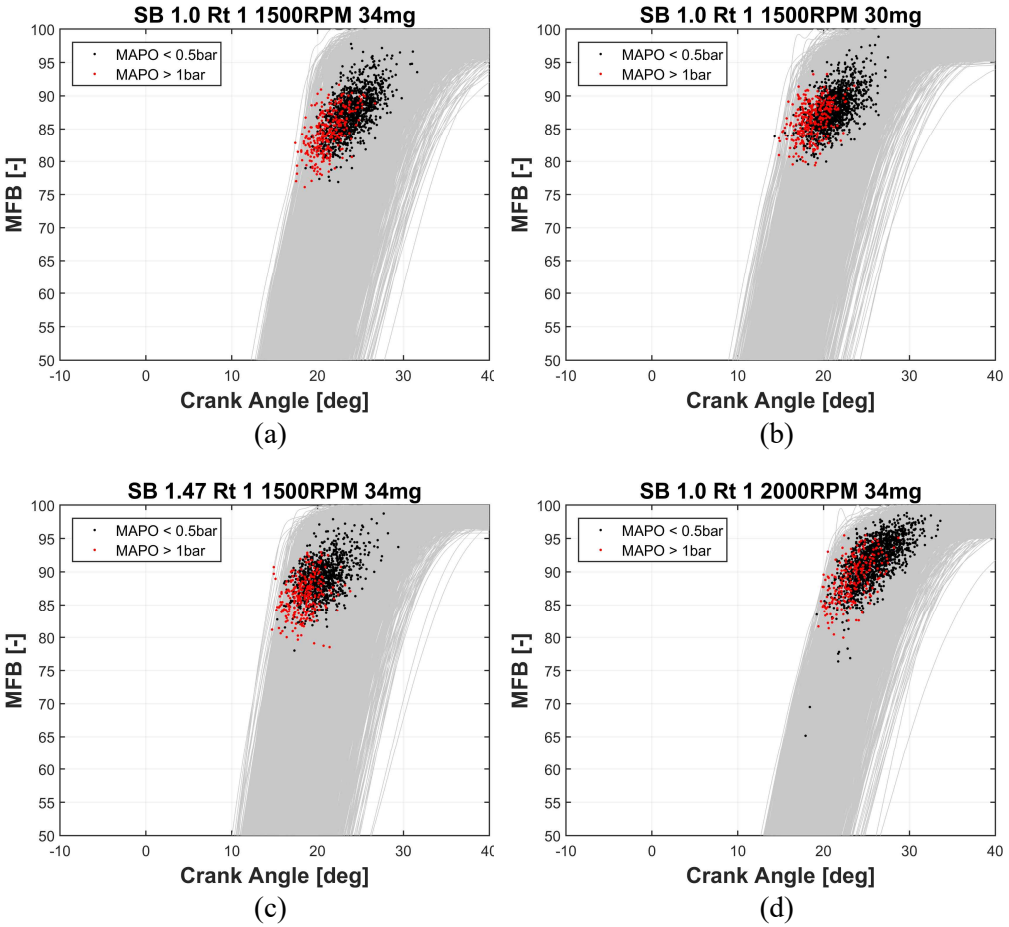

Figure 6.6 Burned mass fraction of 5000 individual cycles with fixed-operating condition with marked MAPO value
(a): SB 1.0, 1500 RPM with 34 mg of fuel rate per cycle
(b): SB 1.0, 1500 RPM with 30 mg of fuel rate per cycle
(c): SB 1.47, 1500 RPM with 34 mg of fuel rate per cycle
(d): SB 1.0, 2000 RPM with 34 mg of fuel rate per cycle

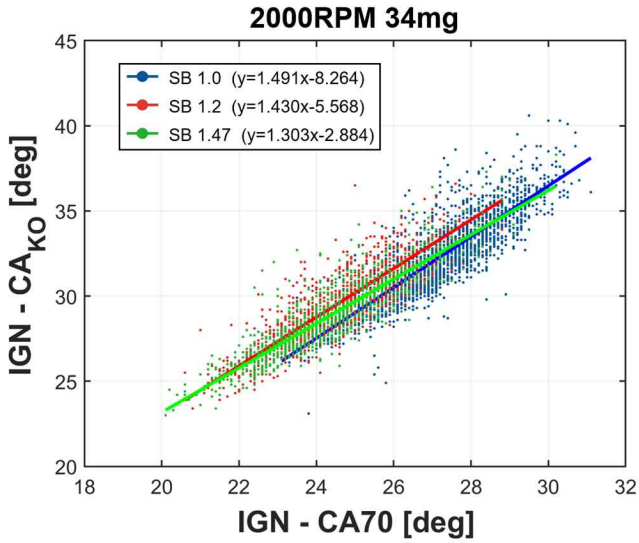

Figure 6.7 Correlation between burn duration (from spark timing to CA70) and duration from spark timing to knock onset timing

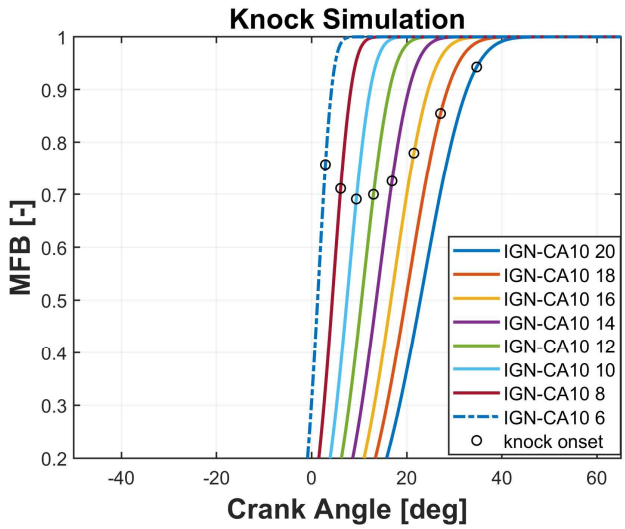

Figure 6.8 Simulation data with different combustion phasing with knock onset mark (SB 1.0, 1500 RPM)

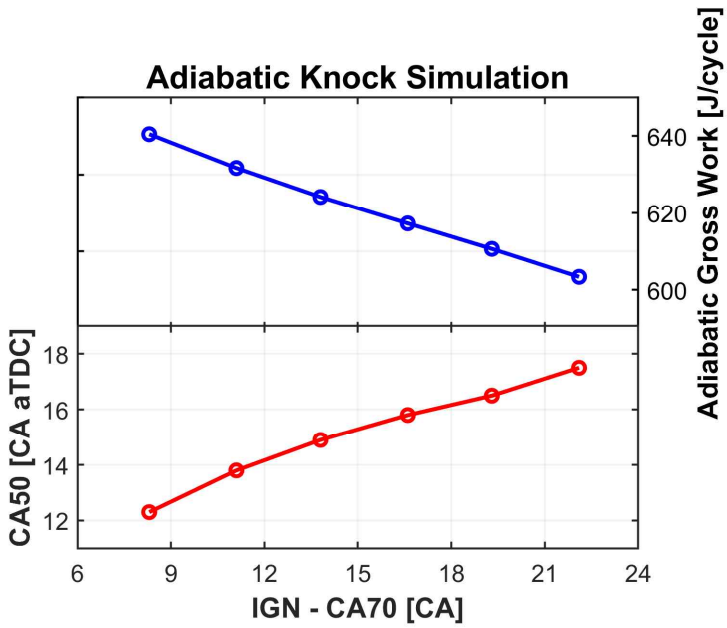

Figure 6.9 Simulation data from adiabatic process under the same knock criterion (SB 1.0, 1500RPM)

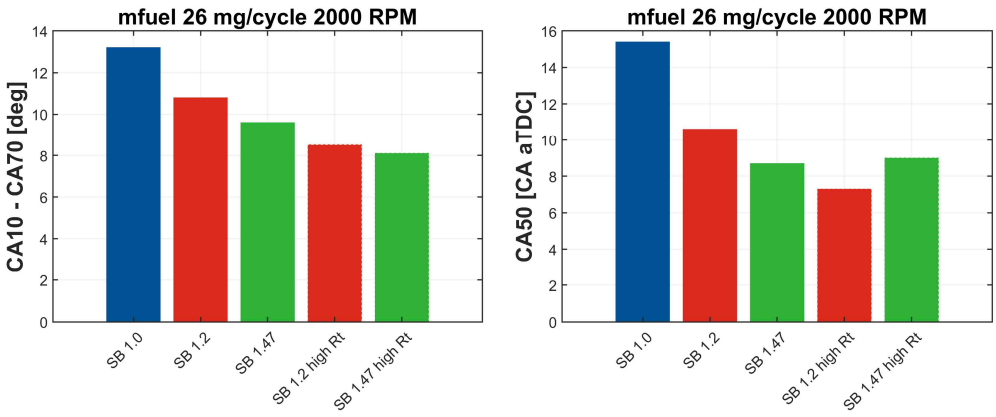

(a)

(b)

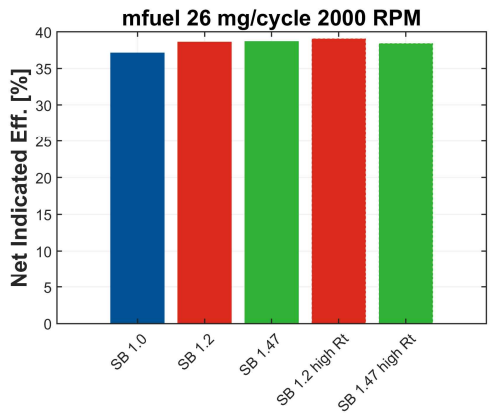

(c)

Figure 6.10 Experimental data for basic three SB ratio with different tumble ratio (fuel rate 26 mg per cycle, 2000 RPM with the best efficiency operation)
(a): burn duration from CA10 to CA70
(b): CA50 combustion phasing
(c): net indicated efficiency

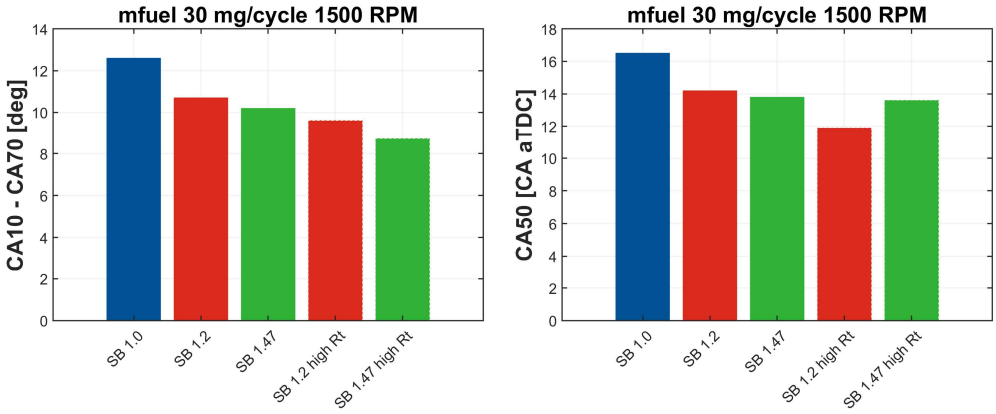

(a)

(b)

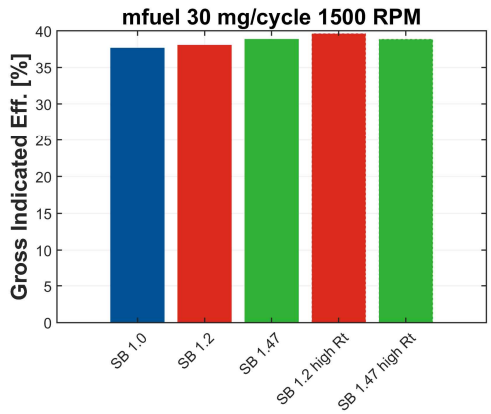

(c)

Figure 6.11 Experimental data for basic three SB ratio with different tumble ratio (fuel rate 30 mg per cycle, 1500 RPM with the best efficiency operation)
(a): burn duration from CA10 to CA70
(b): CA50 combustion phasing
(c): gross indicated efficiency

6.3.2 Geometry and other issue on knock intensity

As discussed in the previous section, certain geometric issues is highly expected with consideration of unexpected results from SB 1.47 and 1.47 high Rt operation, shown in figure 6.10 and 6.11. Therefore, additional knock experiments of which summary was presented in table 6.1 were investigated to find aforementioned issue related to engine geometries caused by different SB ratio.

As shown in figure 6.12 and 6.13, knock-related data followed by averaging process were plotted, selected by similar knock incidence expressed in legend box. In figure 6.12, averaged total burn duration and MAPO values, from 1500 RPM and 26 mg per cycle of fuel rate case, were plotted, following aforementioned tendency that faster burning rate induces higher knock intensity. It should be noted that the tendency was maintained regardless of SB ratio condition, supplemented by fitted curve with black line.

One thing deserves additional discussions related to other reasons why the faster burning rate causes higher knock intensity. First of all, from the several references [49, 108] where the detailed review was achieved in chapter 1, the total volume at knock onset timing was suggested as a main parameter related to knock intensity. This can be explained by the nature of knock onset timing for fast burning rate as the knock onset timing should be advanced for fast burning cycle, literally. Because usual knock occurrence arises after firing TDC, instantaneous volume at the relevant knock onset timing is decreased, which was found to increase knock intensity as shown in figure 6.13 with same case used in figure 6.12. Thus, total volume at knock onset timing was also chosen as a main parameter to determine knock intensity in this study with negative correlation.

Second, rotational speed was mentioned as a parameter that can affect the knock intensity [81]. From this literature, it was mentioned that rotational speed can affect knock-limited condition in terms of knock cyclic frequency which may vary with not only rotational speed condition, but also the features of engine test bench. Shown was corresponding data in figure 6.14, where the averaged unburned mass fraction was plotted with respect to relevant averaged MAPO data. Here, two things should be mentioned – first, overall unburned mass fraction for 2000 RPM case was slightly reduced compared to that for 1500 RPM case, attributed by insufficient time for unburned mixture to be auto-ignited. Second, with same unburned mass fraction, overall increment in knock intensity was found for 2000 RPM case, which means that the correlation mentioned in the reference [81] was correct, using positive correlation between RPM and knock intensity. Thus, in this study, RPM was also used as a main parameter to determine knock intensity with positive correlation.

Finally, and the most important part of this chapter, shape factor was newly suggested from the experimental data in this study, where relevant data was shown in figure 6.15. Here, it was found that slightly higher tendency in MAPO values was detected with same range of unburned mass fraction. Although the instantaneous volume for SB 1.47 case was slightly lower than that of SB 1.2, it was concluded based on the additional approaches (mentioned later) that the parameter that is theoretically related to the knock intensity and has different value for several SB ratio is inevitably required to predict the knock intensity with an unique criterion for various SB ratio conditions. Therefore, suggested was a new parameter called ‘shape factor’ of which definition was graphically expressed in figure 6.16. The definition was listed in equation 6.1.

$$SF\,(\theta) = L(\theta)/V_u^{\frac{1}{3}}(\theta) \tag{6.1}$$

Here, L is defined by subtracting burned radius, calculated by the assumption of spherical flame propagation, from the diagonal[34] length of cylinder at relevant crank angle and V_u is volume of unburned zone at same crank angle. Noted that it is dimensionless parameter. It is the qualitative meaning of the parameter that the hot spot, main source for knock occurrence, can be formed considerably if the volume fraction of thermal boundary layer is reduced. In other words, the larger the L value with same volume for unburned zone, the more the proportion of the hot region (core) in unburned zone, which can make more frequent development of hot spots[35] [30, 31]. Furthermore, same logic can be applied to the suggestion that the greater hot region, the more possible to form larger size of hot spot. In conclusion, the shape factor was related to not only the frequency of hot spot formation, but also the possibility for the size of hot spot to become higher. The entirety of the shape factor was presented in figure 6.17, showing larger value in SB 1.47 case with same volume of unburned zone, which was inevitable due to its compact geometry. Therefore, if the shape factor is found to be effective for the prediction of knock intensity, higher SB ratio will be inevitably disadvantageous for knock-related operation with respect to work extraction.

[34] Pent-roof cylinder head corresponding to the engine design was assumed with combined cone and cylinder of which size was based on the real value of clearance volume and intended gap between piston and liner upper surface at TDC timing.

[35] It was derived by the key matter that knock occurrence may not be usually induced by a single hot spot in real experimental condition, unlike the usual knock simulation based on the several theories.

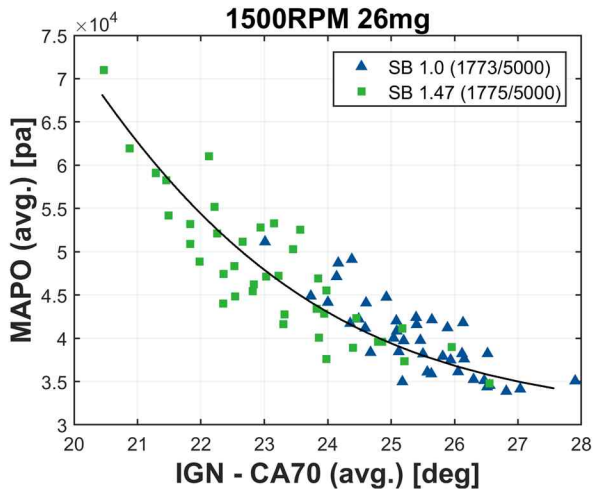

Figure 6.12 Correlation between burn duration (from spark timing to CA70) and MAPO with averaging process for SB 1.0 and 1.47 conditions. (1500 RPM, fuel rate 26 mg per cycle, and ~35% of knock incidence)

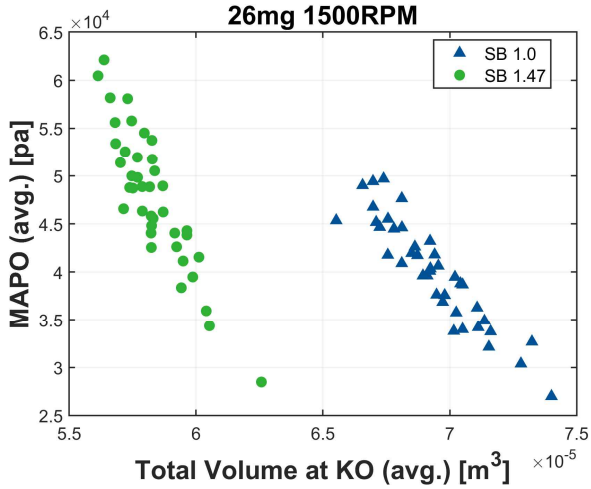

Figure 6.13 Correlation between instantaneous volume at knock onset timing and MAPO with averaging process for SB 1.0 and 1.47 conditions (same as figure 6.13)

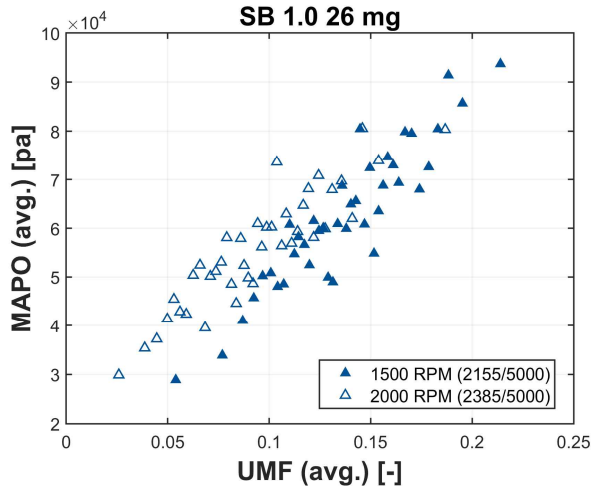

Figure 6.14 Correlation between unburned mass fraction and MAPO with averaging process for 1500 and 2000 RPM of SB 1.0 conditions with fuel rate 26 mg per cycle

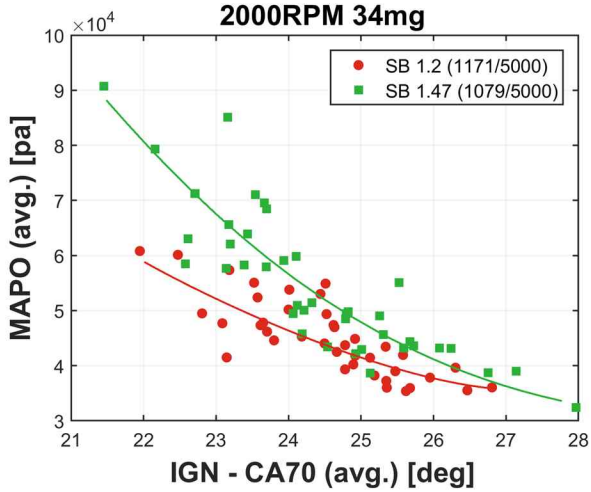

Figure 6.15 Correlation between burn duration and MAPO with averaging process for SB 1.2 and 1.47 with 2000 RPM, fuel rate 34 mg per cycle

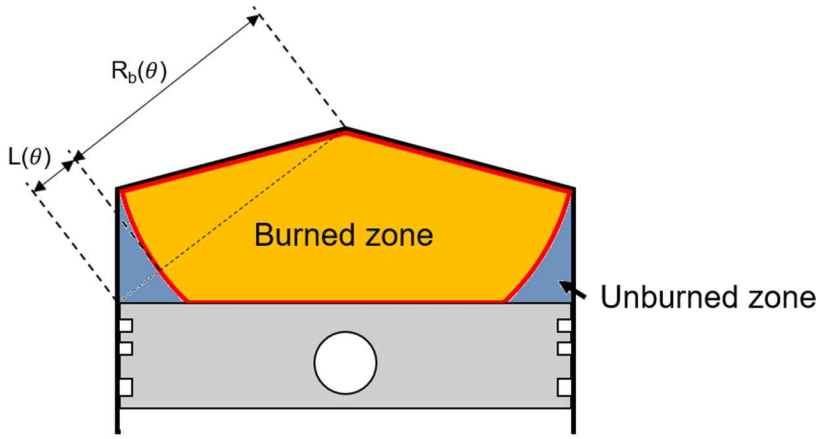

Figure 6.16 Configuration of flame propagation for SI engine operation with flame radius (R) and L value for the newly defined 'shape factor'

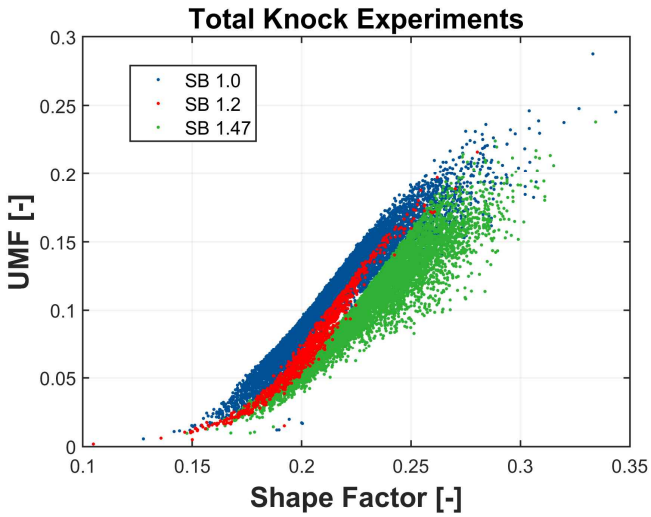

Figure 6.17 Correlation between 'shape factor' and unburned mass fraction with raw data of each individual cycle for SB 1.0, 1.2, and 1.47 conditions.

6.3.3 Suggestions on simulated knock intensity

From the contents in the previous chapter, several parameters, some of which were derived from the previous works [49, 81, 108] and the other of which was firstly suggested in this paper (shape factor), were used to develop the simulated knock intensity corresponding to the averaged MAPO from experimental results[36]. The main purpose of the suggestion was to correlate simulation results into real engine experiments. That is, once the simulated knock intensity is determined based on the entire experimental results, it can be used to simulate various situations which were practically unable to be operated in real experiments such as MBT operation with extreme knock occurrence condition. It is sure that the target value for simulated knock intensity to be matched was the averaged MAPO value for each relevant condition.

Before the suggestion, it should be needed to re-examine the correlation between aforementioned parameters and knock intensity, as summarized below.

1) Positive correlation: unburned mass fraction, shape factor, rotational speed

2) Negative correlation: total volume at knock onset timing

With these, a generalized form of simulated knock intensity was suggested as listed in equation 6.2.

$$KI_{sim} = C_1(LHV_{fuel}\, m_{fuel})\frac{(UMF+C_2SF)}{V_{total,KO}}\, RPM^{C_3} \quad (6.2)$$

[36] For reference, the simulated knock intensity which was mentioned and discussed in this chapter was used for the simulation related to the previous chapter already.

One thing should be noted that the shape factor is added to unburned mass fraction as a role of calibration. The grounds which can supplement the approach mentioned shortly before were plotted in figure 6.18, where the data having 1-2bar of MAPO were normalized with their UMF value to be expressed in the nature of probability density function. Here, one thing was clearly shown that the value of unburned mass fraction assigned to the greatest number of MAPO became smaller as SB ratio increases, attributed by several reasons mentioned before. Furthermore, the theoretical approaches on shape factor and unburned mass fraction on knock intensity resulted in same conclusions that increment in both terms is favorable to increase knock intensity. Thus, it is worthwhile to use the shape factor as a calibration of unburned mass fraction since it has opposite trends with various SB ratios.

As shown in equation 6.2, there are three coefficients that should be determined to make a good correlation with averaged MAPO value – minimizing RMSE between averaged MAPO and simulated knock intensity. This procedure was conducted with using Genetic Algorithm equipped in MATLAB software. After the procedure, each coefficient was determined with minimizing the objective function of the Genetic Algorithm procedure – that is, RMSE. The final definition of simulated knock intensity was listed in equation 6.3.

$$\mathrm{KI_{sim}} = (1.852 \times 10^{-3}) LHV_{fuel}\, m_{fuel}\, \frac{UMF + 0.8392 \times SF}{V_{total,KO}} \left(\frac{RPM}{60} \times 2\pi\right)^{0.3028} \tag{6.3}$$

Here, $\mathrm{LHV_{fuel}}$ has [J/kg] unit, $\mathrm{m_{fuel}}$ has [kg/cycle] unit, UMF and SF are dimensionless parameters, $\mathrm{V_{total,KO}}$ has [m3] unit, and RPM has [rev/min] unit. One thing should be noted that the unit of first coefficient ($\mathrm{C_1}$ in equation 6.2, 1.852E-3 in equation 6.3) should be assigned to cancel the unit of the final RPM-related term, where the term inside the last parenthesis has [rad/sec] unit.

With this, simulated knock intensity has [pa] unit, which is same with averaged MAPO value. The relevant results were plotted in figure 6.19 and 6.20. Firstly, in figure 6.19, several preliminary approaches were conducted, with the simple notion widely used in several simulation-related studies such as – knock intensity was represented as a function of unburned mass fraction (figure 6.19-a) or fuel energy remaining at knock onset timing (figure 6.19-b). The coefficients of determination (R^2) for those approaches, however, were found to be relatively bad compared to that of simulated knock intensity shown in figure 6.20. It should be conceded that the final value of R^2 was still lower than usual value for good correlation case of normal statistical approaches. However, considering the very low value of R^2 mainly attributed by stochastic behavior of knock occurrence, shown in figure 2.13, it can be regarded as considerable strides. Two things should be noted – First, unlike other approaches, the fitted curve from simulated knock intensity only passes the zero point. That is, only the simulated knock intensity satisfied theoretical fact that the averaged MAPO will be zero if the predicted parameters are zero. Second, the absolute value of simulated knock intensity was fairly similar to averaged MAPO value according to the value of slope of fitted curve shown in the text box of figure 6.20.

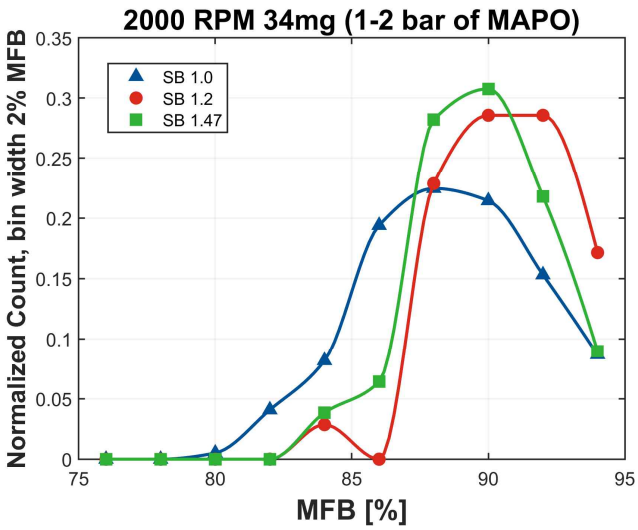

Figure 6.18 Incidence of moderate intensity of MAPO values for each MFB value for SB 1.0, 1.2, and 1.47 with 2000 RPM, fuel rate 34 mg per cycle, normalized by total number of knock cycle for each operating condition

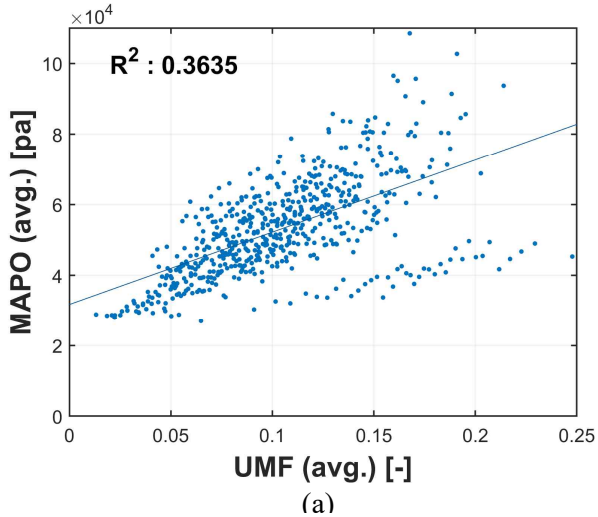

(a)

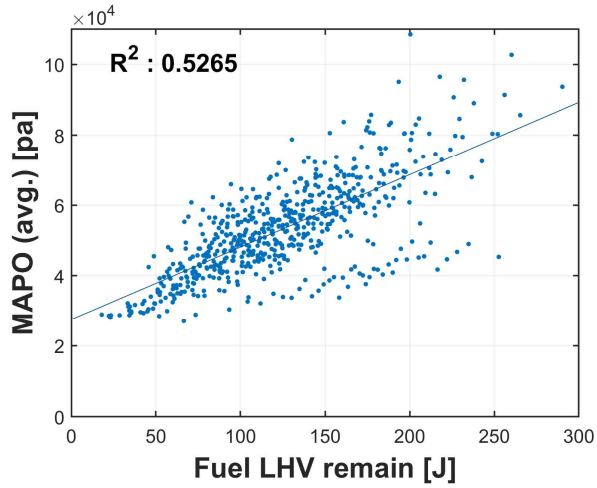

(b)

Figure 6.19 Correlation between unburned mass fraction or fuel LHV remainder in unburned mass at knock onset timing and MAPO with averaging process for all knock experiments
(a) unburned mass fraction and MAPO
(b) fuel LHV remainder at knock onset timing and MAPO

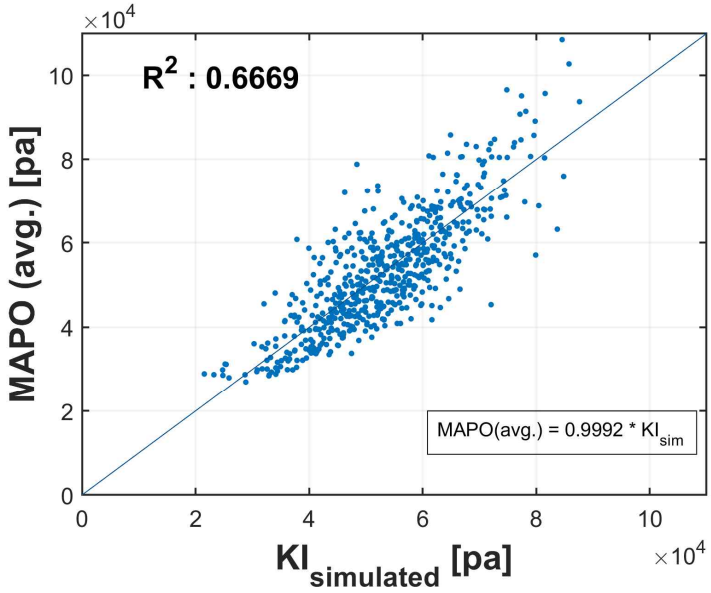

Figure 6.20 Correlation between newly suggested $KI_{simulated}$ and MAPO with averaging process with 1st order curve fitted equation shown in the box

Chapter 7. Conclusions

The sole effect of SB ratio on SI engine efficiency in terms of the parameters from LHV breakdown – cooling loss and exhaust loss – and knock phenomena was comprehensively investigated, preceding the experiments with valve timing variation. In order to investigate these issues, used were sophisticated engine setup including basic three SB ratio with different displacement volume and tumble ratio, and detailed combustion analysis using estimated IVC state and measured in-cylinder pressure.

First of all, the position of valve timing for the best efficiency was determined by numerous experiments with varying load, rotational speed, and SB ratio. Here, it was found that the positions were not significantly affected by SB ratio, but load and rotational speed. In detail, for low load operation, selected were fully advanced intake valve timing and fully retarded exhaust valve timing, attributed by increased residual mass fraction and expansion ratio which can induce lower pumping loss, cooling and exhaust heat loss for engine efficiency. In the case of middle and high load operation, moderate or fully retarded intake valve timing was required because, in this region, knock mitigation is the key thing for higher efficiency. In terms of exhaust valve timing, moderate or retarded operation was required to prevent hot residual gas and too much blowdown loss by earlier EVO timing.

With the valve timing determined previously, additional experiments were conducted to investigate the detailed LHV breakdown (related to cooling and exhaust heat losses) and knock phenomena, which was found to yield unexpected behavior in the preliminary valve timing variation experiments. First of all, heat transfer during closed duration was investigated in detail, by using specific combustion analysis comprised of estimated IVC state and measured in-cylinder

pressure profile with 1st law of thermodynamics. Comparing real experimental data with adiabatic process from combustion analysis, it was found with an assistance of Otto cycle approach that heat transfer which occurs around TDC or peak pressure timing significantly reduced the difference of internal energy value between IVC and EVO timing, which could reduce the total PdV work extraction during closed duration by relatively increased internal energy at EVO timing. Considering this notion, it was shown that higher SB ratio with enhanced flame speed resulted in larger heat transfer around TDC or peak pressure timing, causing not only moderate or large cooling loss but also larger exhaust heat loss attributed by higher value of internal energy remaining at EVO timing, highly correlated to exhaust loss. Therefore, despite enhanced burning rate, SB 1.47 and 1.47 high Rt condition showed no improvement in net indicated efficiency for low load operation. In addition, it was found by additional experiments with larger displacement volume conditions that the effect of reduced SV ratio was mainly dominated by the effect of displacement volume as shown in previous studies. That is, the decrement of cooling loss by increased SB ratio was attributed by larger displacement volume with fixed bore condition. With fixed displacement volume and varying SB ratio, it was shown that enhanced flow dynamics caused not only faster burning rate but also similar or increased cooling loss compared to lower SB ratio operation, attributed by enhanced convective heat transfer coefficient which was estimated by single-zone combustion analysis. Therefore, as a semi-conclusion, there was no advantage for increment in SB ratio to achieve reduced cooling loss.

In the case of knock phenomena, high load operation with fixed fuel rate (26, 30, and 34 mg per cycle) was conducted with using different knock regime, having stronger knock incidence compared to main experiments to obtain clear knock tendency. First of all, as mentioned in recent work, increased knock intensity was found in the individual cycles having faster burning rate, compared to another

individual cycles having slower burning rate which also had weaker or no knock occurrence. Considering previous studies and general notion of autoignition and knock developments, it was expected that relatively smaller volume and higher temperature and pressure attributed by faster flame propagation could cause this situation. Furthermore, an increased unburned mass fraction, which was not expected, at knock onset timing was detected for the individual cycles with faster burning rate, which was generally known as a good indicator of knock intensity from many studies. With these results, endangered was the well-known notion that faster flame propagation can reduce knock occurrence and resultantly, produce knock-robust operation. Thus, new definition of knock-robust operation was suggested as followed; 'the engine which generates more work with same input (i.e. fuel rate related to engine load) under the same knock criterion". In order to supplement the newly suggested definition, 0D simulation with adiabatic process was conducted. From the simulation results, it was found that the operation with faster burning rate still can achieve higher gross indicated efficiency with advanced combustion phasing (expressed as CA50). Therefore, it can be concluded that the strategies related to faster burning rate is still required to operate SI engine with knock-robust characteristics. However, with the results of main experiments including basic three SB ratios and different tumble ratio conditions, it was found that higher SB ratio (i.e. SB 1.47 and 1.47 high Rt) has a decrement in engine efficiency with retarded combustion phasing by enhancing tumble ratio to increase burning rate which was shown in the experiments. In order to implement these trends, comparison between the results of SB 1.2 and 1.47 was conducted by using averaging process. Here, it was found that despite similar burn duration (CA10-CA70), slightly higher knock intensity (expressed as averaged MAPO values) was detected for SB 1.47 operation. Therefore, it can be postulated that there are geometry-related characteristics that can affect knock phenomena and cannot be expected by 0D simulation. In order to find the characteristics, the knock index for knock intensity was newly developed, including 'shape factor'

defined by the characteristic length of unburned zone. Comparing the existing notion related to the correlation between knock intensity and unburned mass fraction or fuel LHV remaining, newly-developed knock index showed good agreement with averaged MAPO values from experiments, which can indirectly prove that such geometric issue should be considered to understand the knock phenomena in the higher SB ratio condition.

References

1. "Share of total U.S. energy used for transportation, 2017." https://www.eia.gov/energyexplained/?page=us_energy_transportation.

2. "Environmental protection agency." 2017, https://www.federalregister.gov/documents/2016/12/28/2016-31140/corporate-average-fuel-economy-standards-credits.

3. "CO2 emission standards for passenger cars and light-commercial vehicles in the european union." 2019, https://www.theicct.org/publications/ldv-co2-stds-eu-2030-update-jan2019.

4. "China passenger vehicle fuel consumption development annual report." 2014, http://www.efchina.org/Attachments/Report/report-ctp-20140801/2014-china-passenger-vehicle-fuel-consumption-development-annual-report.

5. Choi, W. J., Yoo, E., Jang, J. J., Seol, E. et al. "Well-to-Wheel Analysis (WTW) on Greenhouse Gas Emissions of Transportation Fuels in South Korea." Paper presented at the 한국자동차공학회 Workshop, 2018.

6. Teixeira, E. R., Mateus, R., Camoes, A. F., Bragança, L. et al. "Comparative environmental life-cycle analysis of concretes using biomass and coal fly ashes as partial cement replacement material." *Journal of Cleaner Production* 112:2221-30, 2016.

7. Ou, X., Zhang, X., Qin, Y., and Qi, T., "Life cycle analysis of electric vehicle charged by advanced technologies coal-power in future China." *Journal of the China Coal Society* 35(1):169-72, 2010.

8. Yoo, E., Kim, M., and Song, H. H., "Well-to-wheel analysis of hydrogen fuel-cell electric vehicle in Korea." *International Journal of Hydrogen Energy* 43(41):19267-78, 2018.

9. Kalghatgi, G., "Is it really the end of internal combustion engines and petroleum in transport?." *Applied Energy* 225:965-74, 2018.

10. Teng, H., Regner, G., and Cowland, C., "Achieving high engine efficiency for heavy-duty diesel engines by waste heat recovery using supercritical organic-fluid Rankine cycle," SAE Technical Paper 2006.

11. Dolz, V., Novella, R., García, A., and Sánchez, J., "HD Diesel engine equipped with a bottoming Rankine cycle as a waste heat recovery system. Part 1: Study and analysis of the waste heat energy." *Applied Thermal Engineering* 36:269-78, 2012.

12. Wang, E., Zhang, H., Fan, B., Liang, H. et al. "Study of gasoline engine waste heat recovery by organic Rankine cycle." Paper presented at the Advanced Materials Research, 2012.

13. Sprouse III, C. and Depcik, C., "Review of organic Rankine cycles for internal combustion engine exhaust waste heat recovery." *Applied Thermal Engineering* 51(1-2):711-22, 2013.

14. Taymaz, I., Çakır, K., and Mimaroglu, A., "Experimental study of effective efficiency in a ceramic coated diesel engine." *Surface Coatings Technology*

200(1-4):1182-85, 2005.

15. Büyükkaya, E., Engin, T., and Cerit, M., "Effects of thermal barrier coating on gas emissions and performance of a LHR engine with different injection timings and valve adjustments." *Energy conversion and Management* 47(9-10):1298-310, 2006.

16. Edwards, K. D., Wagner, R. M., Briggs, T., and Theiss, T. J. "Defining engine efficiency limits." Paper presented at the 17th DEER Conference, Detroit, MI, October, 2011.

17. Caton, J. A., "The thermodynamic characteristics of high efficiency, internal-combustion engines." *Energy Conversion and Management* 58:84-93, 2012.

18. Heywood, J. B., "Internal combustion engine fundamentals." 1988.

19. Oh, S. and Song, H. H., "Exergy analysis on non-catalyzed partial oxidation reforming using homogeneous charge compression ignition engine in a solid oxide fuel cell system." *International Journal of Hydrogen Energy* 43(5):2943-60, 2018.

20. Sjoberg, C. M. G. and Vuilleumier, D., "Co-Optima Core Fuels: Initial Investigations of Knocking Behavior in a DISI Engine," Sandia National Lab.(SNL-CA), Livermore, CA (United States) 2016.

21. Brassat, A., Thewes, M., Müther, M., and Pischinger, S., "Tailor-made fuels from biomass for gasoline combustion systems." *MTZ worldwide eMagazine* 72(12):56-63, 2011.

22. Li, T., Gao, Y., Wang, J., and Chen, Z., "The Miller cycle effects on improvement of fuel economy in a highly boosted, high compression ratio, direct-injection gasoline engine: EIVC vs. LIVC." *Energy Conversion and Management* 79:59-65, 2014.

23. Luisi, S., Doria, V., Stroppiana, A., Millo, F. et al. "Experimental investigation on early and late intake valve closures for knock mitigation through Miller cycle in a downsized turbocharged engine," SAE Technical Paper 2015.

24. Zheng, B., Yin, T., and Li, T., "Analysis of Thermal Efficiency Improvement of a Highly Boosted, High Compression Ratio, Direct-Injection Gasoline Engine with LIVC and EIVC at Partial and Full Loads," SAE Technical Paper 2015.

25. Söderberg, F. and Johansson, B., "Fluid flow, combustion and efficiency with early or late inlet valve closing." *SAE transactions*:2334-51, 1997.

26. Zeldovich, Y. B., "Regime classification of an exothermic reaction with nonuniform initial conditions." *Combustion and Flame* 39(2):211-14, 1980.

27. König, G., Maly, R., Bradley, D., Lau, A. et al. "Role of exothermic centres on knock initiation and knock damage." *SAE Transactions*:840-61, 1990.

28. Nates, R. and Yates, A., "Knock damage mechanisms in spark-ignition engines." *SAE Transactions*:1970-80, 1994.

29. Fitton, J. C. and Nates, R. J., "Knock erosion in spark-ignition engines." *SAE Transactions*:2318-26, 1996.

30. Yelvington, P. E. and Green, W. H., "Prediction of the knock limit and viable operating range for a homogeneous-charge compression-ignition (HCCI) engine," SAE Technical paper 2003.

31. Bradley, D. and Kalghatgi, G., "Influence of autoignition delay time characteristics of different fuels on pressure waves and knock in reciprocating engines." *Combustion and Flame* 156(12):2307-18, 2009.

32. Bradley, D., Morley, C., Gu, X., and Emerson, D., "Amplified pressure waves during autoignition: relevance to CAI engines." *SAE Transactions*:2679-90, 2002.

33. Kalghatgi, G., "Fuel anti-knock quality-Part I. Engine studies." *SAE Transactions*:1993-2004, 2001.

34. Hwang, K., Hwang, I., Lee, H., Park, H. et al. "Development of new high-efficiency Kappa 1.6 L GDI engine," SAE Technical Paper 2016.

35. Burrows, J., Mixell, K., Reinicke, P., Riess, M. et al. "Corona Ignition-Assessment of Physical Effects by Pressure Chamber, Rapid Compression Machine, and Single Cylinder Engine Testing." Paper presented at the 2nd International Conference on Ignition Systems for Gasoline Engines, 2014.

36. Schenk, M., Schröter, F., Zellinger, F., Klaus, B. et al. "Corona-Ignition vs. Spark Ignition: A Fundamental Comparison for varying thermodynamic conditions of modern turbocharged Gasoline Engines." Paper presented at the International Conference: SIA Powertrain, Versailles, 2015.

37. Yoshihara, Y., Nakata, K., Takahashi, D., Omura, T. et al. "Development of High Tumble Intake-Port for High Thermal Efficiency Engines," SAE Technical Paper 2016.

38. Takahashi, D., Nakata, K., Yoshihara, Y., and Omura, T., "Combustion development to realize high thermal efficiency engines." *SAE International Journal of Engines* 9(3):1486-93, 2016.

39. Omura, T., Nakata, K., Yoshihara, Y., and Takahashi, D., "Research on the measures for improving cycle-to-cycle variations under high tumble combustion," SAE Technical Paper 2016.

40. Nakata, K. and Shimizu, R. "Toyota's new combustion technology for high engine thermal efficiency and high engine output performance." Paper presented at the 37th International Vienna Motor Symposium, 2016.

41. Cairns, A., Blaxill, H., and Irlam, G., "Exhaust gas recirculation for improved part and full load fuel economy in a turbocharged gasoline engine," SAE Technical Paper 2006.

42. Shyani, R. and Caton, J., "A thermodynamic analysis of the use of exhaust gas recirculation in spark ignition engines including the second law of thermodynamics." *Proceedings of the Institution of Mechanical Engineers, Part D: Journal of Automobile Engineering* 223(1):131-49, 2009.

43. Takahashi, D., Nakata, K., Yoshihara, Y., Ohta, Y. et al. "Combustion development to achieve engine thermal efficiency of 40% for hybrid vehicles," SAE Technical Paper 2015.

44. Matsuo, S., Ikeda, E., Ito, Y., and Nishiura, H., "The new Toyota inline 4 cylinder 1.8 L ESTEC 2ZR-FXE gasoline engine for hybrid car," SAE Technical Paper 2016.

45. Wei, H., Zhu, T., Shu, G., Tan, L. et al. "Gasoline engine exhaust gas recirculation–a review." *Applied Energy* 99:534-44, 2012.

46. Asif, M., Giles, K., Lewis, A., Akehurst, S. et al. "Influence of Coolant Temperature and Flow Rate, and Air Flow on Knock Performance of a Downsized, Highly Boosted, Direct-Injection Spark Ignition Engine," SAE Technical Paper 2017.

47. Wang, Z., Liu, H., and Reitz, R. D., "Knocking combustion in spark-ignition engines." *Progress in Energy Combustion Science* 61:78-112, 2017.

48. Wei, H., Yu, J., Shao, A., Zhou, L. et al. "Influence of injection strategies on knock resistance and combustion characteristics in a DISI engine." *Proceedings of the Institution of Mechanical Engineers, Part D: Journal of Automobile Engineering* , 2018.

49. Yu, H., Qi, C., and Chen, Z., "Effects of flame propagation speed and chamber size on end-gas autoignition." *Proceedings of the Combustion Institute* 36(3):3533-41, 2017.

50. Chen, L., Wei, H., Chen, C., Feng, D. et al. "Numerical investigations on the effects of turbulence intensity on knocking combustion in a downsized gasoline engine." *Energy* 166:318-25, 2019.

51. Chen, Y. and Raine, R., "A study on the influence of burning rate on engine knock from empirical data and simulation." *Combustion and Flame* 162(5):2108-18, 2015.

52. Chen, Y. and Raine, R., "Engine knock in an SI engine with hydrogen supplementation under stoichiometric and lean conditions." *SAE International Journal of Engines* 7(2):595-605, 2014.

53. "Cantera: An object-oriented software toolkit for chemical kinetics, thermodynamics, and transport processes." 2018, https://www.cantera.org.

54. Choi, H., Lim, J., Min, K., and Lee, D., "Simulation of knock with different piston shapes in a heavy-duty LPG Engine." *International Journal of Automotive Technology* 6(2):133-39, 2005.

55. Filipi, Z. S. and Assanis, D. N., "The effect of the stroke-to-bore ratio on combustion, heat transfer and efficiency of a homogeneous charge spark ignition engine of given displacement." *International Journal of Engine Research* 1(2):191-208, 2000.

56. Tsuchida, H., Hiraya, K., Tanaka, D., Shigemoto, S. et al. "The effect of a longer stroke on improving fuel economy of a multiple-link VCR engine," SAE Technical Paper 2007.

57. Ikeya, K., Takazawa, M., Yamada, T., Park, S. et al. "Thermal efficiency enhancement of a gasoline engine." *SAE International Journal of Engines* 8(4):1579-86, 2015.

58. Hoag, K. L., Mangold, B., Alger, T., Abidin, Z. et al. "A study isolating the effect of bore-to-stroke ratio on gasoline engine combustion chamber development." *SAE International Journal of Engines* 9(4):2022-29, 2016.

59. Agarwal, A., Filipi, Z., Assanis, D., and Baker, D., "Assessment of single- and two-zone turbulence formulations for quasi-dimensional modeling of spark-ignition engine combustion." *Combustion Science and Technology* 136(1-6):13-39, 1998.

60. Konig, G. and Sheppard, C., "End gas autoignition and knock in a spark ignition engine." *SAE Transactions*:820-39, 1990.

61. Fox, J. W., K. Cheng, W., and Heywood, J. B., "A model for predicting residual gas fraction in spark-ignition engines." *SAE Transactions*:1538-44, 1993.

62. Mladek, M. and Onder, C. H., "A model for the estimation of inducted air mass and the residual gas fraction using cylinder pressure measurements," SAE Technical Paper 2000.

63. Cavina, N., Siviero, C., and Suglia, R., "Residual gas fraction estimation: Application to a GDI engine with variable valve timing and EGR." *SAE Transactions*:1774-82, 2004.

64. Kale, V., Yeliana, Y., Worm, J., and Naber, J., "Development of an improved residuals estimation model for dual independent cam phasing spark-ignition engines," SAE Technical Paper 2013.

65. Gatowski, J., Balles, E. N., Chun, K. M., Nelson, F. et al. "Heat release analysis of engine pressure data." *SAE transactions*:961-77, 1984.

66. Chun, K. M. and Heywood, J. B., "Estimating heat-release and mass-of-mixture burned from spark-ignition engine pressure data." *Combustion Science and Technology* 54(1-6):133-43, 1987.

67. Rassweiler, G. M. and Withrow, L., "Flame Temperatures Vary with Knock and Combustion-Chamber Position," SAE Technical Paper 1935.

68. Brunt, M. F., Rai, H., and Emtage, A. L., "The calculation of heat release energy from engine cylinder pressure data." *SAE Transactions*:1596-609, 1998.

69. Song, H. H. *Low-load extension of residual-effected homogeneous charge compression ignition using recompression reaction.* Stanford University, 2009.

70. Chun, K. M. and Heywood, J. B., "Characterization of knock in a spark-ignition engine," SAE Technical Paper 1989.

71. Cho, S. "Study on the Efffect of Cylinder Wall Temperatures on Knock Characteristics in Spark-Ignited Engine." Ph.D. Dissertation, Department of Mechanical and Aerospace Engineering, Seoul National University, 2018.

72. Cho, S., Park, J., Song, C., Oh, S. et al. "Prediction Modeling and Analysis of Knocking Combustion using an Improved 0D RGF Model and Supervised Deep Learning." *Energies* 12(5):844, 2019.

73. Brunt, M. F., Pond, C. R., and Biundo, J., "Gasoline engine knock analysis using cylinder pressure data." *SAE Transactions*:1399-412, 1998.

74. Draper, C. S., "The physical effects of detonation in a closed cylindrical chamber." 1935.

75. di Gaeta, A., Giglio, V., Police, G., and Rispoli, N., "Modeling of in-cylinder pressure oscillations under knocking conditions: A general approach based on the damped wave equation." *Fuel* 104:230-43, 2013.

76. Kim, K. S. "Study of engine knock using a Monte Carlo method." The University of Wisconsin-Madison, 2015.

77. McKenzie, J. and Cheng, W. K., "The anatomy of knock," SAE Technical Paper 2016.

78. Kalghatgi, G., Algunaibet, I., and Morganti, K., "On knock intensity and superknock in SI engines." *SAE International Journal of Engines* 10(3):1051-63, 2017.

79. Shahlari, A. J. and Ghandhi, J. B., "A comparison of engine knock metrics," SAE Technical Paper 2012.

80. Borg, J. M. and Alkidas, A. C., "Cylinder-pressure-based methods for sensing spark-ignition engine knock." *International Journal of Vehicle Design* 45(1-2):222-41, 2007.

81. Richard, S., Bougrine, S., Font, G., Lafossas, F.-A. et al. "On the reduction of a 3D CFD combustion model to build a physical 0D model for simulating heat release, knock and pollutants in SI engines." *Oil & Gas Science Technology-Revue de l'IFP* 64(3):223-42, 2009.

82. Dahnz, C. and Spicher, U., "Irregular combustion in supercharged spark ignition engines–pre-ignition and other phenomena." *International Journal of Engine Research* 11(6):485-98, 2010.

83. Kalghatgi, G. T. and Bradley, D., "Pre-ignition and 'super-knock'in turbo-charged spark-ignition engines." *International Journal of Engine Research* 13(4):399-414, 2012.

84. Song, H. "Development of Knock Prediction Model by Cool Flame Elimination Method Covering NTC Region: Modeling and Experimental Study." Ph.D. Dissertation, Department of Mechanical and Aerospace Engineering, Seoul National University, 2017.

85. Mehl, M., Pitz, W. J., Westbrook, C. K., and Curran, H. J., "Kinetic modeling of gasoline surrogate components and mixtures under engine conditions." *Proceedings of the Combustion Institute* 33(1):193-200, 2011.

86. Hohenberg, G. F., "Advanced approaches for heat transfer calculations," SAE Technical paper 1979.

87. Livengood, J. and Wu, P. "Correlation of autoignition phenomena in internal combustion engines and rapid compression machines." Paper presented at the Symposium (international) on combustion, 1955.

88. Douaud, A. and Eyzat, P., "Four-octane-number method for predicting the anti-knock behavior of fuels and engines." *SAE Transactions*:294-308, 1978.

89. Chen, L., Li, T., Yin, T., and Zheng, B., "A predictive model for knock onset in spark-ignition engines with cooled EGR." *Energy Conversion and Management* 87:946-55, 2014.

90. Hoepke, B., Jannsen, S., Kasseris, E., and Cheng, W. K., "EGR effects on boosted SI engine operation and knock integral correlation." *SAE International Journal of Engines* 5(2):547-59, 2012.

91. McKenzie, J. and Cheng, W. K., "Ignition Delay Correlation for Engine Operating with Lean and with Rich Fuel-Air Mixtures," SAE Technical Paper 2016.

92. Somers, K. P., Cracknell, R. F., and Curran, H. J., "A chemical kinetic interpretation of the octane appetite of modern gasoline engines." *Proceedings of the Combustion Institute* 37(4):4857-64, 2019.

93. "Single-cylinder research engines." 2019, https://automotive.ricardo.com/engines/single-cylinder-research-engines.

94. Brunt, M. F. and Emtage, A. L., "Evaluation of burn rate routines and analysis errors," SAE Technical Paper 1997.

95. Brunt, M. F. and Lucas, G. G., "The effect of crank angle resolution on cylinder pressure analysis," SAE Technical Paper 1991.

96. Brunt, M. F. and Pond, C. R., "Evaluation of techniques for absolute cylinder pressure correction," SAE technical paper 1997.

97. Kim, M., Lee, S., and Kim, W., "Tumble flow measurements using three different methods and its effects on fuel economy and emissions," SAE Technical Paper 2006.

98. Cho, S., Oh, S., Song, C., Shin, W. et al. "Effects of Bore-to-Stroke Ratio on the Efficiency and Knock Characteristics in a Single-Cylinder GDI Engine," SAE Technical Paper 2019.

99. Cho, S., Song, C., Oh, S., Min, K. et al. "An experimental study on the knock mitigation effect of coolant and thermal boundary temperatures in spark ignited engines," SAE Technical Paper 2018.

100. Oh, S., Cho, S., Seol, E., Song, C. et al. "An Experimental Study on the Effect of Stroke-to-Bore Ratio of Atkinson DISI Engines with Variable Valve Timing." *SAE International Journal of Engines* 11(2018-01-1419):1183-93, 2018.

101. Xu, H., "Some critical technical issues on the steady flow testing of cylinder heads," SAE Technical Paper 2001.

102. Vuilleumier, D., Kim, N., Sjöberg, M., Yokoo, N. et al. "Effects of EGR Constituents and Fuel Composition on DISI Engine Knock: An Experimental and Modeling Study," SAE Technical Paper 2018.

103. Caton, J. A., "On the destruction of availability (exergy) due to combustion processes—with specific application to internal-combustion engines." *Energy* 25(11):1097-117, 2000.

104. Stuhler, H., Kruse, T., Stuber, A., Gschweitl, K. et al. "Automated model-based GDI engine calibration adaptive online DoE approach," SAE Technical Paper 2002.

105. Castagné, M., Bentolila, Y., Chaudoye, F., Hallé, A. et al. "Comparison of engine calibration methods based on design of experiments (doe)." *Oil & Gas Science Technology-Revue de l'IFP* 63(4):563-82, 2008.

106. Sjöberg, M. and Dec, J. E., "An investigation into lowest acceptable combustion temperatures for hydrocarbon fuels in HCCI engines." *Proceedings of the Combustion Institute* 30(2):2719-26, 2005.

107. Aoyama, T., Hattori, Y., Mizuta, J. i., and Sato, Y., "An experimental study on premixed-charge compression ignition gasoline engine," SAE Technical paper 1996.

108. Faghih, M., Li, H., Gou, X., and Chen, Z., "On laminar premixed flame propagating into autoigniting mixtures under engine-relevant conditions." *Proceedings of the Combustion Institute* 37(4):4673-80, 2019.

Appendix A. Proof of the relation between heat transfer and pressure decrement in Otto cycle

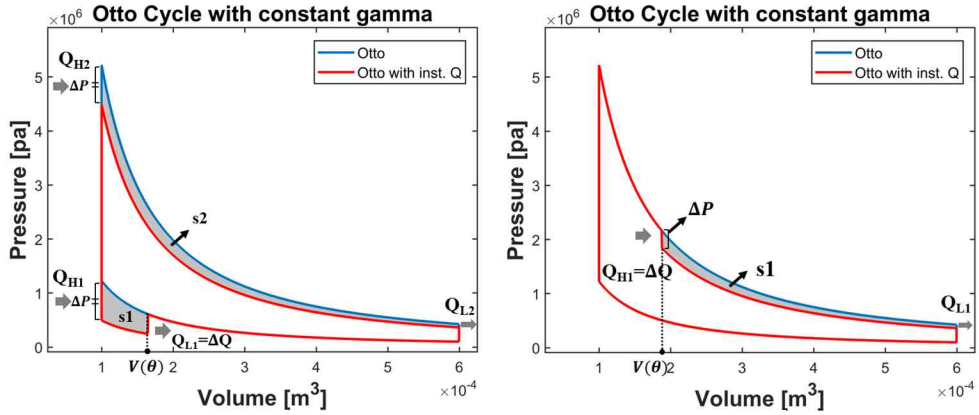

(a) (b)

Figure A1.1 Comparison between Otto cycle and Otto cycle with instantaneous heat transfer added
(a): heat transfer before TDC
(b): heat transfer after TDC

Figure A1.1 showed the P-V diagram of Otto cycle with instantaneous heat transfer added before and after TDC timing. Several assumptions related to this approach were listed below.

- The volume of the start of cycle is expressed as V_{BDC}, and the volume at TDC timing is expressed as V_{TDC}.

- Specific heat ratio (γ) for each point is assumed to be constant, as it is also used for Otto cycle (constant volume cycle) operation. By this assumption, specific heat with constant-volume (isochoric process, c_v) is also constant.

- When the heat addition (ΔQ) occurs, temperature and pressure changes with isochoric process, where the related equations derived by ideal gas law and heat addition with isochoric process were listed below,

$$\Delta P = \frac{R}{c_v V}(\Delta Q) \tag{A1.1}$$

$$\Delta T = \frac{(\Delta Q)}{m\, c_v} \tag{A1.2}$$

where R is gas constant with [J kg^{-1}K^{-1}] unit.

- After the heat addition, the process is operated as same as original cycle, i.e. Otto cycle. Therefore, the area expressed as s1, and s2 for each subfigure can be also treated as 'small' Otto cycle.

First of all, figure A1.1-(a) was covered with detailed equations for proof. When the heat addition (ΔQ) occurs at θ of its volume $V(\theta)$, pressure is decreased. The relevant equations for s1 and s2 from Otto cycle calculation were listed below.

$$s1 = Q_{H1} - Q_{L1}$$

$$= Q_{L1}\left(\frac{Q_{H1}}{Q_{L1}} - 1\right)$$

$$= Q_{L1}\left(\left(\frac{V(\theta)}{V_{TDC}}\right)^{\gamma-1} - 1\right)$$

$$= \Delta Q\ \left(\left(\frac{V(\theta)}{V_{TDC}}\right)^{\gamma-1} - 1\right) \tag{A1.3}$$

$$s2 = Q_{H2} - Q_{L2}$$

$$= Q_{H2}\left(1 - \left(\frac{V_{BDC}}{V_{TDC}}\right)^{1-\gamma}\right)$$

$$= \Delta Q \left(\frac{V(\theta)}{V_{TDC}}\right)^{\gamma-1}\left(1 - \left(\frac{V_{BDC}}{V_{TDC}}\right)^{1-\gamma}\right) \quad \text{(A1.4)}$$

$$Q_{H1} = Q_{H2} = \Delta Q \left(\frac{V(\theta)}{V_{TDC}}\right)^{\gamma-1} \quad \text{(A1.5)}$$

Since s1 can be treated as Otto cycle, Q_{L1} is same with ΔQ. In addition, by using Otto cycle relation and constant specific heat ratio, A1.5 can be derived. Therefore, work loss due to heat addition at crank angle θ can be summarized as below.

$$W_{Otto,loss} = |s2| - |s1|$$

$$= \Delta Q \left(\frac{V(\theta)}{V_{TDC}}\right)^{\gamma-1}\left(1 - \left(\frac{V_{BDC}}{V_{TDC}}\right)^{1-\gamma}\right) - \Delta Q \left(\left(\frac{V(\theta)}{V_{TDC}}\right)^{\gamma-1} - 1\right)$$

$$= \Delta Q \left(1 - \left(\frac{V(\theta)}{V_{BDC}}\right)^{\gamma-1}\right) \quad \text{(A1.6)}$$

Here, the trend of $W_{Otto,loss}$ can be easily expected – as the crank angle where heat addition occurs approaches TDC timing, $W_{Otto,loss}$ increases. That is, the effect of heat addition on the work deficiency is higher as it occurs near TDC (compression stroke only, for now).

Second, the situation of figure A1.1-(b) was covered, which is easily expected compared to former one. The relevant equations were listed below.

$$s1 = Q_{H1} - Q_{L1} = Q_{H1}\left(1 - \frac{Q_{L1}}{Q_{H1}}\right) = \Delta Q\left(1 - \left(\frac{V(\theta)}{V_{BDC}}\right)^{\gamma-1}\right) \quad \text{(A1.7)}$$

$$Q_{H1} = \Delta Q \quad \text{(A1.8)}$$

Since s1 is directly $W_{Otto,bss}$ in this situation, it can be concluded that the value of $W_{Otto,bss}$ is same as former one. Therefore, it can be concluded that regardless of the position at which heat addition occurs, the effect of work loss for Otto cycle operation shows the greatest at TDC timing.

국 문 초 록

점점 강화되고 있는 연비 규제를 맞추기 위해, 가솔린 연료 기반의 전기 점화 엔진의 연구가 계속해서 활발하게 진행되고 있다. 하지만 관련되어 있는 많은 연구들이 엔진의 구동 전략에 대해 집중되고 있으며, 이러한 전략들이 적용되는 엔진의 설계 및 디자인에는 상대적으로 연구가 부족하다. 엔진 설계 또한 구동 전략에 버금가는 효과를 엔진 효율에 미칠 수 있다는 점을 고려하였을 때, 이 또한 중요하게 연구될 필요가 있다. 이러한 엔진 설계 관련 변수들 중 엔진 실린더의 세로와 가로 길이를 대표하는 스트로크 및 보어 길이의 비율이 엔진 구동 결과에 상당한 영향을 줄 수 있다는 것이 이전 연구들에서 확인되었다.

증가된 스트로크 길이에 기반한 전기 점화 엔진 구동에서는 크게 두가지 요소 – 엔진 냉각 손실 및 연소 속도 – 가 중요하게 고려되어 왔다. 우선, 스트로크-보어 비를 상승시킴으로써 (스트로크 증가), 상사점 주변에서의 부피 대비 면적 비가 감소하게 되고 이것이 연소 기간동안의 열전달을 감소시킬 가능성이 있음이 연구되어 왔다. 또한, 늘어난 스트로크 길이에 따른 피스톤 속도 증가로 인해, 엔진 내 유동이 빠르게 되고 이로 인해 난류 화염 속도가 증가함으로써 전기 점화 엔진의 이상적인 사이클인 Otto 사이클에 가까운 구동이 달성될 수 있음이 연구되어 왔다. 하지만 이러한 내용들을 실험적으로 다룬 많은 연구들이 스트로크-보어 비 변경을 보어 고정 상태에서 스트로크를 바꾸면서 진행하였고, 이로 인해 배기량이 증가함으로써 스트로크-보어 비만의 독립적인 효과를 실험 결과로부터 확인하기 어려웠다는 점이 있다.

본 연구는 이러한 사실에 기반하여, 압축비 및 배기량을 모두 고정한 상태에서 스트로크-보어 비 만을 변경하였을 때의 전기 점화

엔진의 구동 특성이 어떻게 바뀌는지를 분석하는 것에 주안점을 두었다. 이를 위해 직접 분사 및 밸브 타이밍 변경이 가능한 단기통 전기 점화 엔진이 실험에 사용되었으며, 압축비 및 배기량을 고정할 수 있는 총 3 가지 스트로크-보어 비에 해당하는 실험 장비가 사용되었다. 또한, 기존의 실험 결과와의 비교 및 연소 속도 상승과 관련된 다른 설계안과의 비교를 위해, 스트로크-보어 비가 기본 3 사양과 비슷한 배기량 변경 2 사양, 그리고 실린더 헤드 텀블비가 개선되었고 스트로크-보어 비가 같은 텀블비 변경 2 사양에 해당하는 실험 장비가 사용되었다. 이를 통해 실험 결과에서의 배기량 변경이 배제된 스트로크-보어 비만의 독립적인 효과, 그리고 연소 속도 증가 전략으로서의 스트로크-보어 비 상승이 타 전략과 비교하여 얼마나 효과적인지를 실험적으로 검증하였다. 이러한 실험 장비들을 바탕으로 밸브 타이밍 변경 실험을 다양한 엔진 부하 및 회전 속도 조건에 대하여 진행하였다. 이를 통해 최고 효율을 나타내는 밸브 타이밍 위치는 스트로크-보어 비에 따라 크게 다르지 않으며, 주로 부하와 회전 속도에 의해 결정되는 것을 확인하였다.

이러한 선행 실험을 바탕으로 다양한 부하 및 회전 속도에서의 밸브타이밍 조건이 결정되었으며, 이러한 선행 실험에서 발견된 예상치 못한 결과들 – 엔진 냉각 손실 및 노킹 특성 – 을 자세하게 분석하기 위해 추가 실험이 진행되었다. 우선 냉각 손실이 효율에 지배적인 저부하 영역에서의 실험이 진행되었으며, 흡기 밸브 닫힘 시점에서의 조건과 실린더 압력 결과를 바탕으로 자세한 연소 분석법을 적용하여 해당 실험 결과를 분석하였다. 그 결과, 엔진 내 폐구간에 해당하는 구동 시점에서 (흡기 밸브 닫힘 – 배기 밸브 열림) 상사점 및 연소압 최대 지점 근처에서의 열전달 비율이 스트로크-보어 비가 큰 사양에서 상대적으로 높은 것이 확인되었으며, 이를 통해 기존 예상과 다른 엔진 내 냉각 손실 상승 및 배기 열손실 증가가 확인되었다. 또한 기존 밸브타이밍 변경 실험보다 더 강한

기준 하에서의 노킹 실험이 추가적으로 진행되었으며, 각 실험 조건에서의 개별 사이클 분석이 진행되었다. 이를 통해, 빠른 연소 속도를 가진 개별사이클에서 더 강한 노킹 강도가 나타나며, 노킹이 발생하지 않은 사이클에서 연소 속도가 더 느린 것이 확인되었다. 이러한 사실이 기존 관념 – 연소속도가 빠른 구동 전략이 노킹에 강건하다 – 에 위배되는지를 확인하기 위해 노킹에 강건하다는 개념을 새롭게 정의하였으며, 이러한 정의를 바탕으로 0 차원 시뮬레이션을 진행한 결과 연소 속도가 빠른 조건에서 여전히 엔진 효율이 높고 연소상 또한 진각될 수 있음이 확인되었다. 하지만 기본 3 사양 및 텀블비 변경 실험을 진행한 결과, 연소 속도가 스트로크-보어 비 및 텀블비 상승에 따라 꾸준히 증가함에 반해, 스트로크-보어 비가 큰 사양에서 동일 노킹 기준 하에 연소상이 지각되고 효율이 감소하는 것이 확인되었다. 이와 같이 예상치 못한 노킹 및 효율 특성은 결국 스트로크-보어 비에 따른 기하학적 요소가 크게 작용되었다고 판단되었으며, 이를 반영하기 위해 새로운 노킹 강도 판단식이 제안되었다. 이를 통해, 스트로크-보어 비 증가를 통해 연소 속도가 향상되더라도 상사점 주변에서 상대적으로 부피 대비 면적이 작고 조밀한 설계 때문에 미연 영역 내 노킹을 유발하는 코어 지점이 생길 가능성이 증가할 수 있음을 새로운 노킹 강도 판단식의 적합도를 통해 간접적으로 확인할 수 있었다. 이러한 결과들을 바탕으로 다양한 전기 점화 엔진 효율 상승 전략을 적용하는 과정에서, 적절한 범위에서의 스트로크-보어 비가 사용되는 것이 엔진 냉각 손실이나 노킹 측면에서 유리할 수 있다는 것이 최종적으로 제시될 수 있다.

주요어: 가솔린 전기 점화 엔진, 스트로크-보어 비, 0 차원 연소 해석, 노킹, 엔진 냉각 손실, 배기 열손실

학 번: 2013-23076